CHARACTERIZING POLYVINYL TOLUENE SCINTILLATOR'S STATE OF HEALTH USING LIGHT READINGS FROM A PHOTOMULTIPLIER TUBE

A Thesis

by

ERNESTO ANDRES ORDOÑEZ FERRER

Submitted to the Office of Graduate and Professional Studies of
Texas A&M University
in partial fulfillment of the requirements for the degree of

MASTER OF SCIENCE

Chair of Committee,	Craig Marianno
Committee Members,	Mark Kimber
	Xiaofeng Qian
Head of Department,	Michael Nastasi

May 2021

Major Subject: Nuclear Engineering

ABSTRACT

Polyvinyl toluene (PVT) based detectors are used in radiation portal monitors (RPM) to detect the illicit trafficking of nuclear materials. These detectors have been observed to internally fog after being subjected to environments with large temperature and humidity fluctuations, potentially decreasing the overall effectiveness of the RPMs. As temperature decreases, PVT fogging is induced by the formation of water-filled voids within the plastic. An Opacity Monitoring System (OMS) was originally developed to measure and track changes in PVT opacity in-situ. This was accomplished by employing an array of different colored light emitting diodes (LED) and optical sensors (OS) to measure light transmission through the detector. Changes in PVT opacity were tracked by intermittently flashing each LED and recording the amount of transmitted light observed by the OS. This method, however, required the aforementioned equipment to be adhered onto the detector and produced a separate data stream from the RPM. An alternative method to track opacity changes was conducted for this research. Here, four OMS/PVT systems were placed in an environmental chamber (EC) at Pacific Northwest National Laboratory (PNNL) and RPM count rates were monitored throughout 360 hours of temperature and humidity cycles ranging from -20°C to 50°C and 40% to 100% relative humidity (RH), respectively. The LED-induced RPM count rates were observed to change in response to temperature fluctuations in the environmental chamber. This aided in establishing a correlation between recorded temperature and count rate, thus proving that RPM electronics can be used to track the onset of fogging within the

detector. Furthermore, a mathematical model establishing the relationship between the onset of fogging and detector temperature was developed to aid RPM operators to predict PVT the onset of fogging on site.

DEDICATION

This Master's thesis is dedicated to my late grandparents, Dr. Joaquin Ordoñez Villalobos and Maria Lourdes Nava.

Abuelito Joaquin: as days progress I recognize your qualities within myself and hope that someday I can become the type of man you were. Your hunger for knowledge and love for life was intoxicating and contagious. Thank you for all your words of wisdom and interest in my nuclear engineering studies. The nuclear engineering book you found for me before your passing stays in my office as a constant reminder of your support.

Abuelita Maria: thank you for always being a loving, caring, and selfless person. Your love and support throughout my life was unwavering. Thank you for always thinking about me and checking on me every day. I miss you and Abuelito Joaquin every day. Rest in Peace

ACKNOWLEDGEMENTS

I would like to thank my committee chair, Dr. Craig Marianno, along with my committee members, Dr. Mark Kimber and Dr. Xiaofeng Qian, for their guidance and support throughout the course of this research.

I would also like to thank my girlfriend, parents, sister, and the rest of my extended family for their encouragement, unwavering support, patience, and love throughout this process. None of this would not have been possible without each of you.

CONTRIBUTORS AND FUNDING SOURCES

Contributors

This work was supervised by a thesis committee consisting of Professor Craig Marianno and Professor Mark Kimber of the Department of Nuclear Engineering alongside Professor Xiaofeng Qian of the Department of Materials Science and Engineering.

Funding Sources

Graduate study was supported primarily by funding from the National Nuclear Security Administration (NNSA). Its contents are solely the responsibility of the author and do not necessarily represent the official views of the NNSA.

NOMENCLATURE

ADC	Analog-to-Digital Converter
CMOS	Complementary Metal-Oxide Semiconductor
EC	Environmental Chamber
FHWA	Federal Highway Administration
hrs	Hours
HSP	Heat Soak Plateau
HTA	Heat Transfer Analysis
HV	High Voltage
IDE	Integrated Development Environment
I^2C	Inter-Integrated Circuit
I/O	Input/Output
LCD	Liquid Crystal Display
LED	Light Emitting Diode
MCA	Multichannel Analyzer
MCAAW	Multichannel Analyzer Alignment Wizard
mm	Milli-meter
MUX	Multiplexer
nm	Nano-meters
NNSA	National Nuclear Security Administration
NR	Normalization Ratio

ORNL	Oak Ridge National Laboratory
OMS	Opacity Monitoring System
OS	Optical Sensor
PMT	Photomultiplier Tube
PNNL	Pacific Northwest National Laboratory
PVT	Polyvinyl Toluene
RPM	Radiation Portal Monitor
RTC	Real Time Clock
SCA	Single Channel Analyzer
SCL	Serial Clock Line
SD	Secure Digital
SDA	Serial Data Line
SPI	Serial Peripheral Interface
TR	Temperature Ratio
TSA	TSA Systems, Ltd
Ω	Ohms
μm	Micro-meters

TABLE OF CONTENTS

Page

LIST OF FIGURES

LIST OF TABLES

Page

1. INTRODUCTION

Polyvinyl toluene (PVT) is a synthetic polymer of alkylbenzenes that, when doped with anthracene, produces a plastic scintillator (Birks 1964). This type of plastic scintillator has been used for over 30 years as part of radiation portal monitors (RPM) that are employed for national security, health physics, and safeguards (Cameron, et al. 2015). This material is prevalent because of cost advantages and moderate scintillation outputs compared to single crystal materials (Myllenbeck, Payne and Feng 2019). Furthermore, PVT is commonly used for gamma ray detection due to its efficiency per unit cost and availability in large proportions compared to other detection materials (Kouzes 2004).

Recently, it was noted that deployed PVT detectors show signs of internal "fogging" after being subjected to environments with cyclical climates of high heat and humidity, followed by freezing temperatures (Cameron, et al. 2015). Consequently, causes and mitigation strategies are needed to prevent loss of radiation detection capabilities within PVT-based systems (Cameron, et al. 2015). The root cause of the internal fogging comes from moisture penetrating the plastic during weather patterns with high heat and humidity. Absorbed water in the plastic acts as a lubricant between the polymer chains of the detector, thus increasing the ductility of the material when subjected to mechanical stresses and leading to water pockets in the lattice of the plastic. (Cameron, et al. 2015). Over time, as temperatures shift to below freezing the moisture within these pockets freeze, stressing the polymer chains in the lattice and resulting in small defects. Therefore, the internal "fogging" that PVT exhibits during colder temperatures is actually the frozen moisture that previously penetrated the plastic.

PVT can experience two types of fogging damage: reversible and irreversible. Reversible damage refers to the aforementioned phenomenon caused by freezing moisture within the plastic. This fogging is comprised of the freezing water situated within the plastic lattice and the moisture that has gradually pooled in voids caused by previous temperature and humidity cycles. Small to the human eye at the time of formation, 10 -100 μm in diameter (Janos, et al. 2018), the defects leading to reversible damage generally do not pose long term problems and fogging tends to dissipate once temperatures rise. After the fogging dissipates, these defects remain in the plastic lattice open to collect more water. Upon closer inspection, Janos, *et al.* noticed that when looking at these defects they were in fact spheroid regions which formed as the plastic attempted to expel the water as temperatures drop. Figure 1, shows a side-by-side comparison of two 14.92 cm x 7.62 cm x 3.81 cm PVT scintillators, where the detector on the left is opaque due to internal fogging after being exposed to high heat and humidity for seven days and subsequently placed in a commercial freezer for 24 hrs. The PVT detector on the right was left at room temperature throughout the experiment. It can be seen that the fogged detector would hinder scintillating light from traveling through the detector. Furthermore, defects are still present once the plastic defogs and will eventually lead to irreversible damage, if given enough time.

Irreversible damage refers to when defects become large enough to permanently fog the plastic. Also referred to as “spider webbing,” irreversible damage forms as moisture continues to penetrate the plastic and settles in already established defects, eventually leading to tears or cracks along void lines which fill with water after cracking or in subsequent environmental cycles (Janos, et al. 2018). Eventually, this spider webbing spreads throughout the detector rendering it completely opaque and useless for radiation detection purposes. Figures 2 and 3 are representations of the irreversible fogging that can occur in PVT. Both images are of the same 89 cm x 15.2 cm x 2.54 cm PVT detector after being exposed to extreme temperature and humidity cycles for over 750 hours in an environmental chamber (EC) at Oak Ridge National Laboratory (ORNL). Figure 2 shows a close-up of the detector, where the spider webbing can be seen within the detector, almost resembling glitter. Figure 3 shows that this effect proliferated throughout the volume of the detector, thus rendering it completely opaque.

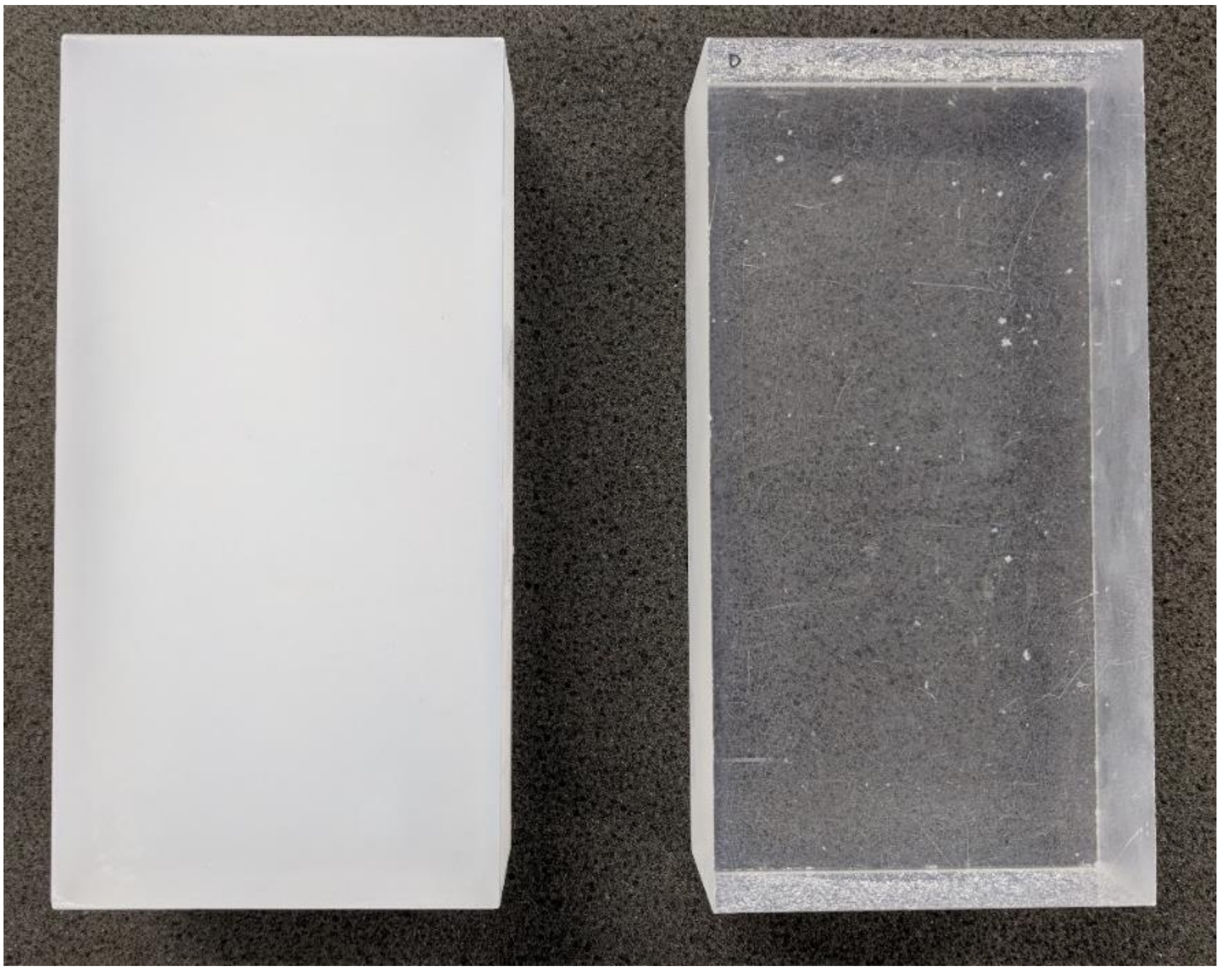

Figure 1. Two 14.92 cm x 7.62 cm x 3.81 cm PVT scintillators demonstrating the effects of reversible fogging.

Figure 2. Close up of a PVT detector exhibiting permanent spider webbing

Figure 3. PVT detector exhibiting permanent fogging after extreme temperature and humidity cycles in an environmental chamber. The clear plastic portion of the detector is composed of Polystyrene, usually adhered onto PVT detectors to aid in scintillation light transmission into the photomultiplier tube.

In uncontrolled environments the PVT can have a lifetime of approximately 10 years (Cameron, et al. 2015); however, PVT fogging does pose premature complications. In addition to the economic burdens of replacing detectors with irreversible fogging, PVT fogging can lead to the disruption of commerce flow at shipping ports and other locations where RPMs are utilized to monitor the illicit trafficking of nuclear materials. The Federal Highway Administration

(FHWA) has calculated that approximately $8 billion in costs per year can be attributed to delays caused by highway bottlenecks (Pant, Barker and Landers 2015). Although RPMs are utilized in shipping ports and other types of checkpoints and not in highways, the economic repercussions can be extrapolated to the given scenario. The decreased functionality of RPM lanes due to fogged PVT detectors can pose a threat to national security and can lead to staggering delays affecting the flow of commerce through a port. This increases the amount of time illegal nuclear materials spend at the port unmonitored as well as financial costs. The objective of this thesis aims to determine the necessary equipment and methodology to track the onset of fogging within PVT detectors and to generate a mathematical relationship between temperature and fogging. Furthermore, the results will demonstrate that fogging can be detected utilizing signals from the detector's photomultiplier tube (PMT). These goals aim to decrease on-site detector maintenance and more effectively identify the RPMs with fogged detectors that are beyond operational specifications.

2. CONCEPTUALIZATION AND HARDWARE

2.1. Opacity Monitoring System

2.1.1. Previous Work

The research outlined in this document is a continuation of the work presented by Suh in her Master's thesis (Suh 2020). The main purpose of Suh's work was to establish a method of tracking in-situ PVT degradation with equipment small enough to fit in the confined spaces of the RPM. The concluding method resulted in the development of an opacity monitoring system (OMS) to track and measure PVT light transmission properties in the field. Opacity is an indication of the amount of light passing through a material; therefore, the higher the material's opacity, the less amount of light traversing through it (Gangakhedkar 2010). Thus, the OMS was implemented to measure variations in recorded light intensity through the plastic during the onset of fogging and defogging. This was accomplished by using a set of light emitting diodes (LED) to periodically illuminate the plastic throughout the experiment and measure the amount of light transmitted through the plastic with a set of optical sensors (OS). This method used the light from the LED array to monitor the amount of light passing through the PVT plastic, which would then decrease as fogging increased within the detector.

The OMS consisted of two TSL2561 OS and a LED array composed of red, white, blue, green, and yellow lights. The OMS was adhered onto the PVT by placing the LED array on the large face of an 89 cm x 15.2 cm x 2.54 cm PVT scintillator, previously shown in Figure 3, with one OS adhered directly across from the array on the opposing face. The second OS was centered on the bottom face of the scintillator with the PMT on the opposing top face of the detector. The LEDs and OSs were controlled by an Arduino Mega 2560 microcontroller, which was also used to record the light intensity data transmitted through the plastic by the lights.

Suh’s PVT/OMS system was subjected to a temperature and humidity profile in an ORNL EC to saturate the plastic with as much moisture as possible during the warmer temperatures and freeze the aforementioned moisture during the lower temperatures. The temperature and humidity cycles within the EC ranged between -20 °C and 55 °C with relative humidity (RH) between 40% and 100%. The experiment lasted approximately 750 hours to induce fogging and track opacity changes utilizing the OMS.

2.1.2. Current Design

Although the recorded data from Suh’s experiment indicated that the OMS successfully tracked fogging and defogging through the duration of the experiment, the conclusions were based on a single set of data. In this iteration of the project, four 89 cm x 15.2 cm x 2.54 cm PVTs, each equipped with its own OMS and PMT, were tested in an EC at Pacific Northwest National Laboratory (PNNL). The number of detectors was increased from one to four to provide redundancies in the case of equipment failure during the experiment and to improve the statistical relevance of the acquired measurements.

A shortcoming of the initial OMS design was that it introduced a data stream in addition to that of the RPM’s. Therefore, the idea of utilizing the PMT, which is already deployed with the detector and RPM, to track the onset of fogging was suggested. Two sets of data were recorded throughout the experiment: light intensity data from the OS and count rate data from the RPM. The OS data would provide more statistical relevance to the results presented by Suh; whereas, the data from the RPM would be used to test the new hypothesis that a PMT can be used to detect fogging. If successful, utilizing the PMT would reduce the amount of extra equipment adhered onto the PVT detector, and the RPM’s inherent data stream could be analyzed to monitor changes in light transmission.

For this iteration of the project, each of the four PVTs was equipped with the same OMS set up as before (i.e. two OSs and an LED array) with the introduction of a TMP36 temperature sensor to measure PVT surface temperature throughout the experiment. This also ensured that temperature data was collected for both the detector and the EC. The OMS was adhered onto the PVT in the same locations as Suh's final experiment, with the temperature sensor located next to the OS directly across from the LED array. The placement of these components is shown in Figure 4.

Though the basis of the setup throughout resembles Suh's work, the approach to analyze the recorded data differed. Suh's work established that PVT fogging can be tracked using OSs and LEDs. The work presented here investigates if the PMT deployed with the detector could be used to track the fogging. The OMSs were still used, but mostly served as a "safety net" to ensure that the detectors fogged during the experiment.

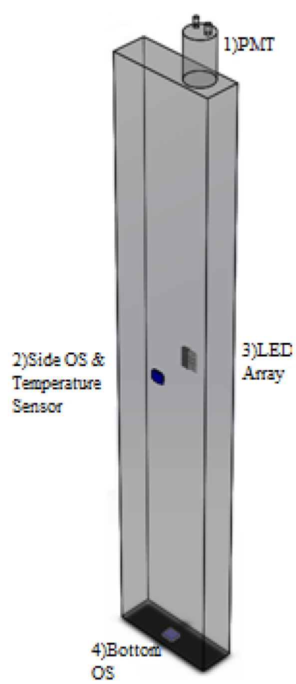

Figure 4. OMS and PMT configuration on PVT detector

2.2. Hardware and Software

2.2.1. TSL2591 Optical Sensors

The optical sensors utilized throughout the experiment were the TSL2591 High Dynamic Range Digital Light Sensor purchased from Adafruit Industries (Figure 5). This converter transforms light intensity into a digital signal output capable of direct inter-integrated circuit (I^2C) interface (AMS n.d.). This component combines one broadband photodiode in order to simultaneously detect visible and infrared light, as well as one infrared-responding photodiode on a single complementary metal-oxide-semiconductor (CMOS). Two analog-to-digital converters (ADC) convert the photodiode currents into a digital output representing the flux of radiant energy per unit area in units of lux (AMS n.d.). These sensors were ultimately chosen due to their low cost and wider response range compared to traditional photoresistors and for their wide lux range. Lux is a unit of measurement for illuminance, which in turn is the measure of luminous flux over a given area. Therefore, illuminance can be thought of as a measurement of illumination intensity on a surface. The TSL2591sensors' lux sensitivity ranges between 188 µlux to 88,000 lux. For reference, 0.0001 lux typically corresponds to a moonless, overcast night sky and approximately 108,000 corresponds to direct sunlight (The Engineering ToolBox n.d.). Given that PVT is naturally transparent, the amount of illumination intensity from the LEDs on one surface should be about the same as on the opposing side. However, as fogging begins to form the detector's opaqueness increases leading to light scattering through fog, subsequently resulting in the apparent reduction in light intensity the OSs experience.

Figure 5. TSL2591 Optical Sensor from Adafruit Industries **(Adafruit Industries n.d.)**

2.2.2. Light Emitting Diodes

In order to implement the light-intensity method utilized in the experiment, a LED array consisting of five colors was constructed to be adhered onto the PVT detector across from one of the TSL2591 OSs (Figure 6). Red, white, blue, green, and yellow LEDs were chosen to provide the widest range of the visible light spectrum as possible during the experiment. Each LED bulb was 5 mm in diameter and were all purchased from Adafruit Industries. Each LED was soldered to a 10 Ω resistor to prevent the lights from burning out during the experiment. Table 1 shows the corresponding brightness (lux) and wavelengths (nm) for each of the LED colors used. The respective datasheets for the LEDs used can be seen in Appendix A.

Figure 6. LED array utilized in the experiment.

Table 1. Brightness and wavelength of utilized LEDs in experiment.

LED	**Brightness (lux)**	**Wavelength (nm)**
Red	1500	630
Yellow	1800	590
Blue	6000	465
Green	8000	525
White	15000 (minimum)	

2.2.3. Inter-Integrated Circuit Communication Protocol

Inter-Integrated Circuit (I^2C) Communication Protocol allows multiple controller chips to communicate with multiple peripheral integrated circuits. Usually, controller components refer to those in charge of executing instruction (in this case the Arduino Mega microcontrollers); whereas, the peripheral integrated circuits generally collect data and report back to the controllers (e.g. the TSL2591 optical sensors). Designed for short distance communications, I^2C was originally developed by Phillips Semiconductors in 1982 and can support up to 1008 peripheral devices (Sparkfun n.d.). Furthermore, controller and peripheral devices communicate via two signal lines: serial data line (SDA) and serial clock (SCL). The clock signal is always generated by the controller device, while the data signal line communicates information and commands between the controller and peripheral devices.

I^2C was chosen for this project since it is user-friendly, easy to implement, and for its low equipment requirements. Given that most I^2C compatible devices are available as "plug and play" devices, implementing this communication protocol between the Arduino Mega and optical sensors was a simple process. Mainly, a simple Arduino script was written utilizing the peripheral's native script functions to establish communication with the microcontroller.

Alternatively, Serial Peripheral Interface (SPI) is another type of data communication between controller and peripheral devices that could have been used in this research. However, this method requires more signal lines between the controller and peripherals leading to more overall wires in the setup (Sparkfun n.d.). SPI establishes controller/peripheral communication with four signal lines, with an additional line for the controller for every additional peripheral. Depending on the amount of peripheral devices, this method can lead to an exponential amount of wires; whereas, I^2C only requires two signal lines between the controller and all peripherals given that I^2C differentiates between all peripherals using different addresses.

2.2.4. TCA9548A 1-to-8 I^2C Multiplexer Breakout

One caveat with using I^2C as the communication protocol for this project was that each OS required a unique address to communicate with the Arduino Mega. However, the TSL2591 was designed to have one static I^2C address. This problem was fixed with the implementation of Adafruit Industries' TCA9548A 1-to-8 I^2C multiplexer breakout board shown in Figure 7. A multiplexer (MUX) is a device that selects between several analog or digital input signals and outputs it into a single output line. The MUX utilized throughout this project had the capability of accepting up toeight different digital signals in an I^2C communication bus and, depending on the selected port, output the selected signal through its output line. This was the best solution to the OSs having a single static I^2C address because multiple sensors could be connected to one Arduino Mega through the MUX.

Figure 7. TCA9548A I^2C Multiplexer **(Adafruit Industries n.d.)**

2.2.5. Arduino Mega 2560 Microcontrollers

The Arduino Mega 2560 is a microcontroller manufactured by the Arduino Company. Illustrated in Figure 8, the Arduino Mega has 54 digital input/output (I/O) pins, 16 analog inputs pins, 4 hardware serial ports, a USB connection, a power jack, and a reset button (Arduino n.d.). This microcontroller was chosen for its “plug-and-play” accessibility where the only software to install was the Arduino Integrated Development Environment (IDE) used to write the script that would control the microcontroller and its associated peripherals. Furthermore, the Arduino Mega, henceforth known as the “Mega”, was also chosen due to its large number of digital I/O pins for the LEDs and SD data logging shield attached to the Mega. Other Arduino microcontroller designs have limited number of digital and analog pins. The Mega’s large number of pins provided the flexibility of utilizing as many peripherals as possible, especially during the preliminary OMS design process. Lastly, the Mega was chosen due to its design having two I^2C pin sets. This was important for conceptualization because it was unknown how many I^2C pin sets would be needed throughout the project. Having the extra set aided in troubleshooting throughout the entire experiment.

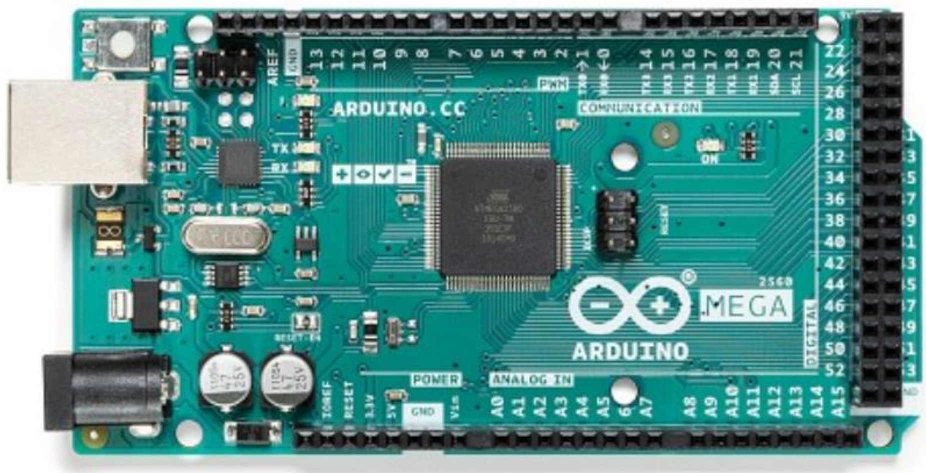

Figure 8. Image of Arduino Mega 2560 microcontroller **(Arduino n.d.)**

2.2.6. Data Logging Arduino Shield

The data logging Arduino shield, otherwise known as the "SD shield", was originally implemented as a way to timestamp and write the collected data into a text file and save it into a secure digital (SD) memory card mounted on the shield. Shown in Figure 9, the SD shield was mounted on the Mega to receive power and to communicate with the microcontroller. The peripherals were connected to the SD shield via stacking headers soldered on the shield, reducing the amount of breadboards needed. The SD shield also included a real time clock (RTC) as part of its circuitry, which produced a data time stamp.

Even though the shield provided the choice of using a SD memory card to save experimental data, this functionality was not used. It was noted that implementing the usage of the SD memory card interfered with the I^2C communication with the OSs. Nevertheless, the shield was still included in the final design of the OMS for its timestamping capabilities.

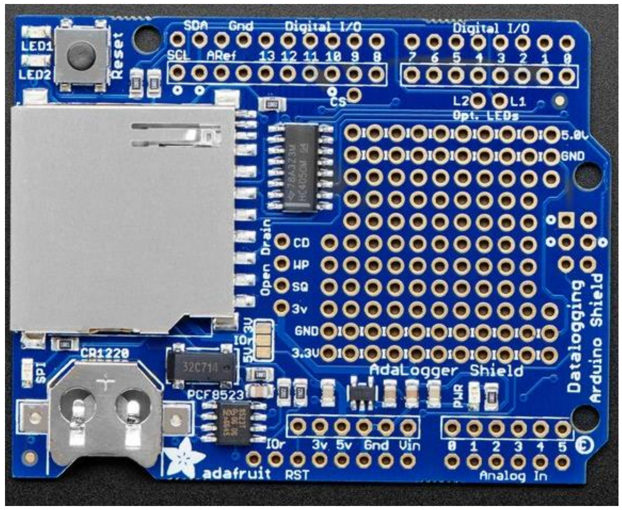

Figure 9. Adafruit Data Logging Shield **(Adafruit n.d.)**

2.2.7. CoolTerm Serial Port Terminal Application

Data collected by the sensors was concatenated into a string of data and sent to the computer via serial communication to be saved in a text file using CoolTerm. Serial communication is the process of transmitting one bit of data at a time over computer bus (Sparkfun n.d.). The Arduino IDE provides a way of displaying the data on a pop-up window but does not offer a way to save it. CoolTerm, a serial port terminal application, was ultimately utilized to save the collected data on the computer. CoolTerm is a free-to-use, serial port application, written by Roger Meier. It is designed to read incoming serial data through the computer serial bus and record it into a text file in real time (Meier n.d.). This provided a simple solution to the SD shield problem since the microcontrollers were connected to the computer throughout the experiment.

2.2.8. RPM System

The RPM system utilized for this research was a TSA Single Channel Analyzer (SCA) 775 model manufactured by Rapiscan Systems. Designed for radiation monitoring, these systems are used to scan pedestrians, vehicles, or cargo containers, and aim to detect any amount of radiation above an established background level for the given environment. These RPM systems include capabilities for gamma ray and neutron detection, where PVT scintillators are utilized to detect gamma rays and ^{3}He tubes for neutrons. Usually, RPM systems consists of two pillars, a "master" and a "slave", with two PVT scintillators in each pillar. However, two RPMs were utilized throughout this experiment. Each RPM consisted of a "desktop" version of the system but had the same functionalities as the master pillar. Shown in Figure 10, the RPM system consisted of an electronics box containing all necessary circuitry for signal processing (i.e. gains settings, upper and lower level discriminators, etc.), connections for the PMT's high voltage (HV), and signal cables. The RPM system also incorporated a controller box, equipped with a liquid crystal display (LCD) screen, where the user can access the RPM's settings.

The RPMs are programmed with two modes of operation: Background Mode and Fast Count Mode. When the system is not actively scanning an object, the RPM is in Background Mode and monitors background radiation. While in this mode the LCD is updated every 5 seconds (TSA Systems, Ltd 2006). Generally, the data displayed on the LCD consists of the average gamma and neutron count rates, but only the average gamma count rate was of importance for this project. When the system is actively scanning an object, the RPM enters Fast Count Mode and while the system does not take counts faster than Background Mode, it does update the LCD more often and tests for alarm conditions every 200 ms (TSA Systems, Ltd 2006). For the purposes of this experiment, the RPM was set to always be unoccupied so that the system updated the display with the detected background every 5 s. Bearing in mind that the entire experiment would last approximately 15 days, it was concluded that keeping the system in Background Mode would be sufficient for the objective of this project.

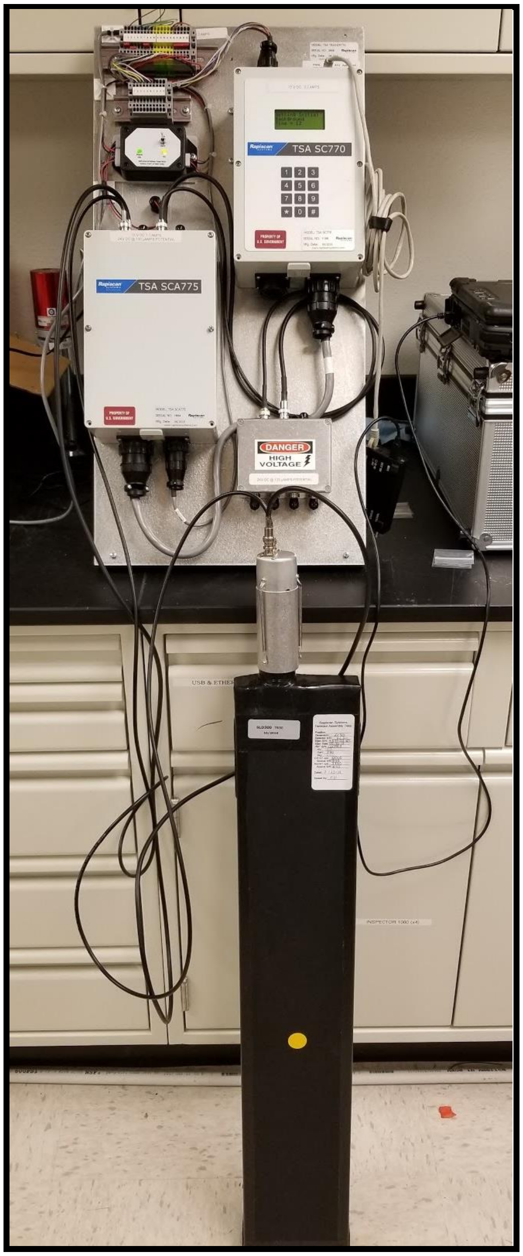

Figure 10. The RPM system used in this experiment connected to a PVT scintillator

The average gamma count rate was calculated using a rolling background algorithm programmed by the manufacturer into the RPM. The RPM recorded counts in 5 s interval windows and used the four most recent intervals to calculate the average background count rate, shown in Figure 11. The algorithm would then delete the oldest 5 s interval to accommodate for the next 5 s window before calculating the new background average. Lastly, the LCD screen was updated every 5 s and the data was sent to the computer via Ethernet cable every 5 s.

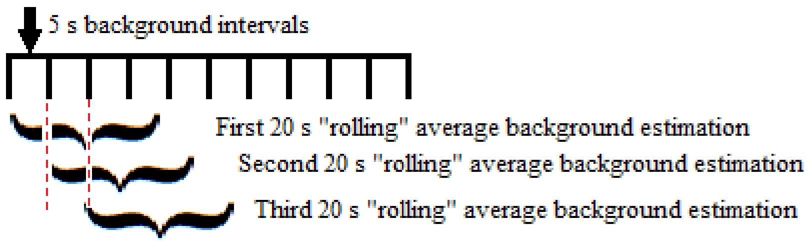

Figure 11. Visual representation of the RPM rolling average algorithm

Two desktop RPMs were used for this experiment since each system could host two gamma ray detectors at a time. The PMTs' HV and signal cables were connected to the RPMs, which in turn were connected to the computer via Ethernet cables. Using a Perl script provided by ORNL, the data from the RPMs was saved onto a text file every time a new string of data was sent.

3. FINAL DESIGN AND TESTING

3.1. Testing and Procedures

To simulate extreme environmental cycles, four 89 cm x 15.2 cm x 2.54 cm PVT detectors were tested in an EC at PNNL. Light intensity data emitted from the LEDs, passing through the detector, and observed by the OSs, in conjunction with temperature data, were collected using the Arduino Mega microcontrollers. Each PVT detector was assigned a microcontroller to manage its respective OMS components and transmit recorded data to the computer where it was saved onto a text file using CoolTerm. Figure 12 shows a schematic of an assembled OMS with Table 2 explaining the wire color legend. Each PVT detector was wrapped with a layer of aluminum foil and a layer of electrical tape to follow industry standards. The OMSs were adhered onto the detectors by cutting slits on the tape and foil layers and inserting each component in their respective locations (Figure 4). Additional electrical tape was utilized to hold these components in place and to light proof these locations.

The optical sensors were integrated with each PVT detector to ensure that the PVT fogged during the experiment and to monitor the LEDs were throughout the experiment. The OMS was programmed to activate each LED in sequence: red, white, blue, green, and yellow. Each color was turned on for 30 continuous seconds with 5 s of no lights in between. A period of 600 s without any lights followed before the entire LED sequence repeated. This sequence occurred four times after which all LEDs were continuously turned on for 60 s to introduce a "light flag" in the data stream. The purpose of the light flag was to introduce a marker in the RPM data which would aid in aligning RPM and OMS measurements post-experiment. These flags were needed due to the 6 independent clocks (2 for each RPM and 4 for each Mega) which would inevitably get out of sync at some point of the experiment. Afterwards, the LED sequence would start the first LED cycle again and the process would repeat. The optical sensors recorded light intensity once per second whenever any, or all, LEDs were turned on. Detector count rate data was recorded by the RPMs through the PMTs on each of the PVT detectors. Count rate data was transmitted every 5 seconds by the RPMs via Ethernet connection to the computer throughout the experiment.

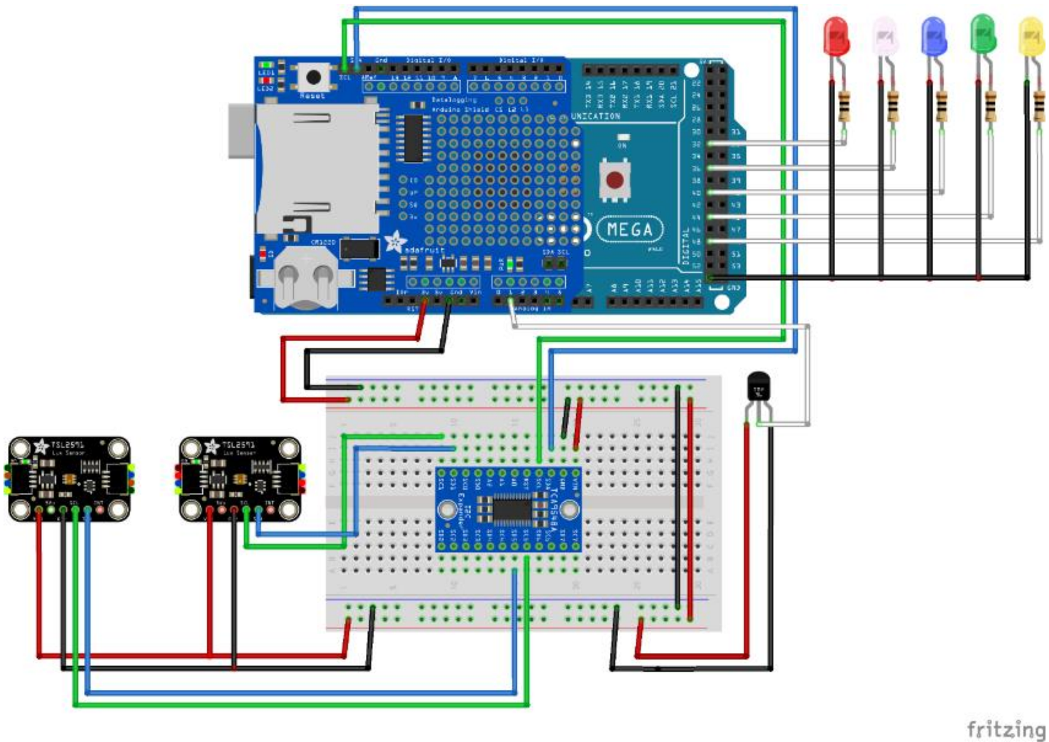

Figure 12. Final OMS design layout. Image generated using Fritzing

Table 2. OMS wire color legend

Wire Color	Functions
Red	Power
Black	Ground
Green	SCL
Blue	SDA
White	LED/Temperature sensor signal

Both RPMs were calibrated using the Multichannel Analyzer Alignment Wizard (MCAAW) software provided by the project sponsors in conjunction with the Amptek multichannel analyzer (MCA)-8000-D (Figure 13), known as the “Pocket MCA”. The Pocket MCA was connected to the computer via USB and used meter probes to read incoming signals from the RPM. Both RPMs were calibrated by following the instructions from MCAAW’s calibration function. The MCA probes were connected to the RPM’s circuit box and the system’s gain settings were adjusted to meet alignment specifications per MCAAW.

Figure 13. AMPTEK MCA8000D Pocket MCA used in this experiment. Image used with permission from manufacturer. **(AMPTEK n.d.)**.

In addition to the four PVT detectors and OMSs, a 14.92 cm x 7.62 cm x 3.81 cm wood block, also with OMS components, was placed in the EC to monitor LED light output at different temperatures throughout the experiment. Temperature fluctuations have an inverse effect on electrical current. As temperature increases, electrical current decreases; and as temperature decreases, electrical current increases. Emission intensity of LEDs decreases with increasing temperature, yet tends to increase with decreasing temperature (Schubert 2012). Therefore, it was expected that LED light output would change as temperatures varied in the experiment resulting in the implementation of the wood block as a pseudo-PVT detector. Shown in Figure 14, a rectangular hole was cut out from the center of the wood block where the LED array, one OS, and a temperature sensor were adhered to it on either side to simulate the OMS-detector configuration. This was done to ensure that measured light intensity changes registered with the PVT were in fact due to the onset of fogging rather than drastic changes in LED light outputs from temperature effects. The wood block was wrapped with a layer of black electrical tape similar to the PVT detectors. Aluminum foil, however, was not used as the inner wrapping layer of the wood block since light transmission through the medium was not a concern like it was for the PVT detectors.

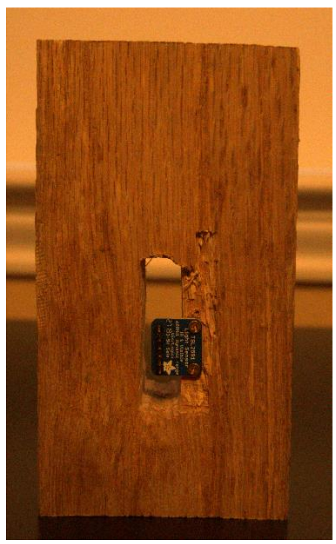

Figure 14. Image of wood block used a pseudo-PVT detector to aid in LED control experimental measurements

The environmental chamber at PNNL was programmed to cycle through a temperature and relative humidity (RH) profile consisting of approximately 1.3E+6 s (~360 hr). The initial 300,000 s (~83 hours) of the profile consisted of a “heat soak plateau” (HSP) at 50 °C and 100% RH. This was done to saturate the PVT with moisture and to establish a baseline RPM count rate and OMS light intensities at the beginning of the experiment. The EC was programmed to decrease at a rate of 7 °C hr^{-1} at 40% RH until reaching -20 °C; hold at -20 °C for four hours; and return to 50 °C at the same rate and RH. Due to issues with the EC's cooling coil and heating mechanisms, a consistent temperature profile could not be achieved. Nonetheless, temperature and RH were controlled to expose the PVT detectors to temperature and humidity cycles after the mechanical issues were addressed by the EC's operators.

Given that the microcontrollers and RPMs had different clock speeds (16 MHz and 2 MHz, respectively) and independent data streams, careful consideration was given when booting up these systems at the beginning of the experiment. Data acquisition via a Perl script was first set up for the RPMs, followed by setting up OMS data acquisition via CoolTerm for the Megas. Given that there were 6 components with independent internal clocks, it was imperative for all of these components to start recording data at the same time. This was achieved by executing the Perl script and letting it run while CoolTerm was setup for the Megas. Four CoolTerm windows were established, one for each of the four microcontrollers. Once data was being recorded from all four Megas, the reset button was pressed and held for all four microcontrollers at the same time. This stopped the Megas from executing the script and commanded the boards to start from the beginning. The four reset buttons were released at the same time and the timestamps for the first line of data were recorded for each microcontroller. Timestamps for the RPM correlating to the first OMS line of data were also recorded. This process ensured that all 6 components had the same experiment starting point.

Following experiment completion, all the data was compiled into text files for analysis. The main data of interest was the LED-induced RPM count rate and its fluctuations as a result of fogging. RPM data was analyzed in two ways: 1) sequentially to understand count rate behavior throughout the experiment, and 2) compared with respect to temperature to see changes in magnitude of the data. To quantify the latter, a normalization ratio (NR), Eq. 1, was calculated to compare the average count rate detected during the initial 300,000 s to the rest of the experiment. The results of this analysis would indicate if the PMT can be used to track changes in light transmission through PVT, and therefore changes in the onset of fogging. Furthermore, the results of this analysis could also estimate the magnitude by which count rate varies from the baseline values.

$$Normalization\ Ratio\ (NR) = \frac{Average\ Count\ Rate}{Average\ Count\ Rate\ During\ Heat\ Soak\ Plateau} \qquad \text{Eq. 1}$$

3.2. Heat Transfer Analysis (HTA)

The temperature sensors were incorporated onto the OMS design to measure PVT surface temperature since it was deemed necessary to calculate the detector's temperature through its thickness. Given that PVT fogging originates from the center of the detector, we were wondering if there was a correlation between inner detector temperature and fogging. Temperature sensors were adhered on the surface of the detector rather than inside the plastic given than drilling holes into the plastic would disturb the transparency and efficiency of the detector by generating cracks.

To effectively calculate the temperature at the center of the PVT plastic, the system was treated as a transient conduction heat transfer problem where the main objective was to determine the temperature gradient through the thickness of the detector (2.54 cm) as well as throughout the duration of the experiment. The air surrounding the PVT detectors was considered as the working fluid of the problem where its temperature was determined by the temperature profile programmed into the EC's computer. The PVT detectors were propped against one of the EC walls, but they were assumed to be upright for the purposes of this HTA allowing it to be treated as a plane wall. Furthermore, the detectors were treated as one dimensional considering that their heights and lengths were assumed to be infinitely larger than its thickness. When compared to the 2.54 cm detector thickness, the 89 cm height and the 15.2 cm length of the detectors were 35 and six times larger than the thickness, respectively.

This HTA was done with equations and concepts explained in the book *Principles of Heat and Mass Transfer* (Incropera, et al. 2003). Generally, transient conduction problems are described by the three dimensional heat equation (Eq. 2),

$$\frac{\partial}{\partial x}\left(k\frac{\partial T}{\partial x}\right)+\frac{\partial}{\partial y}\left(k\frac{\partial T}{\partial y}\right)+\frac{\partial}{\partial z}\left(k\frac{\partial T}{\partial z}\right)+\dot{q}=\rho c_p\frac{\partial T}{\partial t} \qquad \text{Eq. 2}$$

where c_p is specific heat $\left(\frac{J}{kg\ K}\right)$, k is thermal conduction coefficient $\left(\frac{W}{m\ K}\right)$, $\dot{q}$ is internal heat generation rate $\left(\frac{W}{m^3}\right)$, ρ is density $\left(\frac{kg}{m^3}\right)$, t is time (s), and T is temperature (K). However, it was previously explained that the PVT detectors would be considered one dimensional to easily enable an analytical analysis. The adequacy of this assumption will be discussed in the respective results section of this heat transfer analysis. Furthermore, with the assumptions of no internal heat generation and constant thermal conductivity, Eq. 2 simplifies to

$$\frac{\partial^2 T}{\partial x^2}=\frac{1}{\alpha}\frac{\partial T}{\partial t} \qquad \text{Eq. 3}$$

where $\alpha=\frac{k}{\rho c_p}\ \left(\frac{m^2}{s}\right)$ and is referred to as the thermal diffusivity, or the measure of a materials ability to conduct thermal energy relative to its ability to store it.

In order to solve Eq. 3 for the temperature distribution with respect to time and space, T(x,t), the following initial condition and two boundary conditions were implemented. For a typical transient conduction problem, the initial condition is

$$T(x,0) = T_i \quad \text{Eq. 4}$$

stating that a uniform temperature distribution at t = 0 is present, and the boundary conditions are

$$\frac{\partial T}{\partial x} = 0, at\ x = 0 \quad \text{Eq. 5}$$

$$-k\frac{\partial T}{\partial x} = h[T(L,t) - T_\infty], at\ x = L \quad \text{Eq. 6}$$

Equation 5 establishes the symmetrical requirement for the midplane of the wall; whereas, Eq. 6 establishes the surface condition experienced for t > 0, where h is the convective heat transfer coefficient $\left(\frac{W}{m^2K}\right)$ and T_∞ is the temperature of the surrounding air (K). Equation 6 also establishes the connection between convective heat transfer from the air surrounding the detectors to conductive heat transfer within the detectors themselves. It is also worth noting that in addition to the relationships outlined in Eqs. 3-6, the temperature profile through detector thickness also varies depends on the physical parameters of the PVT. Namely, these are

$$T = T(x, t, T_i, T_\infty, L, k, \alpha, h) \quad \text{Eq. 7}$$

This problem was solved analytically by nondimensionalizing relevant parameters in the equations outlined above. The first parameter to be nondimensionalized was temperature, where the temperature difference is defined as $\theta = T - T_\infty$ and the maximum temperature difference possible is $\theta_i = T_i - T_\infty$. Therefore the nondimensional form resulted in

$$\theta^* \equiv \frac{\theta}{\theta_i} = \frac{T - T_\infty}{T_i - T_\infty}\text{, where } 0 \leq \theta^* \leq 1 \quad \text{Eq. 8}$$

a dimensionless spatial coordinate was also defined as

$$x^* \equiv \frac{x}{L} \qquad \text{Eq. 9}$$

where L is the half-thickness of the PVT detector, and a dimensionless time can be defined as

$$t^* \equiv \frac{\alpha t}{L^2} \equiv Fo \qquad \text{Eq. 10}$$

where t^* can be regarded as the dimensionless Fourier number and is used to characterize transient conduction problems.

By substituting Eqs. 8-10 into Eqs. 3-6, the governing equation as well as the initial and boundary conditions for this transient conduction problem become

$$\frac{\partial^2 \theta^*}{\partial x^{*2}} = \frac{\partial \theta^*}{\partial Fo} \qquad \text{Eq. 11}$$

$$\theta^*(x^*, 0) = 1 \qquad \text{Eq. 12}$$

$$\frac{\partial \theta^*}{\partial x^*} = 0, at\ x^* = 0 \qquad \text{Eq. 13}$$

$$\frac{\partial \theta^*}{\partial x^*} = -Bi\ \theta^*(1, t^*), at\ x^* = 1 \qquad \text{Eq. 14}$$

where the Biot number is $Bi = \frac{hL}{k}$ and L in this case is known known as the “characteristic length” of the PVT detectors determined by the ratio of their volume to surface area. The Biot number represents the ratio of heat transfer resistances inside and at the surface of a body. In dimensionless form the functional dependence of the problem can now be expressed as

$$\theta^* = f(x^*, Fo, Bi) \qquad \text{Eq. 15}$$

Comparing Eqs. 7 and 15, it can be seen that the latter is a more manageable problem to tackle given that its dependency decreased from eight parameters to three dimensional ones.

As previously stated, the PVT detectors were assumed to be one dimensional plane walls leading to the subsequent assumption that conduction only occurs through the thickness. Furthermore, the detectors were also assumed to be at a constant initial temperature, $T(x, 0) = T_i$, and were eventually exposed to the EC air where $T_\infty \neq T_i$. Therefore, the resulting temperature changes given these parameters can be calculated by solving Eq. 11 using Eq. 12-14, resulting in the exact solution to this problem as

$$\theta^* = \sum_{n=1}^{\infty} C_n \exp(-\xi_n^2 Fo) \cos(\xi_n x^*) \qquad \text{Eq. 16}$$

where the coefficient C_n is

$$C_n = \frac{4 \sin \xi_n}{2\xi_n + \sin(2\xi_n)} \qquad \text{Eq. 17}$$

and the eigenvalues, ξ_n, are the positive roots to the transcendental equation

$$\xi_n \tan \xi_n = Bi \qquad \text{Eq. 18}$$

The values for the first four roots, ξ_n, of Eq. 18 and the corresponding C_n values were provided in Appendix B.3 by Incropera *et al*. The exact solution for θ^* is valid for any time, $0 \leq Fo \leq \infty$, and since the convection conditions stated in Eq. 9 must be $x^* = \pm 1$ then it can be assumed that the temperature distribution is symmetrical about the midplane ($x^* = 0$).

The Biot number, Bi, was calculated using measured data throughout the experiment. In order to calculate Bi, the convective heat transfer coefficient, h, needed to also be determined using the surface temperature of the PVT detectors, ambient temperature of the air inside the EC, and the corresponding, temperature-dependent physical properties of air. These properties for air include the thermal conductivity, k $\left[\frac{W}{m\,K}\right]$, the Prandtl number, Pr, and the kinematic viscosity, ν $\left[\frac{m^2}{s}\right]$. The Prandtl number offers a measure of the relative effectiveness of momentum and energy transport by diffusion in the velocity and thermal boundary layers, respectively (Incropera, et al. 2003). The air within the EC was also assumed to be an ideal gas, and the full set of values determined via interpolation of Appendix B.3 (Incropera, et al. 2003) for these properties can be found in Appendix C at the end of this document.

The following number that was calculated was the Grashof number, Gr, which measures the ratio of buoyancy forces to viscous forces of the working fluid where for this experiment is air. The Grashof number for vertical flat plates (i.e. the PVT detectors) were calculated by using

$$Gr = \frac{g\beta(T_s - T_\infty)L^3}{\nu^2} \qquad \text{Eq. 19}$$

where g is the acceleration due to gravity $\left(\frac{m}{s^2}\right)$, β is the coefficient of thermal expansion (usually $\frac{1}{T}$ for ideal gases) $\left(\frac{1}{K}\right)$, T_s is the surface temperature of the detectors (K), T_∞ is the surrounding air temperature (K), L is the vertical length, or height, of the detectors (m), and ν is the kinematic viscosity the air. This was followed by the calculation of the Nusselt number, Nu, which is the ratio of convection to pure conduction heat transfer occurring at the interface of the air and the surface of the PVT detectors. The Nusselt numbers were determined by using

$$Nu = 0.68 + \frac{0.670Ra^{\frac{1}{4}}}{\left(1 + \left(\frac{0.492}{Pr}\right)^{\frac{9}{16}}\right)^{\frac{4}{9}}}; Ra \lesssim 10^9 \qquad \text{Eq. 20}$$

where Ra shown represents the Rayleigh number, a dimensionless number measuring the flow of natural convection, and is determined by

$$Ra = Gr * Pr \qquad \text{Eq. 21}$$

Equation 20 is suitable for vertical plates and laminar flow, both of which can be applied to the PVT detectors and air flow, respectively, within the environmental chamber. Vertical plates refer to rectangular prism geometries, such as the PVTs, where the height of the object is oriented in the z-axis (i.e. parallel to the pull from gravity). Laminar flow corresponds to fluid flow that is highly ordered and it is possible to identify streamlines along which the fluid particles are moving (Incropera, et al. 2003). The air flow within the environmental chamber was assumed to be laminar, where further proof supporting this claim can be seen in Section 4.5.

Once the Nusselt number was determined it was then used to calculate h with the following equation, which was then used to calculate the Biot number

$$h = \frac{Nu * k}{L} \qquad \text{Eq. 22}$$

The Biot number was determined for various parts of the experiment, therefore resulting in the iterative calculations of the parameters described above to address changes in temperature and to have temperature gradients within the PVT detectors throughout the experiment. Bi was used to determine the first four positive roots of Eq. 18 as well as for the first four values of the series outlined in Eq. 17. Once evaluated, these values, along with distances between the PVT centerline (x = 0) and the surface $\left(x = \frac{2.54\ cm}{2} = 1.27\ cm\right)$, were used in Eq. 16 to determine θ^*. Notice that the nondimensional parameter θ^* is the ratio of the difference in the surrounding temperature and the temperature at thickness x of the detector over the maximum temperature difference between the surface temperature of the detector and the surrounding temperature. The results from calculating θ^* will be used to quantify by how much the temperature at the center of the detector varies from the surface temperature. A θ^* value close to unity would indicate that there was not a quantifiable difference between the surface and centerline temperatures.

However, a θ^* closer to 0 would indicate a much larger difference between the surface and centerline temperatures.

4. RESULTS

4.1. Lux vs Time Results

Out of the four PVT detectors used for the experiment, three yielded results along with measurements from the wood block. Both of PVT_4's OSs failed at the beginning of the experiment and were not connected throughout the duration of the experiment. PVT_3's Bottom OS failed at the beginning of the experiment and its Side OS failed approximately halfway through the experiment. It is suspected that the OSs failed due to an electrical short after the experiment began, but the source of this short is unknown. During the OMS design and assembly process, electrical shorts within the OSs were usually caused by overheating sensor components when soldering the sensors' pins or by applying excess voltage to the sensors via the Mega. During this process, it was also determined that the Arduino script would continue running if the broken sensor was disconnected from the board. This meant that the remaining OMS components would continue executing with the OMS reporting 0 lux for the broken OS in the output string. All OSs utilized for the PNNL experiment were tested before the experiment began and all were found to be functioning. However, given that the experiment had already begun and to the limited time allotted with the environmental chamber, the broken optical sensors were disconnected from their respective Megas to allow the Arduino script to continue executing. Again, this meant that light intensity for failed OSs was recorded as 0 lux, even though the LEDs were operational. Furthermore, operational LEDs meant that the RPM still detected changes in light intensities through the PVT, ultimately still recording data for the main objective of this project.

As previously explained, the first 300,000 s of the experiment consisted of the HSP, the period of time at the beginning of the experiment used to introduce moisture into the plastic at high temperatures and to set a measurement baseline for the RPM count rate and recorded light intensity. As shown by the EC temperature profile in Figure 15, temperature decreased after 300,000 s at a rate of 7 °C hr^{-1} and 40% RH until reaching -20 °C where it remained for four hours before increasing to 50 °C at the same rate and RH. Environmental chamber temperature and RH were cycled at this rate throughout the experiment. Figure 15, however, shows that temperature cycle duration was not consistent after approximately 700,000 s into the experiment. This inconsistency in cycle duration was caused by technical malfunctions with the chamber's heating and cooling mechanisms. The EC operators managed to work around these technical malfunctions, but it resulted in shorter temperature and RH cycles for the second half of the experiment.

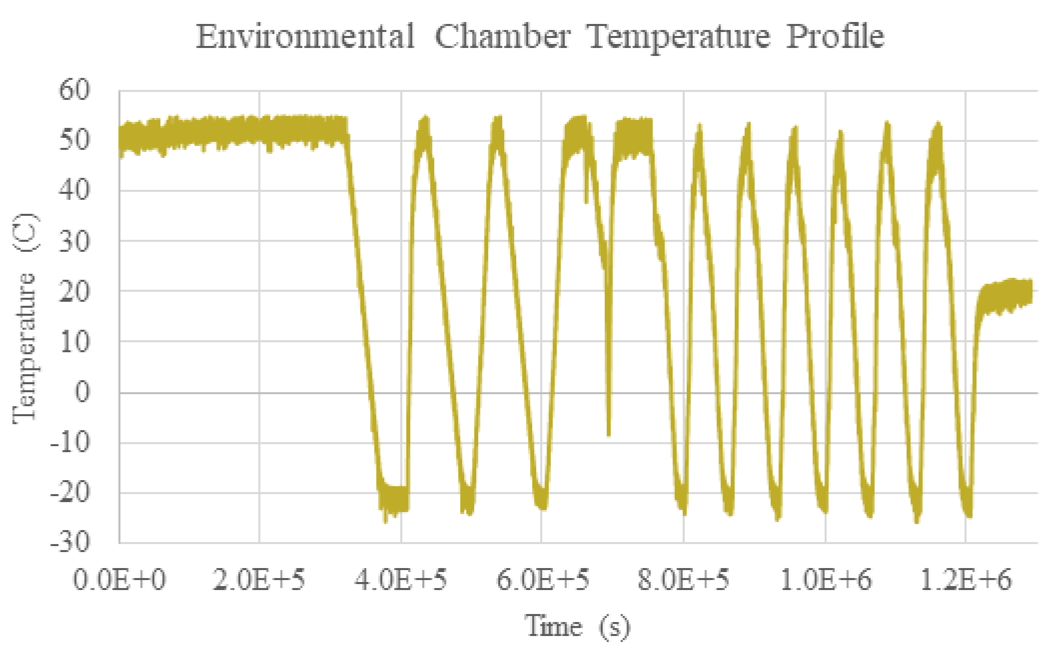

Figure 15. Environmental chamber temperature profile

Figures 16 and 17 respectively show recorded temperature and flag data for both PVT_1 OSs throughout the experiment. These figures were chosen as representative subsets of the data, where Figures for PVT_3 and PVT_4 can be found in Appendix B. The abscissa for both figures represents time in seconds, the left ordinate represents recorded light intensity in lux, and the right ordinate represents temperature in celsius. For all detectors, data from both optical sensors were separately plotted due to each sensor recording different magnitudes of light intensity. As shown in Figures 16 and 17, recorded light intensity for the Side OS ranged from 0 to 5000 lux, whereas for the Bottom OS it ranged from 0 to 250 lux. This drastic difference in lux magnitude is due to the placement of the sensors on the PVT detector. Shown in Figure 4, the Side OS was adhered on the detector directly across from the LED array and the Bottom OS was adhered onto the detector on the bottom face across from the PMT. Given that the detector is 2.54 cm thick and 89 cm tall, it makes sense that the OS directly across the LED array would register brighter light intensity than the OS placed at the bottom of the detector and at an angle from the LED array. LED flag data was utilized throughout the entire data analysis process since it was a common data source across all data sets. As it will be explained in more detail in Section 4.2, individual LED data was easily recorded by the OMS, but not by the RPMs due to its rolling average algorithm. The combination of the rolling average algorithm and the desynchronization between the RPM and Mega internal clocks resulted in the mixed response by the RPM to the LED sequence. The lux data presented in both figures may also seem discontinuous, especially in Figure BB, however these discontinuities are attributed to erratic data points collected during the experiment.

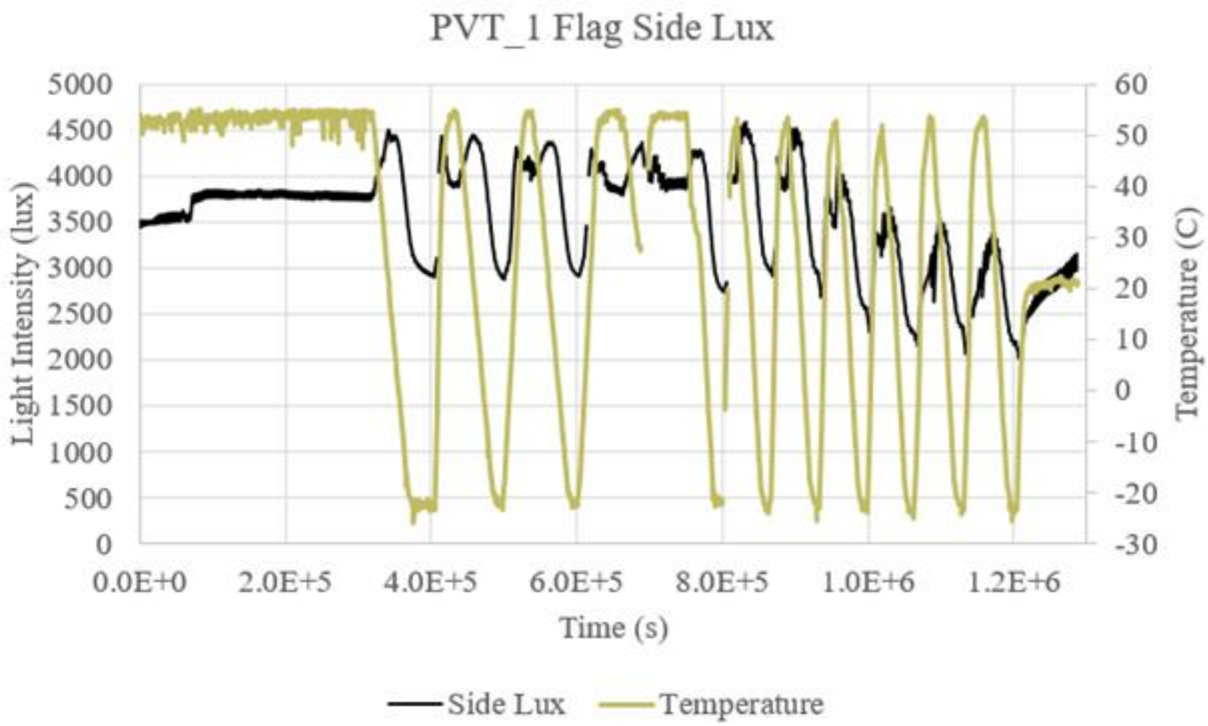

Figure 16. Side OS light intensity and experiment temperature profile for PVT_1

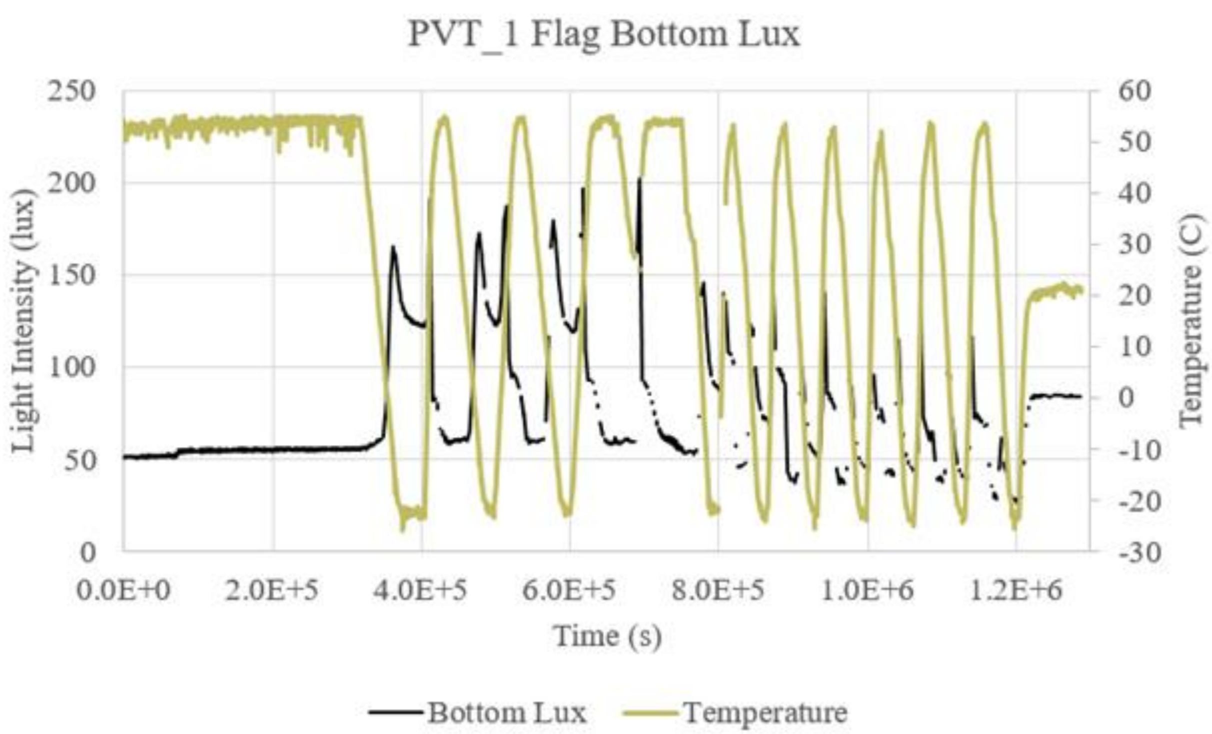

Figure 17. Bottom OS light intensity and experiment temperature profile for PVT_1

Figures 18 and 19 show an interesting behavior between recorded light intensity and temperature. These two figures are magnified versions of Figures AA and BB, respectively, in order to better show the data. Both figures show that changes in recorded light intensity do not immediately occur in response to temperature changes. With PVT being a plastic, and therefore an insulator, it takes time for temperature changes to propagate throughout the volume of the detector. Furthermore, it also takes time for the fogging to propagate from the center of the detector to the remainder of the volume. Therefore, even though changes in LED light output may respond quickly to changes in temperature, changes in recorded LED light intensity experience a lag caused by the propagation of fogging through the plastic.

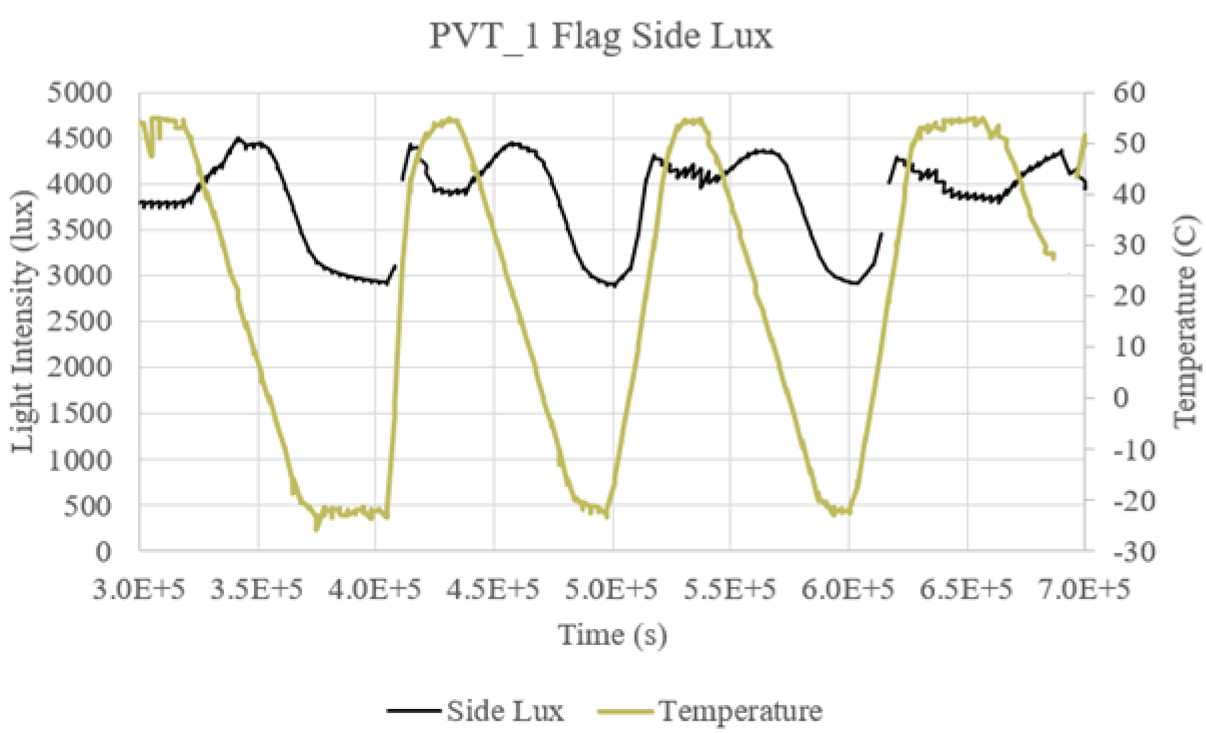

Figure 18. Zoomed in version of PVT_1 Side OS light intensity and temperature profile.

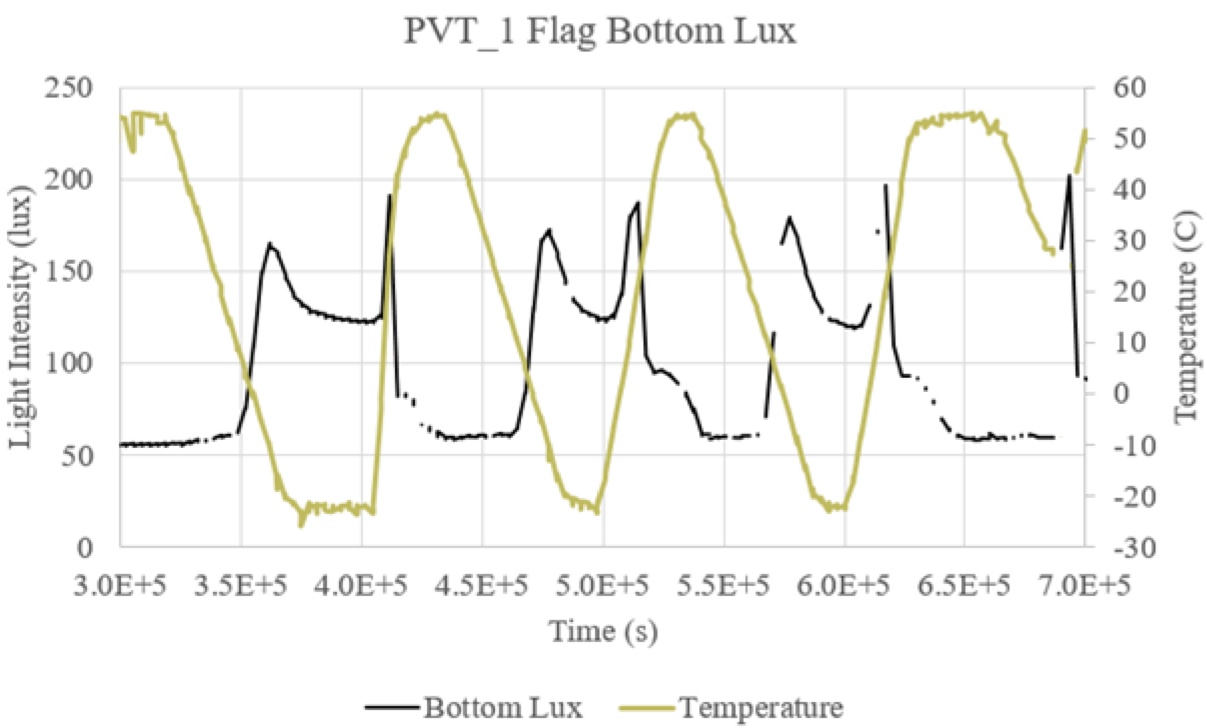

Figure 19. Zoomed in version of PVT_1 Bottom OS light intensity and temperature profile.

Light readings for both Figures 18 and 19 also tend to briefly equalize during the peaks and valleys of the temperature profile. It is also evident that there are local maxima in light intensity at the leading and trailing ends of these regions of the profile. This behavior can also be seen in the remaining figures in Appendix B. The first local maxima can be seen shortly after 300,000 s with light intensity increasing by 17% for the Side OS and 88% for the Bottom OS before decreasing in response to the decrease in temperature. It is theorized that this is a result from the way light scatters as fogging spreads within the detector. As fogging increases and the plastic becomes more opaque, LED light transitions from being preferentially scattered to being absorbed by the fog resulting in the brief increase in light intensity (Marianno, et al. 2020). This is analogous to driving through fog since the car's light scatters more in thin fog allowing the light to travel further, but is absorbed in dense fog resulting in little visibility (Marianno, et al.

2020). This phenomena also explains the light intensity maxima shortly after 400,000 s. As temperature increases and PVT fogging dissipates, light scattering starts to dominate over absorption resulting in the brief maxima before returning to baseline values. Marianno *et al* noted that the magnitude of these maxima depends on how each light color scatters differently depending on its wavelength, but it is worth noting that the recorded flag data is a summation of all LED wavelengths since all five lights were turned simultaneously. Therefore, these maxima represent light scattering from all five LED color wavelengths combined. This local maxima phenomenon can also be seen in Figure DD, however it occurs as temperature decreases to -20 °C rather than when it increases to 50 °C. This behavior was not observed for the flag data collected from the wood block since the only medium between the lights and OSs was air.

Figure 18 also shows a direct relationship between lux and temperature, whereas Figure 19 shows an inverse relationship between lux and temperature. The direct relationship for the Side OS refers to the decrease in light intensity as temperature decreases, and a return to baseline values when temperature returns to 50 °C. On the other hand, the inverse relationship for the Bottom OS refers to the increase in light intensity as temperature decreases, and the decrease in light intensity as temperature returns to 50 °C. These two relationships are also attributed to the transition from light being scattered to being absorbed as fogging sets in. PVT fogging occurs from the middle of the detector and spreads outwards. This results in the decrease in recorded light intensity by the Side OS due to its location across the LED array. However, as fogging spreads throughout the detector, LED light is scattered causing more light to be registered by the bottom OS and PMT resulting in the observed inverse relationship between light intensity and temperature shown in Figure DD. This relationship has not been previously observed in literature.

The results from this section validate the conclusions stated by Suh in her thesis and by Marianno *et al* in their findings. The OMS can successfully track opacity changes in the plastic as well as changes in light transmission through the plastic due to the onset of fogging. However, the most important conclusions from these figures are those of the direct and inverse relationships between temperature and the optical sensors.

4.2. Average Count Rate vs Experiment Time Results

Count rate data, in counts per second (cps), was collected throughout the experiment by each RPM every 5 s. Figure 20 shows the complete set of count rate data from PVT_1. The first 300,000 s of the data corresponds to the HSP, followed by peaks and valleys corresponding to the RPM's response to cold and hot portions of the temperature profile, respectively. Each RPM data set consists of the system's response to illumination caused by the individual LEDs and by the LED flags.

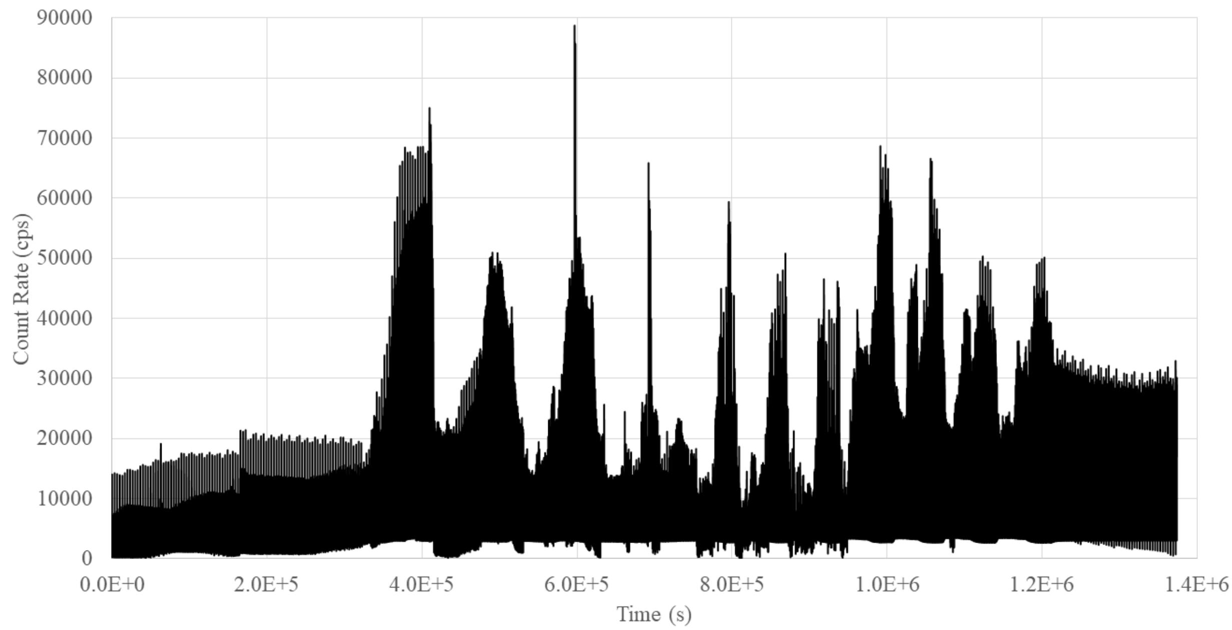

Figure 20. Complete count rate data for PVT_1.

Figures 21 and 22 show two representative light cycles from Figure 20 at -20 °C and 50 °C, respectively. Each data point on both graphs represent the average count rate over the previous 20 s. As mentioned earlier this data was recorded every 5 s by the RPM because it was in Background Mode. LED flags were identified as the increase in count rate data, followed by a brief plateau at the maximum height followed by a sharp decrease. The two count rate “peaks” following the flags represent LED cycles where each light is individually turned on for 30 s, trailed by 600 s of no lights. Notice that in both figures it is difficult to discern between LED colors during periods where the RPM registered the normal LED cycles, but it is quite simple to pick out which periods belonged to the flags. Flags were also easy to identify, compared to the light cycles, considering that they only occurred once every four LED cycles.

Figures 21 and 22 also show that RPM response to the individual LEDs is not consistent throughout the experiment. Although the count rates in response to the LEDs seem consistent in their respective figures, it is worth remembering that these two figures are from the same set of data. Due to the RPM’s rolling average algorithm and clock desynchronization between the RPMs and Megas, RPM response to individual LEDs was not consistent as the experiment progressed resulting in “muddled” LED peaks. This data muddling made it difficult to discern which data points belonged to each LED color. Therefore, averages seen below may correspond to data constituting of multiple LED colors at the same time. For these reasons, it was decided that RPM flag data would be used to analyze the systems’ responses throughout the experiment.

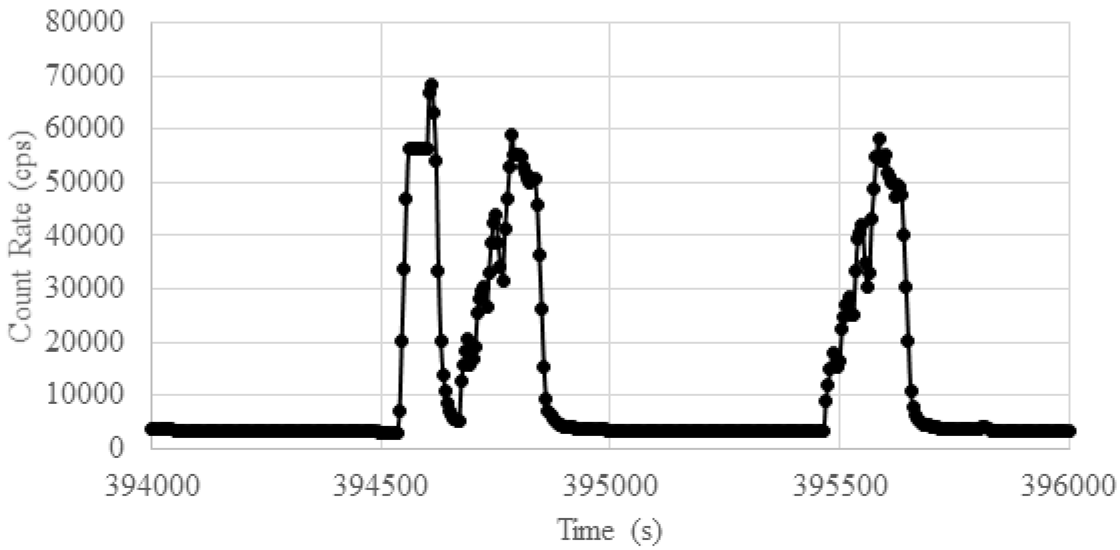

Figure 21. PVT_1 response to a flag and LED sequence at -20°C

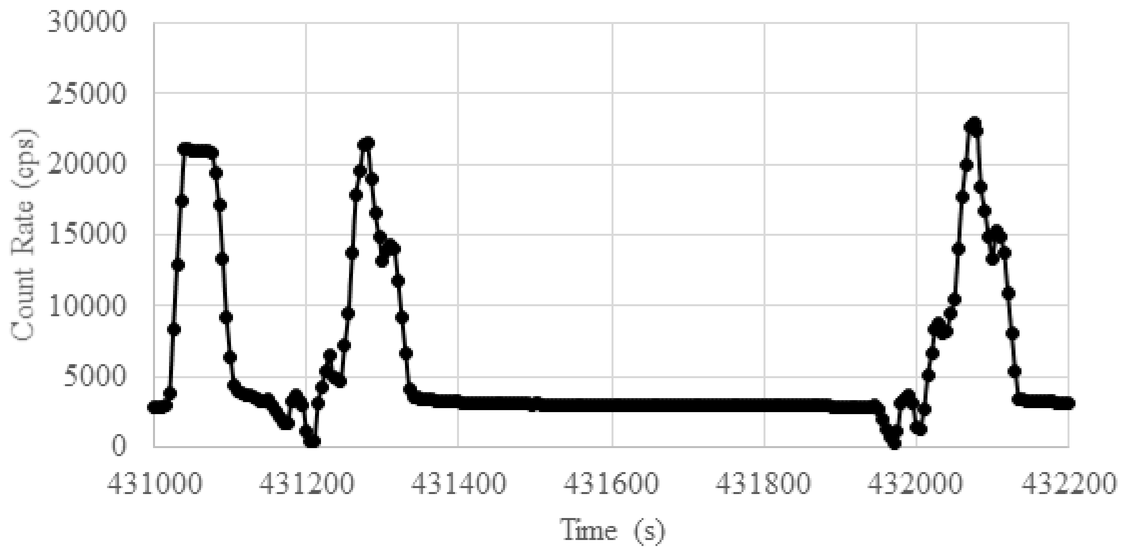

Figure 22. PVT_1 response to a flag and LED sequence at 50 °C

Figures 23-26 show the cleaned RPM data for PVTs 1, 2, and 4 where the top three count rates from each flag region was extracted, averaged, and utilized in the analysis. The abscissa for these figures represents time in seconds, the left ordinate represents count rate in cps, and the right ordinate represents temperature in celsius. As previously stated, PVT_3 and PVT_4 experienced technical malfunctions with their respective OSs resulting in disconnecting these components during the experiment. PVT_4's OSs were disconnected early into the experiment, allowing its Mega to execute the LED lighting sequence and its PMT to measure changes in count rate. PVT_3's Bottom OS was also disconnected at the beginning of the experiment, however its Side OS failed around the 700,000s. PVT_3's LEDs were still functional resulting in the slight count rate increases seen in Figure 16's first two cold periods. However, PVT_3's malfunctioning equipment was not immediately discovered resulting in an increase in count rate between 4 and 5 times higher than what had been measured prior to this point. The increase in count rate is due to the Arduino script getting stuck after the Side OS failed, resulting in an LED remaining on for approximately 300,000 s. Count rates returned to near baseline values after the Side OS was disconnected. Increases in count rate were also not detected by the RPM after this point, most likely due to complete OMS failure.

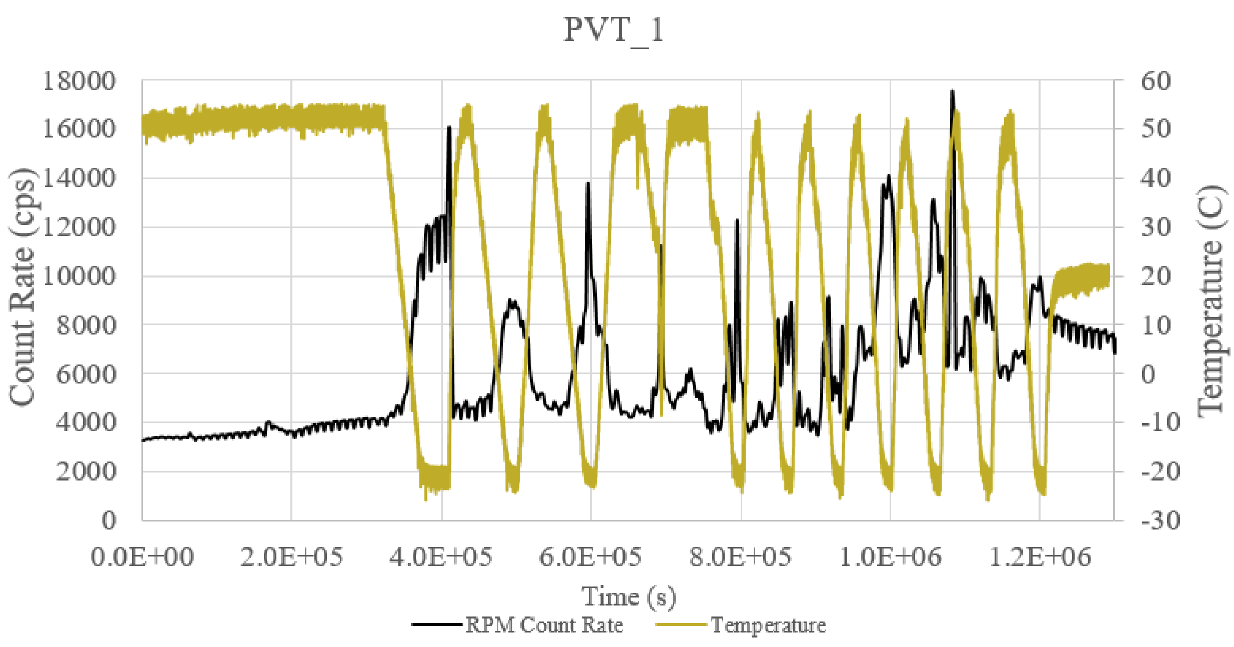

Figure 23. Temperature and count rate data for PVT_1

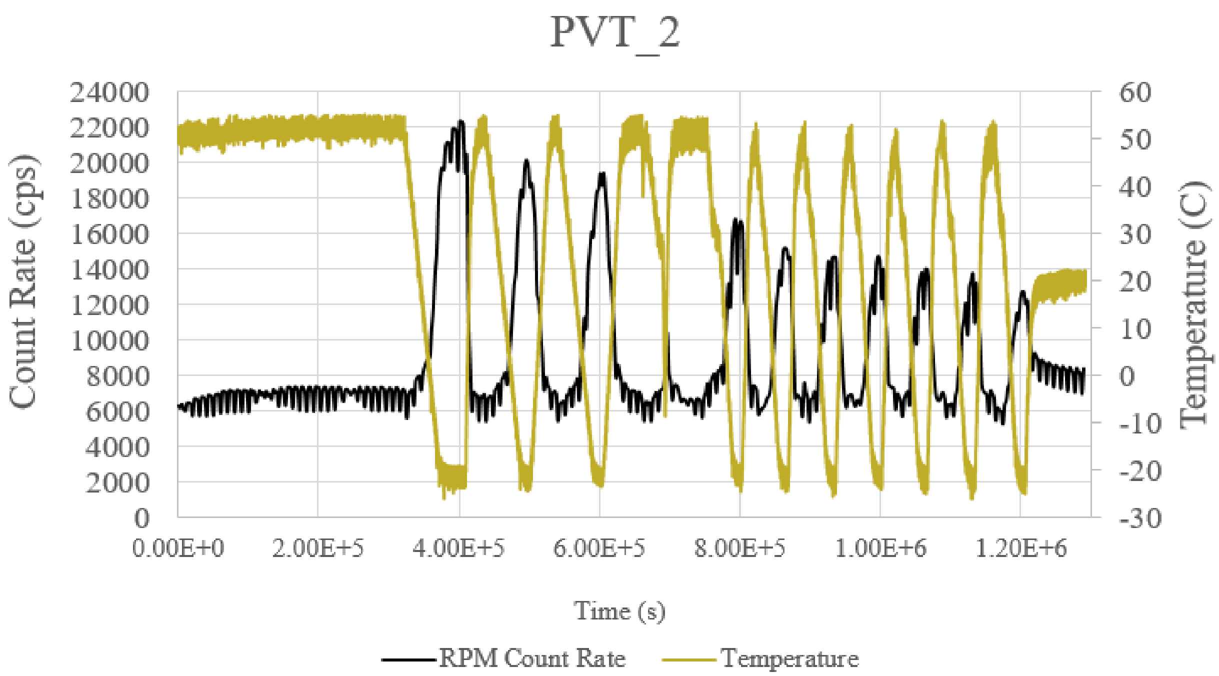

Figure 24. Temperature profile and count rate data for PVT_2

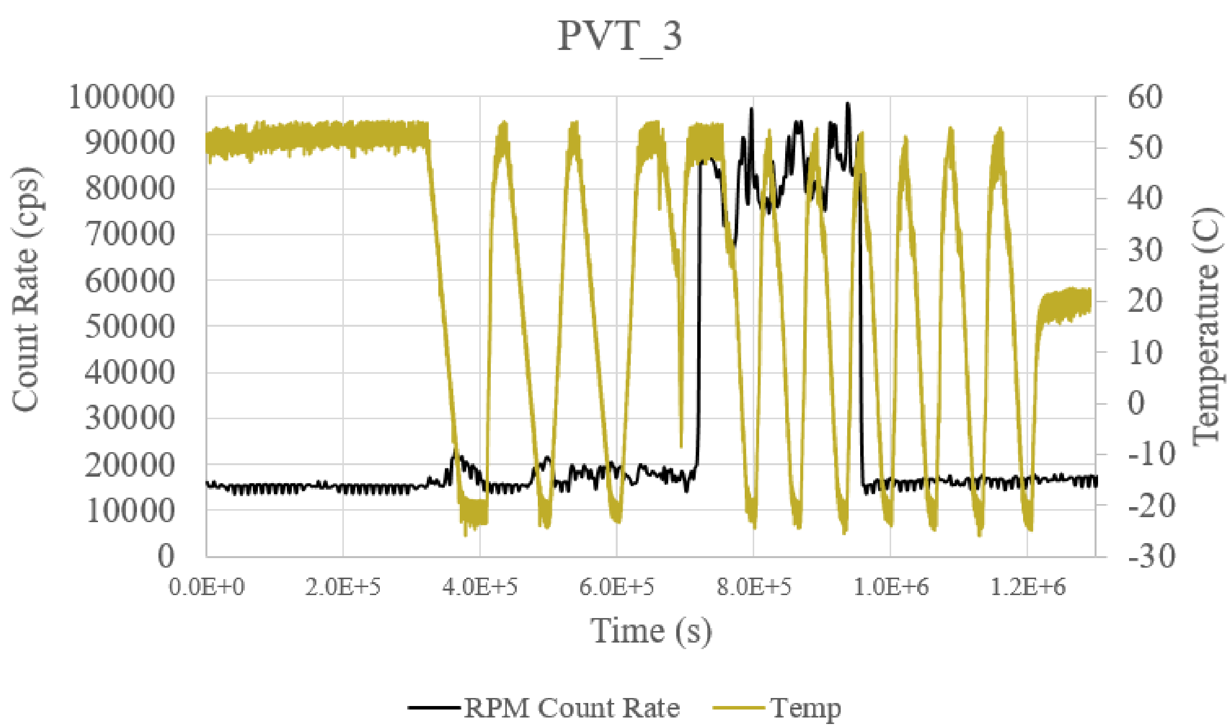

Figure 25. Temperature profile and count rate data for PVT_3

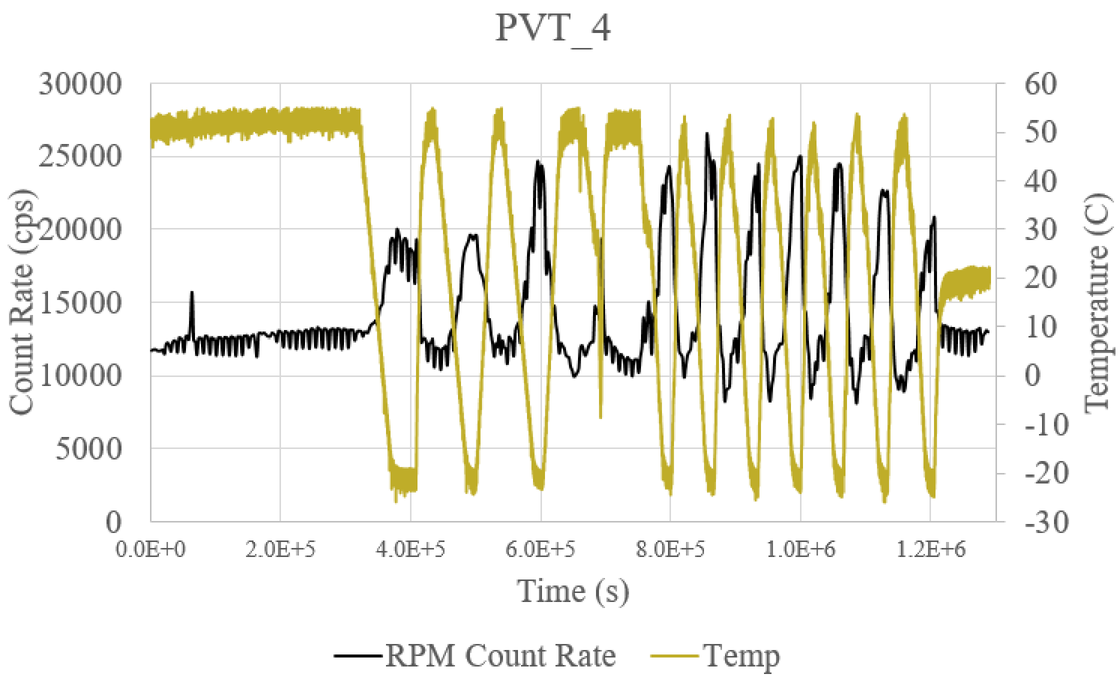

Figure 26. Temperature profile and count rate data for PVT_4

Figures 27-30 show magnified versions of Figures 23-26 to emphasize that count rates and detector opacity increased as temperature decreased. The increase in count rate is a result of scattered LED light caused by PVT fogging. As explained in Section 4.2, LED light is preferentially scattered as the fogging forms in the detector volume. Note that this increase in count rate during cold temperatures resembles the same inverse trend exhibited by the Bottom OSs rather than the direct trend shown by the Side OSs. As fogging spreads through the detector, light was scattered to the PMT and to the Bottom OS, resulting in the increase in count rates.

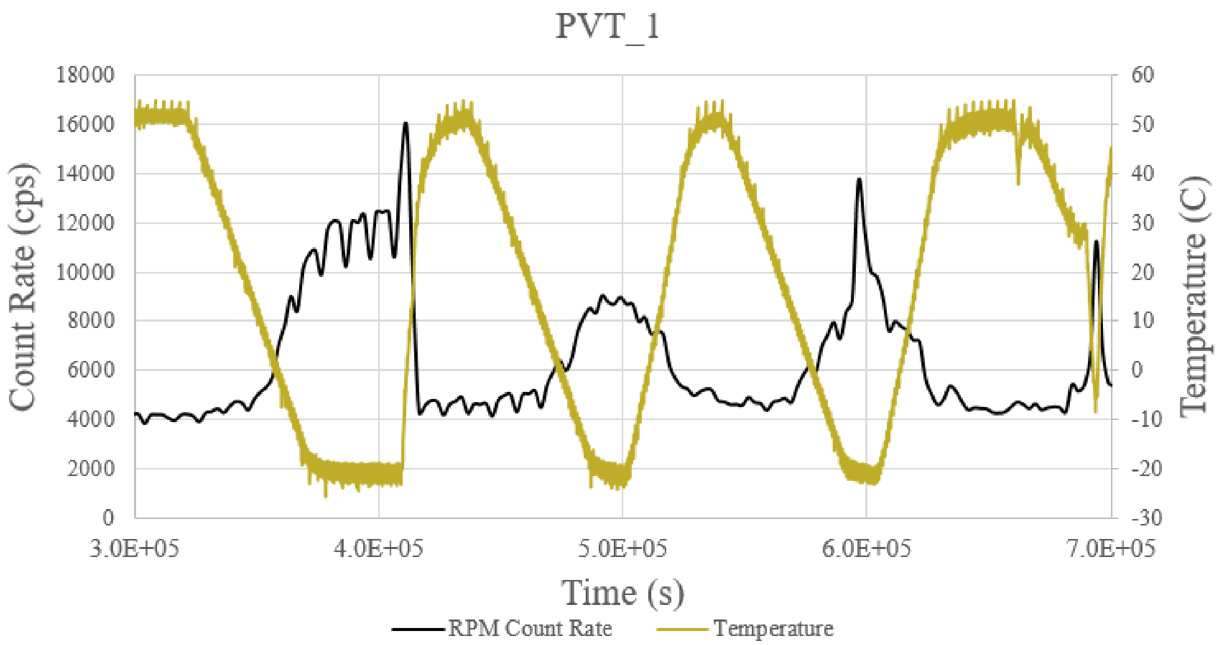

Figure 27. Zoomed in version of PVT_1 count rate and temperature data

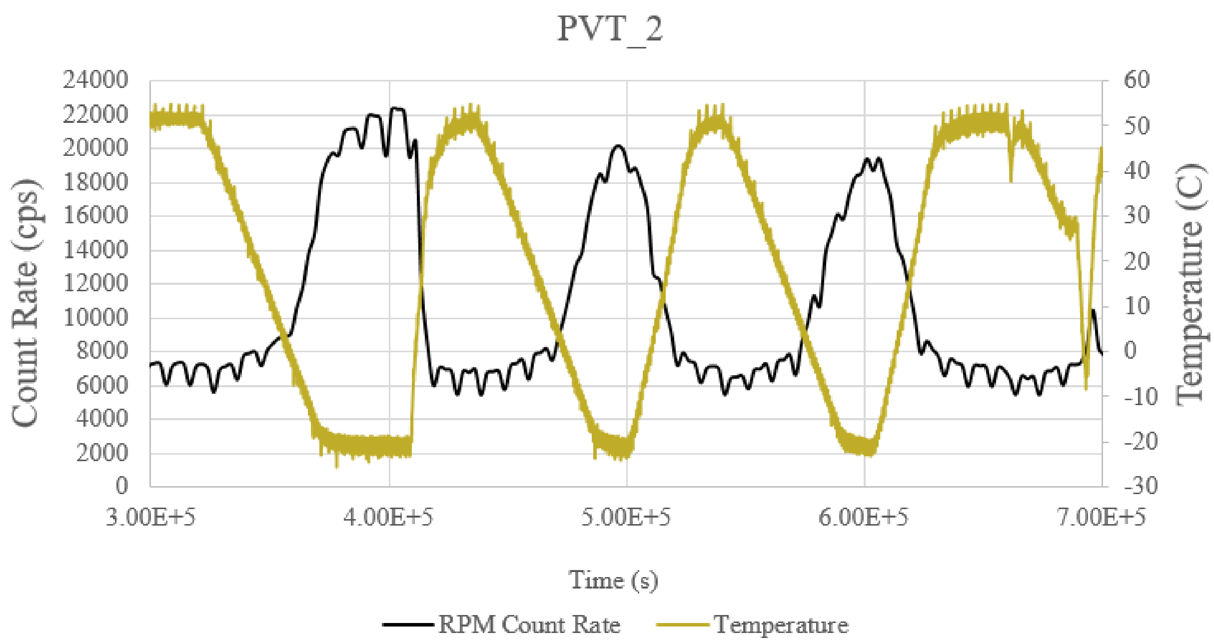

Figure 28. Zoomed in version of PVT_2 count rate and temperature data

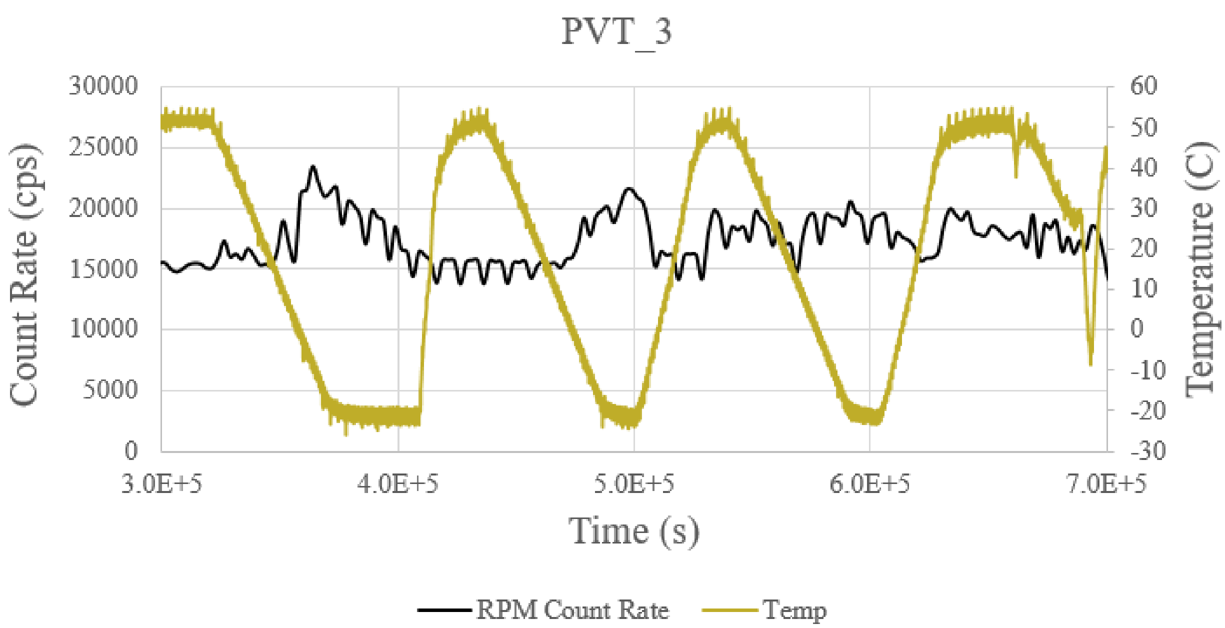

Figure 29. Zoomed in version of PVT_3 count rate and temperature data

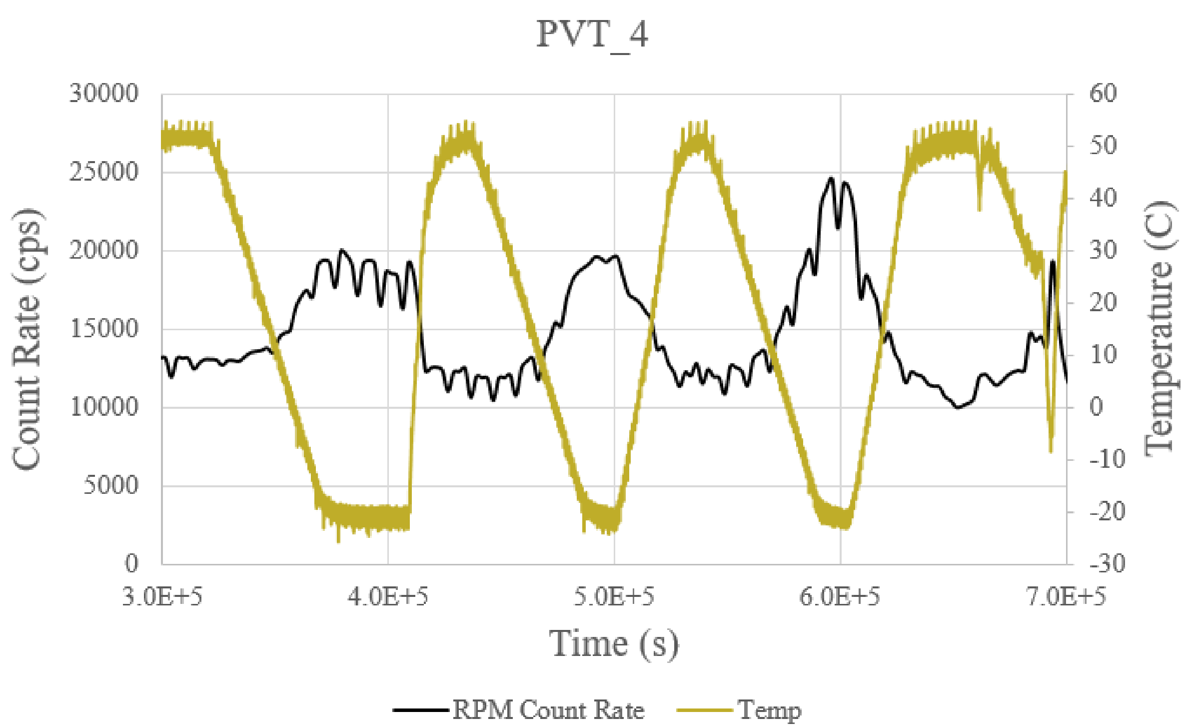

Figure 30. Zoomed in version of PVT_4 count rate and temperature data

These figures also show oscillations in the count rate data, especially during cold and warm periods. These oscillations are thought to be caused by the asynchronous behavior between the RPMs' and Megas' clocks. The RPMs and Megas had clock speeds of 2 MHz and 16 MHz, respectively. Meaning that the Arduino microcontrollers were able to execute about 8 times more instructions per second than the RPMs. Having 6 different clocks (i.e. 2 RPM clocks and 4 Arduino clocks) meant that they would behave independently of each other and eventually un-sync, even though they were all synchronized at the beginning of the experiment. This led to instances where the RPMs would measure count rates at different point of the LED light sequence.

The inverse relationship between count rate and temperature leads to the conclusion that the PMT can in fact be utilized to track changes in PVT opacity caused by fogging at cold temperatures. This conclusion also suggests that the OMS is superfluous equipment and that PVT fogging can be tracked by simply implementing a LED array with the RPM electronics. This would decrease the amount of unneeded equipment introduced by the OMS. Eliminating the OMS would also remove the additional data stream introduced by the Megas since the RPMs count rate data can be used to monitor deviations from baseline values. Lastly, even though the PMT exhibits a similar trend to the Bottom OS, it does not, however, show the local maxima at the leading and trailing ends of the temperature peaks and valleys as shown by both OSs. Therefore, we can assume that reported count rates are in fact directly in response to temperature extremes rather than allowing the system to stabilize before reaching a conclusion.

4.3. Normalized Count Rate vs Temperature Results

Figures 31-33 show the normalized count rates from PVT_1, PVT_2, and PVT_4, respectively, with respect to temperature. The normalized data presented in these figures consists of the flag data extracted from the complete RPM measurement sets. As shown in Figures 21 and 22, flags usually resulted in higher detected count rates, and were easier to discern, compared to those of the individual LED lights. Flag count rates were normalized to the baseline flag count rates using Eq. 1. Error bars showing 1σ were included in both figures, but cannot be seen in Figure 33 due to their small size. Normalized data for PVT_3 could not be calculated due to OMS malfunction as described in previous sections.

These figures show that at temperatures near 50 °C, detector count rates are found near unity, whereas count rates increase when subjected to colder temperatures. At -20 °C, count rate for PVT_1 increased between 2 to 4 times the baseline, between 2.5 and 3.5 times for PVT_2, and up to 2 times for PVT_4. These results further prove that PMTs can be used to track changes in count rates in response to changes in detector opacity caused by fogging. Further testing is required to fine tune the relationship temperature and the increase in count rate due to fogging, but these figures do indicate that detector fogging can be quantified by monitoring how much count rate values increase during, and after, the onset of fogging.

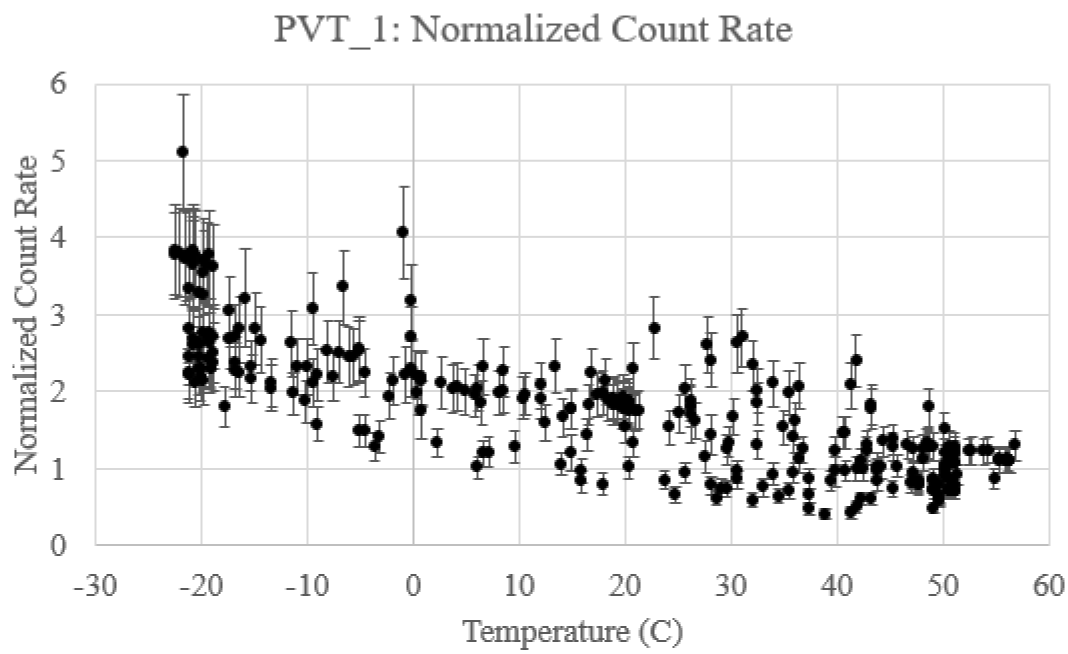

Figure 31. Normalized count rate with respect to temperature for PVT_1

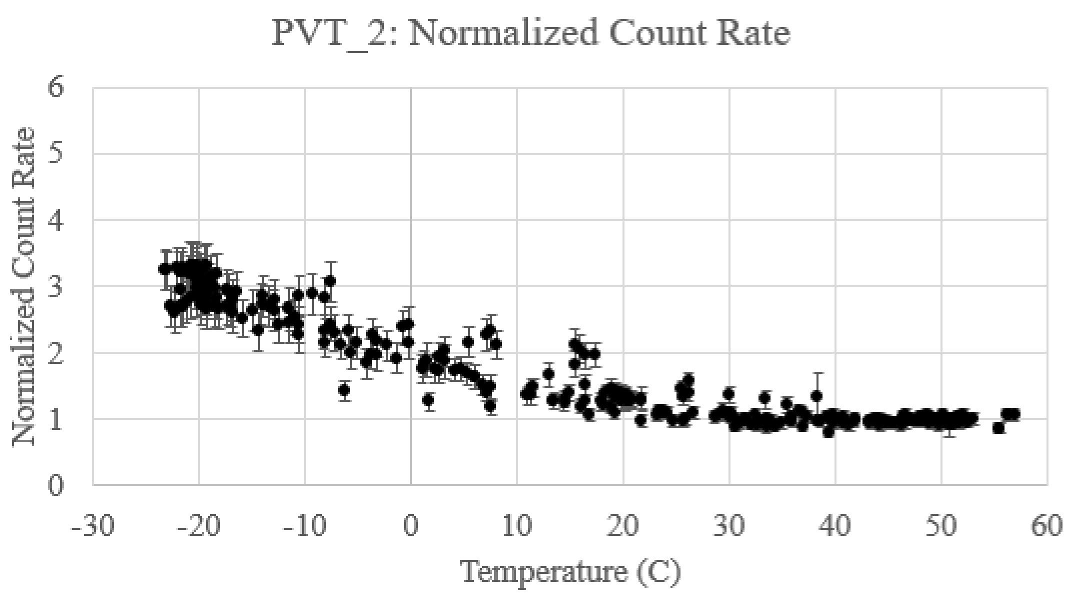

Figure 32. Normalized count rate with respect to temperature for PVT_2

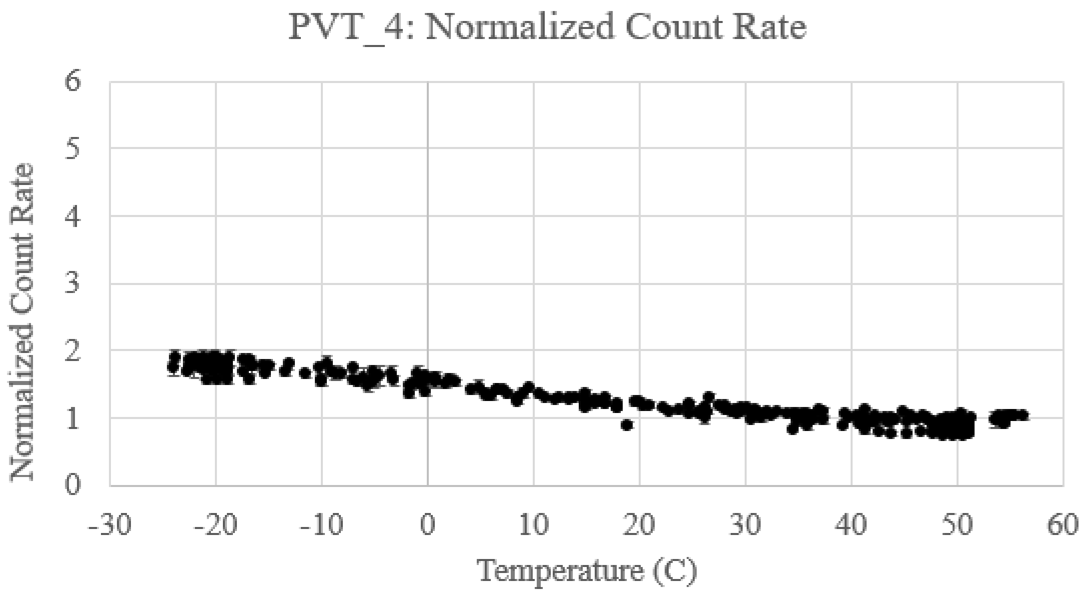

Figure 33. Normalized count rate with respect to temperature for PVT_4

4.4. Wood Block Results

Figure 34 shows flag light intensity and temperatures for the wood block OMS throughout the experiment. The wood block was placed in the EC to monitor LED light output throughout the experiment without PVT plastic between the LED array and OS. Figure 35 shows a subset of Figure 34 within 300,000 s and 700,000s. Both figures show that flag light intensity exhibited an inverse relationship with temperature similar to that of the Bottom OS and PMT. This is to be expected since electrical current also has an inverse relationship with temperature, resulting in higher LED light output during the cold periods of the experiment. Figure 36 shows that the normalized flag light output increased between 15% and 25% at -20 °C and returned to unity when the EC returned to 50 °C.

Even though LED light marginally increased during cold periods of the experiment, it did not interfere with the measured light intensity from the OSs and count rate from the PMT. Since

PVT fogging starts at the beginning of the detector before spreading out, most of the fogging would be found in the center of the detector volume. Coincidentally, since this is also where the LED array and Side OS are located on the PVT, the increase in light emission at cold temperatures would be negated by the fogging. Meaning that the fog attenuates the increase in light emission, thus preventing the OS and PMT from registering higher readings. Furthermore, LED light output only increased by 25% at -20 °C, but RPM count rates increased by at least 200% at -20 °C. Thus, validating that the increase in recorded count rates was due to light scattering during the onset of fogging and not due to an increase in LED light output during colder temperatures.

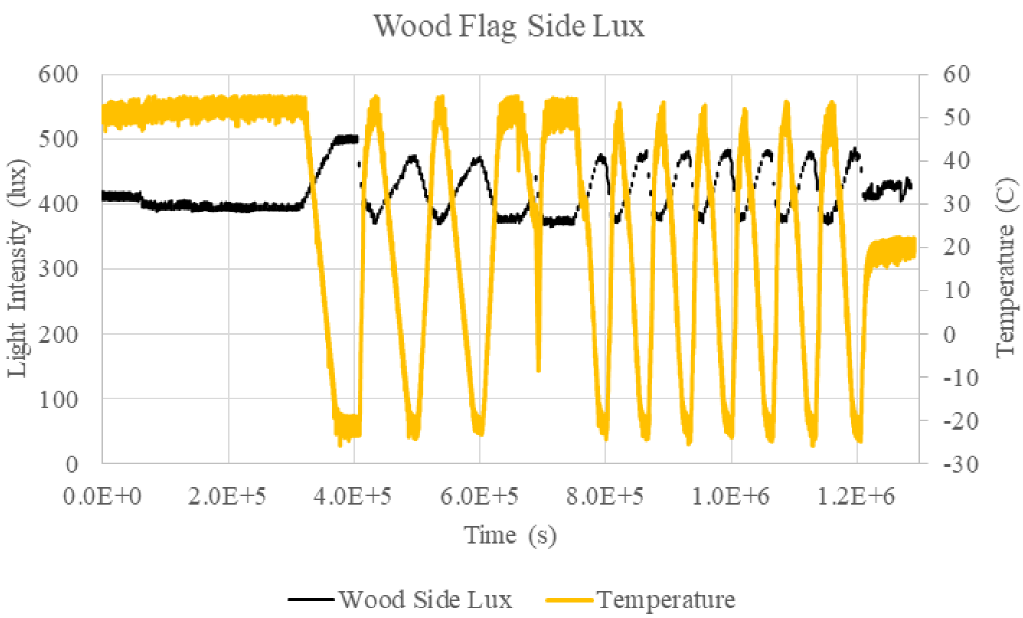

Figure 34. Light intensity and temperature data for LED flags for wood block side OS

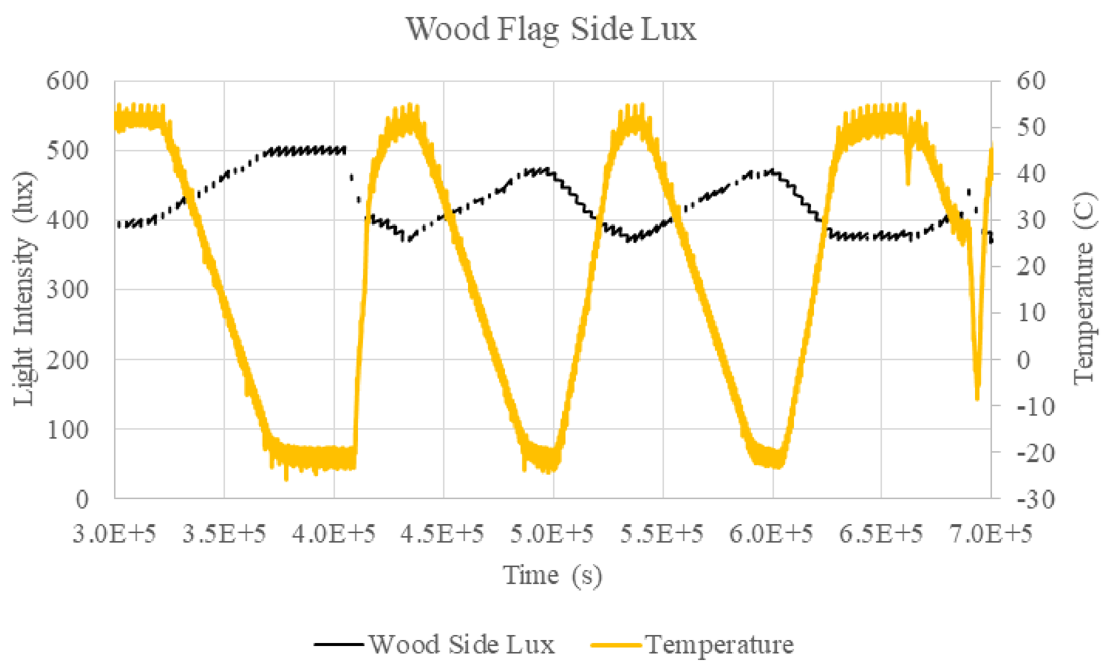

Figure 35. Zoomed in version of light intensity and temperature data for the Wood block

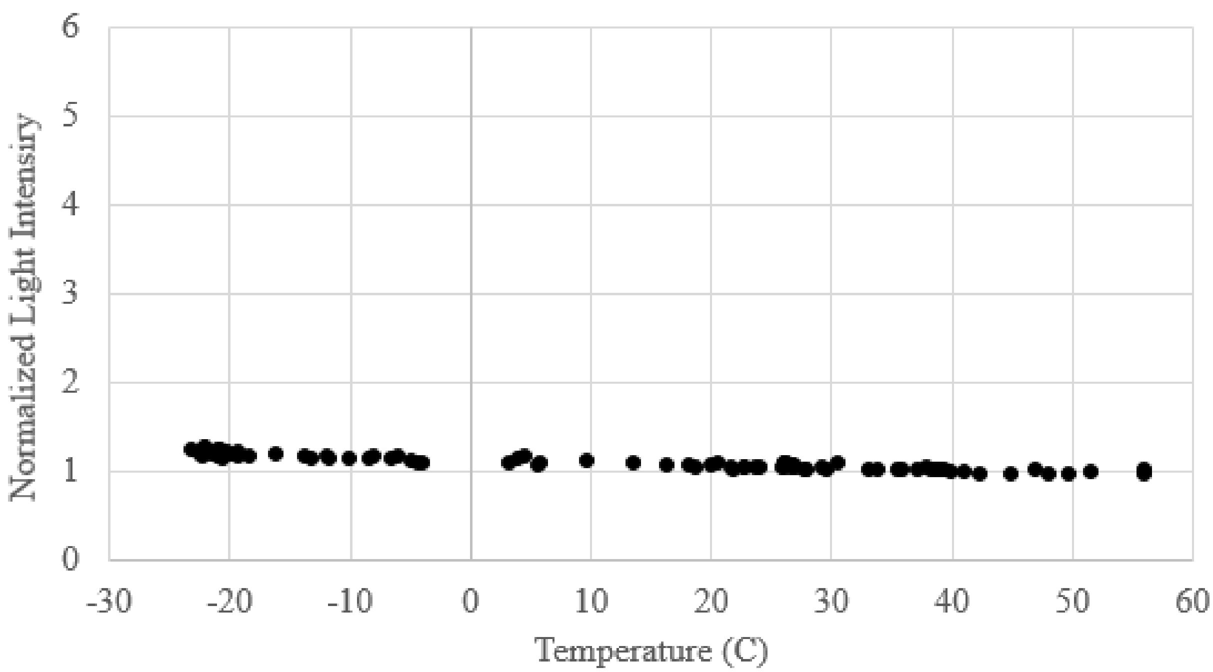

Figure 36. Normalized lux readings for flag data within the wood block.

4.5. HTA Results

A summary of the results from the HTA analysis utilizing the equations outlined in Section 3.2 are listed in Tables 3 with the complete set of results being shown in Appendix C. Table 3 shows the cases for PVT_1 and PVT_2 with the largest temperature gradients between the calculated surface and centerline temperatures. Data for PVT_4 was not included due to OMS malfunction at the start of the experiment. Starting from the leftmost column, the first column corresponds to the experiment time, followed by the measured PVT surface temperature and the surrounding ambient temperature dictated by the environmental chamber. The next column corresponds to the calculated Rayleigh numbers. The Rayleigh (Ra) number was calculated for each row of the table presented in Appendix C since its values are dependent on the initial environmental conditions of the heat transfer problem. The fifth column shows the calculated Biot numbers, followed by the resulting centerline temperature calculated using the equations presented in Section 3.2. Lastly, the θ_C^* column shows the nondimensional temperature ratio used to quantify the difference between the centerline and surface temperatures of the detectors.

The HTA analysis was performed for temperatures after the 700,000 s mark of the experiment since that was the EC temperature data that was provided by the EC operators. The convective heat transfer coefficient (h) as well as the Grashof (Gr), Rayleigh (Ra), and Nusselt (Nu) numbers were calculated using Equations 19-22, where the Surface Temperature and Surrounding Temperature columns were used to calculate Gr. Bi was calculated using h, and was subsequently used to determine the eigenvalues, ξ_n, of Eq. 18 via interpolation of the data presented in Appendix B.3 of Incropera *et al*. Once the eigenvalues were determined, C_n was determined using Eq. 17 to ultimately determine θ^* using Eq. 16.

As explained in Section 3.2, the nondimensional parameter θ^* represents the ratio of the temperature difference between a certain thickness of the PVT and the surrounding temperature over the maximum difference between the PVT surface and surrounding temperatures. Knowing this, Table 3 shows the maximum and minimum θ_C^* for both detectors to determine the largest temperature difference between the surface and the centerline of the PVT. As shown in Table 3, the biggest temperature difference was between a calculated centerline temperature of 30.40 °C and a measured surface temperature of 30.08 °C for PVT 1, whereas the biggest temperature difference for PVT_2 was between 12.63 °C at the centerline and 12.50 °C at the surface. Given that these were the largest temperature differences calculated, it can be assumed that no appreciable difference between the calculated temperatures was observed. Therefore, it can be safely assumed that for the purposes of this project, the center and surface temperatures of the PVT detectors are approximately equal and that the temperature gradient through the detector thickness is negligible.

Table 3. Calculated HTA values for PVT_1 and PVT_2

	Experiment Time (s)	**Surface Temperature (C)**	**Surrounding Temperature (C)**	**Ra**	**Bi**	**Tc (C)**	$\boldsymbol{\theta_C^*}$
PVT_1	1034829	30.08	27.00	1.973E+8	0.128	30.40	1.102
	1060439	-22.66	-20.00	3.825E+8	0.130	-22.25	0.847
PVT_2	945071	31.05	43.50	6.335E+8	0.179	32.68	0.869
	1213218	12.50	16.00	2.684E+8	0.134	12.63	0.963

The validity of the laminar fluid flow assumption, and therefore the validity of using Eq. 20 in this HTA, can be seen in the results presented in the Ra column. Equation 20 shows that the Nusselt number can be calculated using this relationship for situations with a Ra magnitude of less than, or approximately equal to, $1x10^9$. As shown in Appendix C, none of the calculated Ra values exceeded a magnitude of $1x10^8$ therefore proving that the air flow within the environmental chamber was indeed laminar.

Lastly, the one-dimensional geometry assumption for the HTA can be validated in two ways. The first proof also comes from the results shown in the Ra column for each PVT, where Eq. 20 is only valid for vertical planar walls (i.e. one-dimensional) in a laminar flow environment which was proven to correctly apply to the PVT detectors in this section. The second proof can be seen in Tables 4 and 5, where the results presented in these tables are based on the same scenarios from Table 3 but for PVT detectors whose thicknesses have been changed to 89 cm and 15.2 cm, respectively. This was done to quantify the temperature gradient for PVT thicknesses much larger than 2.54 cm. As shown in Table 4, the centerline temperature did not exceed 1.6% for PVT_1 and 2.1% for PVT_2 when compared to the maximum temperature difference between the surface and surrounding temperatures and having an 89 cm thickness. Table 5 shows that there was not a discernable difference between the calculated centerline temperature and the measured surface PVT temperature when assuming a detector thickness of 15.2 cm. Therefore, it can be concluded that the one-dimensional assumptions was correct for the HTA performed on this set of experimental data.

Table 4. HTA analysis assuming a PVT detector thickness of 89 cm.

	Experiment Time (s)	Surface Temperature (C)	Surrounding Temperature (C)	Ra	Bi	Tc (C)	θ_C^*
PVT_1	1034829	30.08	27.00	1.973E+8	0.128	30.13	1.016
	1060439	-22.66	-20.00	3.825E+8	0.130	-22.70	1.016
PVT_2	945071	31.05	43.50	6.335E+8	0.179	30.78	1.021
	1213218	12.50	16.00	2.684E+8	0.134	12.44	1.017

Table 5. HTA analysis assuming a PVT detector thickness of 15.2 cm

	Experiment Time (s)	Surface Temperature (C)	Surrounding Temperature (C)	Ra	Bi	Tc (C)	θ_C^*
PVT_1	1034829	30.08	27.00	1.973E+8	0.128	30.08	1.000
	1060439	-22.66	-20.00	3.825E+8	0.130	-22.66	1.000
PVT_2	945071	31.05	43.50	6.335E+8	0.179	31.05	1.000
	1213218	12.50	16.00	2.684E+8	0.134	12.50	1.000

5. CONCLUSIONS

Polyvinyl toluene based detectors have been used in RPMs to help detect the illicit trafficking of nuclear materials. These detectors have been observed to internally fog after being subjected to environments with large temperature and humidity fluctuations, potentially decreasing the effectiveness of the equipment. An OMS comprised of an array of five different colored LEDs (red, white, blue, green, and yellow), two optical sensors, and a temperature sensor was developed to detect fogging in-situ, but was found to introduce extra equipment to the already limited space within the RPMs. Therefore, the idea of utilizing the PMT already deployed with the RPM to track fogging was suggested.

Four PVT detectors were placed within an environmental chamber at PNNL to be exposed to temperature and humidity cycles ranging from -20 to 50 °C and 40% to 100% relative humidity, respectively. Each detector was equipped with an OMS and a PMT, where the OMSs were used to ensure that the PVTs were indeed fogging during the experiment. PMT data was monitored and exported to the computer by the RPMs via Ethernet cables; whereas, the OMS data was monitored and exported to the computer by Arduino Megas 2560 microcontrollers. Each LED was programmed to individually turn on for 30 s, followed by a 5 s period of no light, were LED light intensity data was recorded by the optical sensors once every second. A 600 s period of no lights followed the last LED before staring the light sequence again. After the fourth cycle, all five LEDs turned on for 60 s to introduce a light flag in the RPM data stream to aid in post-experiment data analysis.

The overall collected data consisted of two sets: OMS data and RPM data. The OMS data consisted of recorded light intensities emitted by the LEDs and detected by the optical sensors. Once analyzed, it was determined that the Side OS, placed across the LED array, experienced a direct relationship with temperature; whereas, the Bottom OS, placed at the bottom face of the PVT detector, experienced an inverse relationship with temperature. The direct relationship exhibited by the Side OS was expected given that PVT fogging originates at the center of the detector; thus, resulting in a decrease in recorded light intensity as fogging spread through the detector. The inverse relationship exhibited by the Bottom OS was due to light being preferentially scattered in different directions as fogging spread through the detector volume. Coincidentally, this inverse relationship was also exhibited by the count rate data collected by the PMT. RPM data demonstrated that count rates increased as temperature decreased, and returned to near baseline values when temperature increased. This phenomena can also be attributed to the spread of fogging through the detector volume since LED light was scattered towards the PMT as well. Therefore, leading to the first indication that the PMT can indeed be used to track the onset of fogging in PVT.

A second indication that the PMT can be used to detect fogging came from normalizing the RPM data. Given that the LED flags provided a discernable and periodic feature in the collected RPM data set, the top three LED flag data points for each light cycle were extracted, averaged, and normalized to the baseline measurements. Once normalized, it was determined that PVT_1 experienced an increase between 2 and 4 times the baseline values during the cold periods of the experiment. PVT_2 experienced an increase between 2.5 and 3.5 times the baseline values at similar temperatures. PVT_4 showed an increase of up to 2 times baseline values at similar temperatures. Data for PVT_3 could not be determined due to equipment malfunction during the experiment. The results from this normalization method led to the second indication that PMTs can be used to detect fogging by showing that there can be significant changes in count rates at colder temperatures than during warm temperatures.

In addition to the PVT detectors, a wood block with OMS components was introduced in the environmental chamber to measure changes in LED light output during the experiment. The wood block served as a pseudo-PVT detector, where a hole was carved through the center of the wood block, and the LED array and an optical sensor were adhered on either side. As like the data collected with the PMT, temperature also has an inverse relationship with electrical current. As temperature increases, electrical current decreases; and as temperature decreases, electrical current increases. This phenomena can be translated into LED light output by this same inverse relationship. Results from the wood block OMS showed the same inverse relationship exhibited by the PMT and Bottom OS data, where recorded light intensity increased between 15-25% at cold temperatures. However, the RPM data showed that recorded count rates increased by at least 200% during the cold periods. Therefore, showing that not only did fogging negate changes in recorded counts by the 15-25% increase in light output, but also showed that increases in recorded count rates were indeed due to the fogging.

Lastly, a heat transfer analysis of the PVT detectors was conducted to determine the temperature gradient through the thickness of the detectors. Given that fogging originates at the center of the detectors, it was important to determine the difference, if any, between the centerline and surface temperature of the detectors. After developing a transient conduction heat transfer problem, it was determined that there were no discernable differences between the centerline temperature and surface temperatures. Therefore, it was assumed that the calculated centerline temperatures were approximately equal to the measured surface temperatures.

The findings in this project indicate that the PMTs deployed with the RPM systems can indeed be used to monitor changes in PVT opacity due to fogging. By utilizing the PMTs, no extra equipment would have to be introduced into the limited space within the RPM.

Furthermore, this conclusion states that RPM operators will be able to utilize count rate data collected from deployed systems, compare to an established baseline, and better determine which systems, if any, have been overly degraded by PVT fogging.

REFERENCES

Adafruit. n.d. *Adafruit Assembled Data Logging Shield for Arduino.* Accessed September 30, 2020. https://www.adafruit.com/product/1141.

Adafruit Industries. n.d. *Adafruit TSL2591 HIgh Dynamic Range Digital Light Sensor.* Accessed September 25, 2020. https://learn.adafruit.com/adafruit-tsl2591.

—. n.d. *TCA9548A I2C Multiplexer.* Accessed September 28, 2020. https://www.adafruit.com/product/2717.

AMPTEK. n.d. *MCA-8000D Digital Multichannel Analyzer.* Accessed March 29, 2021. https://www.amptek.com/products/multichannel-analyzers/mca-8000d-digital-multichannel-analyzer.

AMS. n.d. "TSL2591 Light-to-Digital Converter." Accessed September 25, 2020. https://cdn-learn.adafruit.com/assets/assets/000/078/658/original/TSL2591_DS000338_6-00.pdf?1564168468.

Arduino. n.d. *Arduino Mega 2560 Rev3.* Accessed September 30, 2020. https://store.arduino.cc/usa/mega-2560-r3.

Birks, J.B. 1964. *The Theory and Practice of Scintillation Counting.* Vol. 27. Pergamon Press.

Cameron, R.J., B.G. Fritz, C. Hurlburt, R.T. Kouzes, A. Ramey, and R. Smola. 2015. "Fogging in Polyvinyl Toluene Scintillators." *IEEE Transactions on Nuclear Science* 62 (1): 368-371. doi:10.1109/TNS.2015.2390076.

Gangakhedkar, N.S. 2010. *Opacity.* https://www.sciencedirect.com/topics/chemistry/opacity.

Incropera, F. P., D. P. Dewitt, T. L. Bergman, and A. S. Lavine. 2003. *Principles of Heat and Mass Transfer.* 7th. Hoboken, New Jersey: Wiley.

Janos, A., S. Payne, N. Zaitseva, M. Lance, R.T. Kouzes, P.L. Feng, N. Myllenbeck, G.C. Slovik, and M. Goswami. 2018. "Root cause analysis and solutions for plastic gamma detector degradation in challenging environments - An Overview." *Nuclear Instruments and Methods in Physics Research Section A: Accelerators, Spectrometers, Detectors, and Associated Equipment* 954. Accessed 2020.

Kouzes, R.T. 2004. "Radiation Detection at Borders for Homeland Security." *Physics and Society Newsletter*, July.

Marianno, C.M., E.A. Ordonez, J.W. King, and R. Suh. 2020. "Development of an optical sensor for measuring opacity changes in polyvinyl toluene scintillators." *Radiation Physics and Chemistry* (Elsevier).

Meier, Roger. n.d. *Roger Meier's Freeware.* https://freeware.the-meiers.org/.

Myllenbeck, N.R., S. Payne, and P.L. Feng. 2019. "Environmental conditions leading to fogging in commercial poly(vinyltoluene) plastic scintillators." *Nuclear Instruments and Methods in Physics Research Section A: Accelerators, Spectrometers, Detectors, and Associated Equipment* 954. Accessed 2020.

Ordonez, E.A., and C. Marianno. 2020. "Characterizing the state of health of polyvinyl toluene scintillators using light readings from photomultiplier tube." *Institute of Nuclear Materials Management (INMM) Annual Conference.*

Pant, Raghav, Kash Barker, and Thomas L. Landers. 2015. "Dynamic impacts of commodity flow disruptions in inland waterway networks." *Computers & Industrial Engineering* (Elsevier) 89: 137-149. Accessed September 2020. doi:https://doi.org/10.1016/j.cie.2014.11.016.

Schubert, E. Fred. 2012. *Light-Emitting Diodes.* New York: Cambridge University Press.

Sparkfun. n.d. *I2C.* Accessed September 28, 2020. https://learn.sparkfun.com/tutorials/i2c/all.

—. n.d. *Serial Communication.* Accessed February 9, 2021. https://learn.sparkfun.com/tutorials/serial-communication/all.

Suh, R.Y. 2020. "PVT/PMT System Feedback Design and Feasibility Study." College Station, Texas: Department of Nuclear Engineering at Texas A&M University, May.

The Engineering ToolBox. n.d. *Illuminance - Rommended Light Level.* Accessed February 8, 2021. https://www.engineeringtoolbox.com/light-level-rooms-d_708.html.

TSA Systems, Ltd. 2006. "Vehicle and Pedestrian Monitor: VM-250AGN / PM-700AGN Operations & Service Manual." January 30.

APPENDIX A

OMS COMPONENT DATASHEETS

Blue LED

深 圳 市 昱 申 科 技 有 限 公 司
CHINA YOUNG SUN LED TECHNOLOGY CO., LTD.
TEL: (86) 755-28079401 28079402 28079403 28079404 28079405
FAX: (86) 755-28079407 E-mail: info@100LED.com Web: www.100LED.com

Model No.: YSL-R542B5C-A11

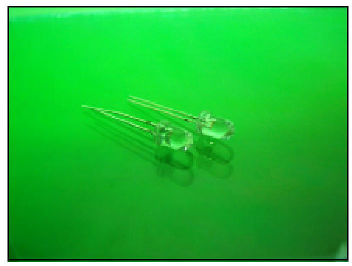

Applications:

- Decorations
- Advertising Sign
- Indicators
- Illuminations
- Traffic Lights
- Flashlights

Absolute Maximum Ratings: (Ta=25℃) .

ITEMS	Symbol	Absolute Maximum Rating	Unit
Forward Current	I_F	20	mA
Peak Forward Current	I_{FP}	30	mA
Suggestion Using Current	I_{su}	16-18	mA
Reverse Current (V_R=5V)	I_R	10	uA
Power Dissipation	P_D	105	mW
Operation Temperature	T_{OPR}	-40 ~ 85	℃
Storage Temperature	T_{STG}	-40 ~ 100	℃
Lead Soldering Temperature	T_{SOL}	Max. 260℃ for 3 Sec. Max. (3mm from the base of the expoxy bulb)	

Absolute Maximum Ratings: (Ta=25℃)

ITEMS	Symbol	Test condition	Min.	Typ.	Max.	Unit
Forward Voltage	V_F	I_F=20mA	3.2	---	3.4	V
Wavelength (nm) or TC(k)	Δλ	I_F=20mA	465	---	467.5	nm
*Luminous intensity	I_V	I_F=20mA	3000	---	5000	mcd
50% Viewing Angle	2θ1/2	I_F=20mA	---	---	10	deg

Address: 5/F, Building B, Anzhilong Indl., Qinghua East Road., Longhua Town, Shenzhen CHINA. 518109

深圳市昱申科技有限公司
CHINA YOUNG SUN LED TECHNOLOGY CO., LTD.
TEL: (86) 755-28079401 28079402 28079403 28079404 28079405
FAX: (86) 755-28079407 E-mail: info@100LED.com Web: www.100LED.com

Light Degradation in mcd: (I_F=20mA)

Hours / Colors	Light Degradation in mcd after Different Hours					
	216 Hrs	360 Hrs	792 Hrs	1104 Hrs	1992 Hrs	2328 Hrs
Red	1.52%	-1.22%	-3.10%	-4.68%	-5.72%	-8.27%
Yellow	-1.71%	-2.97%	-5.93%	-8.13%	-8.90%	-11.10%
Blue	3.13%	-0.33%	-3.84%	-8.23%	-21.32%	-24.92%
Green	-8.02%	-9.78%	-14.25%	-17.37%	-20.79%	-22.30%
Hours	48 Hrs	168 Hrs	336 Hrs	360Hrs	720 Hrs	1008 Hrs
Cool White	10.56%	6.72%	-2.29%	-7.68%	-17.32%	-22.48%
Pure White	13.66%	8.22%	-1.45%	-8.50%	-19.52%	-25.26%
Warm White	3.02%	-4.38%	-15.18%	-21.15%	-27.19%	-29.97%

Mechanical Dimensions:

- All dimension are in mm, tolerance is ±0.2mm unless otherwise noted
- An epoxy meniscus may extend about 1.5mm down the leads.
- Burr around bottom of epoxy may be 0.5mm Maximum

Unit: mm

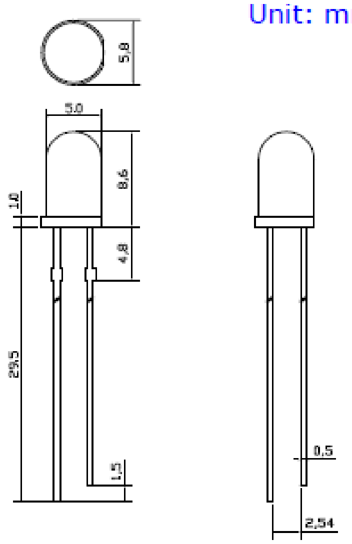

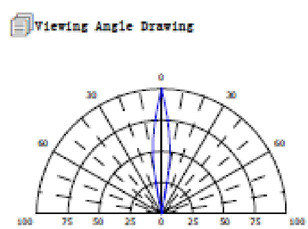

Address: 5/F, Building B, Anzhilong Indl., Qinghua East Road., Longhua Town, Shenzhen CHINA. 518109

深 圳 市 昱 申 科 技 有 限 公 司
CHINA YOUNG SUN LED TECHNOLOGY CO., LTD.
TEL: (86) 755-28079401 28079402 28079403 28079404 28079405
FAX: (86) 755-28079407 E-mail: info@100LED.com Web: www.100LED.com

Packing Information:

1. Anti-static bag

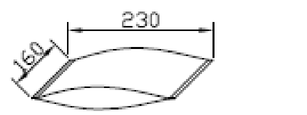

Unit: mm

- 200 - 500pcs per bag
- With 1 little bag of drier inside

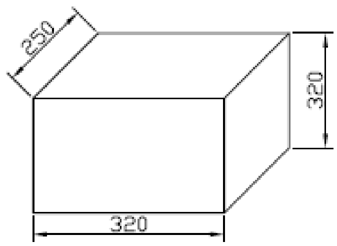

Middle Box

- 30 - 40 bags per box
- 15-20K pcs per box

Anti-static Tube Packaging Information:

Unit: mm

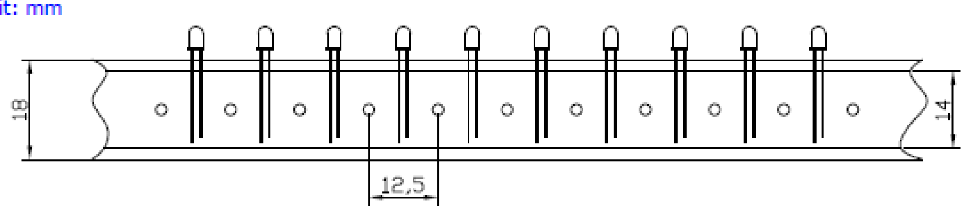

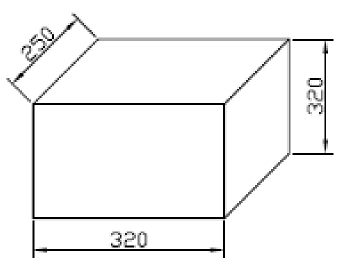

Middle Box

- Taping dimension can be adjusted to customer's requirements.
- 8-10 Layers per box
- 16K-20K pcs per box

Address: 5/F, Building B, Anzhilong Indl., Qinghua East Road., Longhua Town, Shenzhen CHINA. 518109

TEL: (86) 755-28079401 28079402 28079403 28079404 28079405
FAX: (86) 755-28079407 E-mail: info@100LED.com Web: www.100LED.com

Code System:

YSL-R542B5C-A11

1 2 3 4 5 6 7 8 9 10

1. Company Code, short for Young Sun
2. Code for LED series.
3. Code for LED Type.
   R: Round B: Bullet C: Columnar O: Ovai
   H: Helmet Q: Square V: Concave P: Pagoda
   S: Strawhat D: Special
4. Code for LED Lens Type.
5. Code for Lead Frame of LED
6. Code for Lead Frame Code of LED
7. Code for Wavelength Color
8. Code for Lens color
   C: Water Clear W: White Diffused D: Color Diffused T: Color Transparent
9. Code for Viewing Angle
   A: 1-10 B: 10-20 C: 20-30 D: 30-40 E: 40-60 F: 60-90 G: 90-120 H: >120
10. Luminous Intensity Grade:

1: 1-50mcd	4: 200-300mcd	7: 800-1000mcd	10: 2000-3000mcd	14: 10000-13000mcd
2: 50-100mcd	5: 300-500mcd	8: 1000-1500mcd	11: 3000-5000mcd	15: 13000-15000mcd
3: 100-200mcd	6: 500-800mcd	9: 1500-2000mcd	12: 5000-8000mcd	16: 15000-20000mcd
			13: 8000-10000mcd	17: 20000~mcd

Warrantee:

- In order to make the LEDs lifespan longer, please set the input current below 20mA.
- Electrical & Optical Characteristics consistency of same items all shippments.

Notes:

- Please use LEDs based on our datasheet.
- LED is senstive to statics, be sure your equipments are anti-static when you use our LEDs.
- Pay more attention to your heat dissipation system when you use it, the better heat dissipation, the longer LED lifespan.

Green LED

深 圳 市 昱 申 科 技 有 限 公 司

CHINA YOUNG SUN LED TECHNOLOGY CO., LTD.

TEL: (86) 755-28079401 28079402 28079403 28079404 28079405
FAX: (86) 755-28079407 E-mail: info@100LED.com Web: www.100LED.com

Model No.: YSL-R542G5C-A14

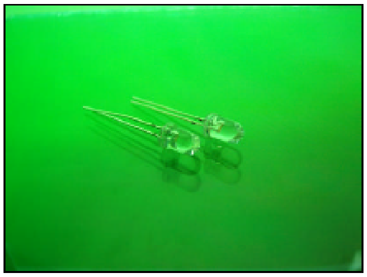

Applications:

- Decorations
- Advertising Sign
- Indicators
- Illuminations
- Traffic Lights
- Flashlights

Absolute Maximum Ratings: (Ta=25 ℃) .

ITEMS	Symbol	Absolute Maximum Rating	Unit
Forward Current	I_F	20	mA
Peak Forward Current	I_{FP}	30	mA
Suggestion Using Current	I_{su}	16-18	mA
Reverse Current (VR=5V)	I_R	10	uA
Power Dissipation	P_D	105	mW
Operation Temperature	T_{OPR}	-40 ~ 85	℃
Storage Temperature	T_{STG}	-40 ~ 100	℃
Lead Soldering Temperature	T_{SOL}	Max. 260℃ for 3 Sec. Max. (3mm from the base of the expoxy bulb)	

Absolute Maximum Ratings: (Ta=25 ℃)

ITEMS	Symbol	Test condition	Min.	Typ.	Max.	Unit
Forward Voltage	V_F	IF=20mA	3.2	---	3.4	V
Wavelength (nm) or TC(k)	Δ λ	IF=20mA	520	---	525	nm
*Luminous intensity	Iv	IF=20mA	10000	---	13000	mcd
50% Viewing Angle	2 θ 1/2	IF=20mA	---	---	10	deg

Address: 5/F, Building B, Anzhilong Indl., Qinghua East Road., Longhua Town, Shenzhen CHINA. 518109

www.100LED.com ONE HUNDRED LED PERFECT LED

深 圳 市 昱 申 科 技 有 限 公 司
CHINA YOUNG SUN LED TECHNOLOGY CO., LTD.
TEL: (86) 755-28079401 28079402 28079403 28079404 28079405
FAX: (86) 755-28079407 E-mail: info@100LED.com Web: www.100LED.com

Light Degradation in mcd: (I_F=20mA)

Colors \ Hours	Light Degradation in mcd after Different Hours					
	216 Hrs	360 Hrs	792 Hrs	1104 Hrs	1992 Hrs	2328 Hrs
Red	1.52%	-1.22%	-3.10%	-4.68%	-5.72%	-8.27%
Yellow	-1.71%	-2.97%	-5.93%	-8.13%	-8.90%	-11.10%
Blue	3.13%	-0.33%	-3.84%	-8.23%	-21.32%	-24.92%
Green	-8.02%	-9.78%	-14.25%	-17.37%	-20.79%	-22.30%
Hours	48 Hrs	168 Hrs	336 Hrs	360Hrs	720 Hrs	1008 Hrs
Cool White	10.56%	6.72%	-2.29%	-7.68%	-17.32%	-22.48%
Pure White	13.66%	8.22%	-1.45%	-8.50%	-19.52%	-25.26%
Warm White	3.02%	-4.38%	-15.18%	-21.15%	-27.19%	-29.97%

Mechanical Dimensions:

- All dimension are in mm, tolerance is ±0.2mm unless otherwise noted
- An epoxy meniscus may extend about 1.5mm down the leads.
- Burr around bottom of epoxy may be 0.5mm Maximum

Unit: mm

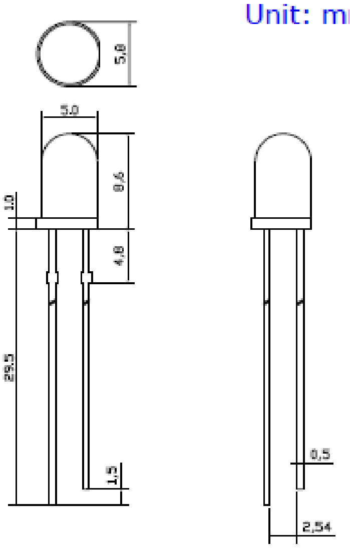

Viewing Angle Drawing

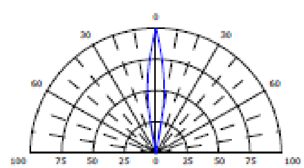

Address: 5/F, Building B, Anzhilong Indl., Qinghua East Road., Longhua Town, Shenzhen CHINA. 518109

TEL: (86) 755-28079401 28079402 28079403 28079404 28079405
FAX: (86) 755-28079407 E-mail: info@100LED.com Web: www.100LED.com

Packing Information:

1. Anti-static bag

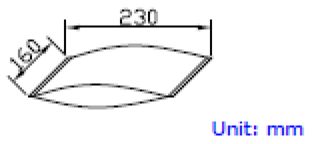

- 200 - 500pcs per bag
- With 1 little bag of drier inside

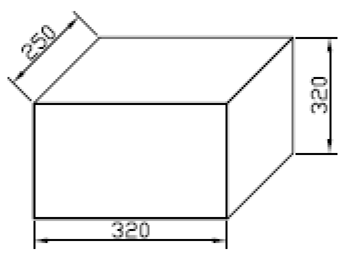

Middle Box

- 30 - 40 bags per box
- 15-20K pcs per box

Anti-static Tube Packaging Information:

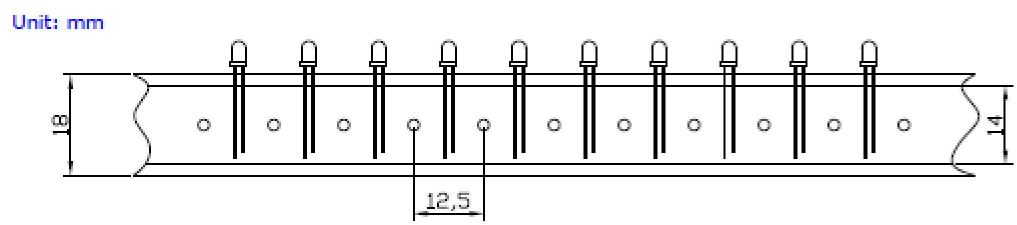

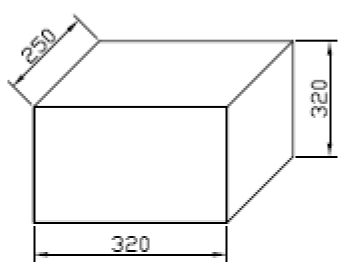

Middle Box

- Taping dimension can be adjusted to customer's requirements.
- 8-10 Layers per box
- 16K-20K pcs per box

深圳市昱申科技有限公司
CHINA YOUNG SUN LED TECHNOLOGY CO., LTD.
TEL: (86) 755-28079401 28079402 28079403 28079404 28079405
FAX: (86) 755-28079407 E-mail: info@100LED.com Web: www.100LED.com

Code System:

YSL-R542G5C-A14
1 2 3 4 5 6 7 8 9 10

1. Company Code, short for Young Sun
2. Code for LED series.
3. Code for LED Type.
   R: Round B: Bullet C: Columnar O: Ovai
   H: Helmet Q: Square V: Concave P: Pagoda
   S: Strawhat D: Special
4. Code for LED Lens Type.
5. Code for Lead Frame of LED
6. Code for Lead Frame Code of LED
7. Code for Wavelength Color
8. Code for Lens color
   C: Water Clear W: White Diffused D: Color Diffused T: Color Transparent
9. Code for Viewing Angle
   A: 1-10 B: 10-20 C: 20-30 D: 30-40 E: 40-60 F: 60-90 G: 90-120 H: >120
10. Luminous Intensity Grade:

1: 1-50mcd	4: 200-300mcd	7: 800-1000mcd	10: 2000-3000mcd	14: 10000-13000mcd
2: 50-100mcd	5: 300-500mcd	8: 1000-1500mcd	11: 3000-5000mcd	15: 13000-15000mcd
3: 100-200mcd	6: 500-800mcd	9: 1500-2000mcd	12: 5000-8000mcd	16: 15000-20000mcd
			13: 8000-10000mcd	17: 20000~mcd

Warrantee:

- In order to make the LEDs lifespan longer, please set the input current below 20mA.
- Electrical & Optical Characteristics consistency of same items all shippments.

Notes:

- Please use LEDs based on our datasheet.
- LED is senstive to statics, be sure your equipments are anti-static when you use our LEDs.
- Pay more attention to your heat dissipation system when you use it, the better heat dissipation, the longer LED lifespan.

Address: 5/F, Building B, Anzhilong Indl., Qinghua East Road., Longhua Town, Shenzhen CHINA. 518109

Red LED

深 圳 市 昱 申 科 技 有 限 公 司
CHINA YOUNG SUN LED TECHNOLOGY CO., LTD.
TEL: (86) 755-28079401 28079402 28079403 28079404 28079405
FAX: (86) 755-28079407 E-mail: info@100LED.com Web: www.100LED.com

Model No.: YSL-R531R3C-A13

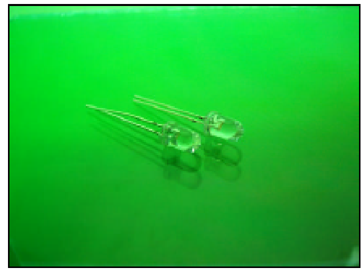

Applications:

- Decorations
- Illuminations
- Advertising Sign
- Traffic Lights
- Indicators
- Flashlights

Absolute Maximum Ratings: (Ta=25 ℃) .

ITEMS	Symbol	Absolute Maximum Rating	Unit
Forward Current	I_F	20	mA
Peak Forward Current	I_{FP}	30	mA
Suggestion Using Current	I_{su}	16-18	mA
Reverse Current (VR=5V)	I_R	10	uA
Power Dissipation	P_D	65	mW
Operation Temperature	T_{OPR}	-40 ~ 85	℃
Storage Temperature	T_{STG}	-40 ~ 100	℃
Lead Soldering Temperature	T_{SOL}	Max. 260℃ for 3 Sec. Max. (3mm from the base of the expoxy bulb)	

Absolute Maximum Ratings: (Ta=25 ℃)

ITEMS	Symbol	Test condition	Min.	Typ.	Max.	Unit
Forward Voltage	V_F	IF=20mA	2.0	---	2.4	V
Wavelength (nm) or TC(k)	Δλ	IF=20mA	620	---	625	nm
*Luminous intensity	Iv	IF=20mA	8000	---	10000	mcd
50% Viewing Angle	2θ1/2	IF=20mA	---	---	10	deg

Address: 5/F, Building B, Anzhilong Indl., Qinghua East Road., Longhua Town, Shenzhen CHINA. 518109
www.100LED.com ONE HUNDRED LED PERFECT LED

深 圳 市 昱 申 科 技 有 限 公 司
CHINA YOUNG SUN LED TECHNOLOGY CO., LTD.
TEL: (86) 755-28079401 28079402 28079403 28079404 28079405
FAX: (86) 755-28079407 E-mail: info@100LED.com Web: www.100LED.com

Light Degradation in mcd: (I_F=20mA)

Hours / Colors	Light Degradation in mcd after Different Hours					
	216 Hrs	360 Hrs	792 Hrs	1104 Hrs	1992 Hrs	2328 Hrs
Red	1.52%	-1.22%	-3.10%	-4.68%	-5.72%	-8.27%
Yellow	-1.71%	-2.97%	-5.93%	-8.13%	-8.90%	-11.10%
Blue	3.13%	-0.33%	-3.84%	-8.23%	-21.32%	-24.92%
Green	-8.02%	-9.78%	-14.25%	-17.37%	-20.79%	-22.30%
Hours	48 Hrs	168 Hrs	336 Hrs	360Hrs	720 Hrs	1008 Hrs
Cool White	10.56%	6.72%	-2.29%	-7.68%	-17.32%	-22.48%
Pure White	13.66%	8.22%	-1.45%	-8.50%	-19.52%	-25.26%
Warm White	3.02%	-4.38%	-15.18%	-21.15%	-27.19%	-29.97%

Mechanical Dimensions:

- All dimension are in mm, tolerance is ±0.2mm unless otherwise noted
- An epoxy meniscus may extend about 1.5mm down the leads.
- Burr around bottom of epoxy may be 0.5mm Maximum

Unit: mm

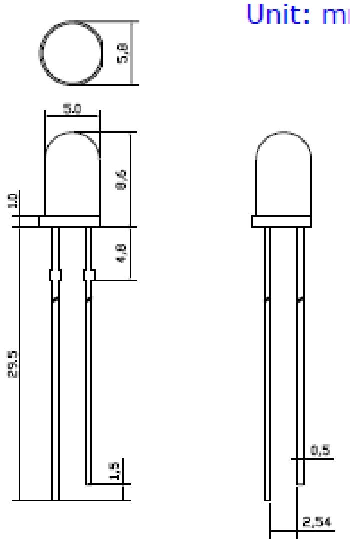

Viewing Angle Drawing

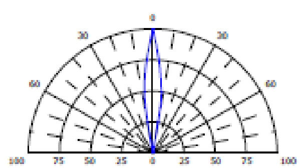

Packing Information:

1. Anti-static bag

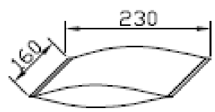

Unit: mm

- 200 - 500pcs per bag
- With 1 little bag of drier inside

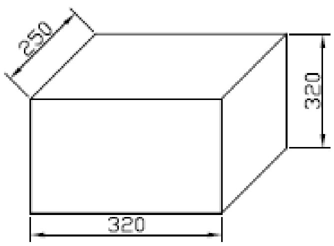

Middle Box

- 30 - 40 bags per box
- 15-20K pcs per box

Anti-static Tube Packaging Information:

Unit: mm

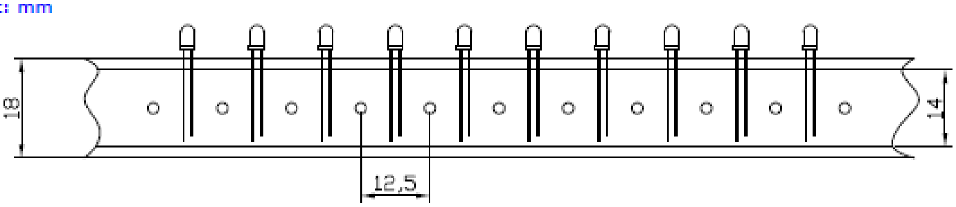

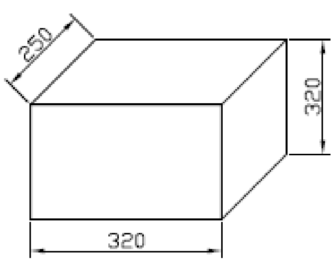

Middle Box

- Taping dimension can be adjusted to customer's requirements.
- 8-10 Layers per box
- 16K-20K pcs per box

Code System:

YSL-R531R3C-A13

1 2 3 4 5 6 7 8 9 10

1. Company Code, short for Young Sun
2. Code for LED series.
3. Code for LED Type.

   R: Round B: Bullet C: Columnar O: Ovai
   H: Helmet Q: Square V: Concave P: Pagoda
   S: Strawhat D: Special

4. Code for LED Lens Type.
5. Code for Lead Frame of LED
6. Code for Lead Frame Code of LED
7. Code for Wavelength Color
8. Code for Lens color

   C: Water Clear W: White Diffused D: Color Diffused T: Color Transparent

9. Code for Viewing Angle

   A: 1-10 B: 10-20 C: 20-30 D: 30-40 E: 40-60 F: 60-90 G: 90-120 H: >120

10. Luminous Intensity Grade:

1: 1-50mcd	4: 200-300mcd	7: 800-1000mcd	10: 2000-3000mcd	14: 10000-13000mcd
2: 50-100mcd	5: 300-500mcd	8: 1000-1500mcd	11: 3000-5000mcd	15: 13000-15000mcd
3: 100-200mcd	6: 500-800mcd	9: 1500-2000mcd	12: 5000-8000mcd	16: 15000-20000mcd
			13: 8000-10000mcd	17: 20000~mcd

Warrantee:

- In order to make the LEDs lifespan longer, please set the input Current below 20mA.
- Electrical & Optical Characteristics consistency of same items all shippments.

Notes:

- Please use LEDs based on our datasheet.
- LED is senstive to statics, be sure your equipments are anti-static when you use our LEDs.
- Pay more attention to your heat dissipation system when you use it, the better heat dissipation, the longer LED lifespan.

White LED

CHINA INTERNATIONAL CO.

SHENZHEN FURUIER PHOTOELECTRIC CO., LTD.

SPECIFICATION FOR APPROVAL

CUSTOMER :

ARTICLE : 5mm Standard Round White LED

PART NO : FLR-50T04-HW7

DATE : 2011-03-22

CUSTOMER MODEL:

RoHS PRODUCT

Authorized Signature

ATTENTION
OBSERVE PRECAUTIONS
ELECTROSTATIC
SENSITIVE DEVICES

Http://www.furuier.en.alibaba.com E-mail:ledexport@furuier.com
Tel:86-755-61563456 Fax:86-755-61568736 Rev:A0 Page:1 of 5
Add:Rd.HuaChang Nan.Tongfuyu Zone.Dalang.Longhua.Baoan District.Shenzhen.China.

∅Absolute Maximum Rating

Item	Symbol	Absolute Maximum Rating	Unit
Forward Current	I_F	20	mA
Peak Forward Current	I_{FP}	120	mA
Reverse Voltage	V_R	5	V
Power Dissipation	P_D	85	mW
Operation Temperature	Topr	-35~+80	℃
Storage Temperature	Tstg	-40~+80	℃
Lead Soldering Temperature	Tsol	Max.260° for 3sec Max.	

*I_{FP} Conditions:Pulse Width≤10msec duty≤1/10
*Tsol Conditions:4mm from the base of the epoxy bulb

∅TypicalOptical/ElectricalCharacteristics

Item	Symbol	Condition	Min.	Typ.	Max.	Unit
Forward Voltage	VF	IF=20mA	—	3.0	3.4	V
Reverse Current	IF	V_R=5V	—	—	10	uA
50% Power Angle	$2\theta_{1/2}$	IF=20mA	—	12	—	deg
Luminous Intensity	IV	IF=20mA	15000	20000	—	mcd
Chromaticity coordinates		IF=20mA	—	x=0.33 y=0.32	—	nm
Recommend Forward Current	I_F(rec)	—	—	10~20	—	mA

Notes:

1. Absolute maximum ratings Ta=25° C .
2. Tolerance of measurement of forward voltage±0.1V.
3. Tolerance of measurement of peak Wavelength±2.0nm.
4. Tolerance of measurement of luminous intensity±15%.

Add:Rd.HuaChang Nan.Tongfuyu Zone.Dalang.Longhua.Baoan District.Shenzhen.China.
Http://www.furuier.en.alibaba.com E-mail:ledexport@furuier.com
Tel:86-755-61563456 Fax:86-755-61568736 Designed By:

∅Package Dimensions And Materials

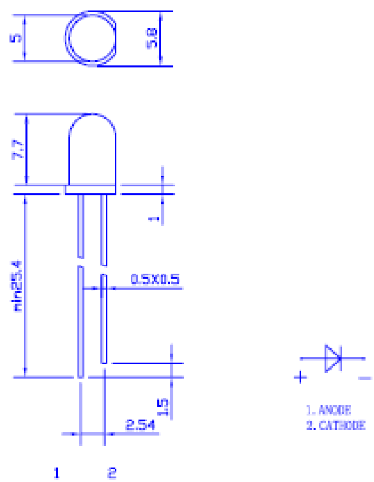

□ 0.5 SQUARE*2

Chip		Lens Color
Dice Material	Emitting Color	
InGaN	WHITE	WATER CLEAR

Notes:

1. All dimension units are millimeters
2. All dimension tolerance is ±0.2mm unless otherwise noted
3. An epoxy meniscus may extend about 1.5mm down the leads
4. Burr around bottom of epoxy may be 0.5mm max

Add:Rd. HuaChang Nan. Tongfuyu Zone. Dalang. Longhua. Baoan District. Shenzhen. China.
Http://www.furuier.en.alibaba.com E-mail:ledexport@furuier.com
Tel:86-755-61563456 Fax:86-755-61568736 Designed By:

∅Spatial Distribution

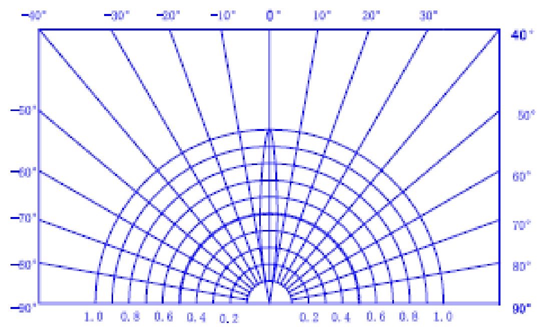

Rev lative Luminous Intensity Angle

∅Reflow Temp/Time

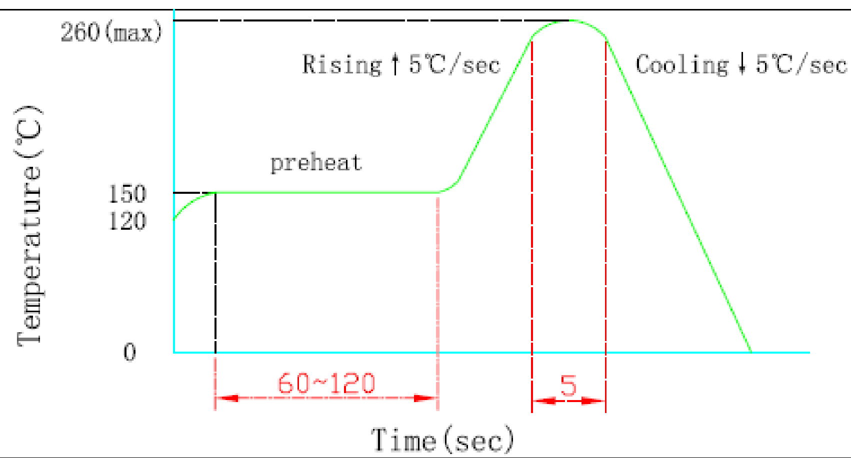

∅Soldering iron

Basic spec is≤5sec when 260℃. If temperature is higher, time should be shorter (+10℃-1sec) Power dissipation of iron should be smaller than 15W, and temperatures should be controllable. surface temperature of the device should be under 230℃

Electro-Optical Characteristic(Ta=25℃)

PARAMETER	SYMBOL	TEST CONDITTIONS	Green		Orange		GaP Red		HI-EFF		Yellow		GaAlAs		Blue		UNIT
			TYP.	MAX.	TYP.	MAX.	TYP.	MAX.	TYP.	MAX.	TYP.	MAX.	TYP.	MAX.	TYP.	MAX.	
Forward Voltage	VF	IF=20mA	2.3	2.8	2.2	2.8	2.3	2.8	2.2	2.8	2.2	2.8	1.8	2.5	3.5	4.5	V
Reverse Current	IR	VR=5V		100		100		100		100		100		100		100	uA
Wavelength	λP	IF=20mA	570		635		700		625		590		660		430		nm
Spectral Line Halfwidth	△λ	IF=20mA	30		35		100		35		35		20		30		nm

Absolute Maximum Ratings(Ta=±25℃)

PARAMETER	Green	Orange	Gap Red	HI-EFF	Yellow	GaAlAs	Blue	UNIT
Reverse Voltage Per Segment or D.P.	5	5	5	5	5	5	5	V
Average Forward Current (IF)	25	25	25	25	25	30	50	mA
Peak Forward Current Per Segment Or Dp	200	200	200	200	200	200	200	mA
Power Dissipation	85	85	85	85	85	100	120	mW
Operating Temperature Range	-35℃~+80℃							
Recommend Storage Temperature Range	-35℃~+80℃							
Lead Solder Temperature(4mm From Body) 260℃for3sec								
Life:100000H								

Typical Electron-Optical Characteristic Curves25℃
Free Air Temperature Unless Otherwise Specified

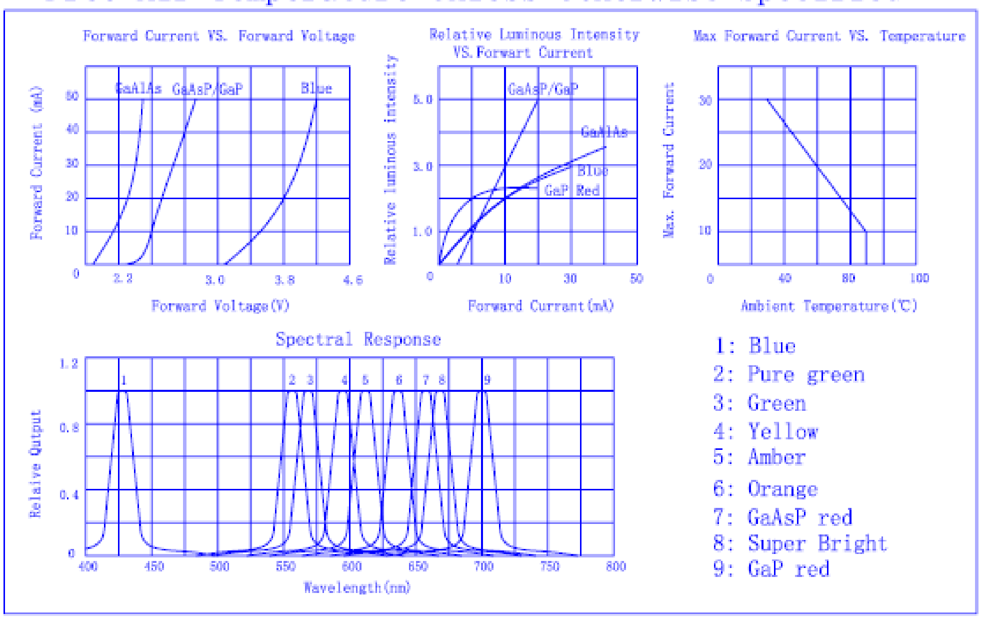

Add:Rd.HuaChang Nan.Tongfuyu Zone.Dalang.Longhua.Baoan District.Shenzhen.China.
Http://www.furuier.en.alibaba.com E-mail:ledmarket@furuier.com

Tel:86-755-61563456 Fax:86-755-61568736

Yellow LED

FRE CHINA INTERNATIONAL CO.

SHENZHEN FURUIER PHOTOELECTRIC CO., LTD.

SPECIFICATION FOR APPROVAL

CUSTOMER :

ARTICLE : ∅5 Round Water clear Pure yellow LED

PART NO : FLR-50T04-PY6

DATE : 2012-02-22

CUSTOMER MODEL:

RoHS PRODUCT

Authorized Signature

ATTENTION
OBSERVE PRECAUTIONS
ELECTROSTATIC
SENSITIVE DEVICES

Http://www.furuier.en.alibaba.com E-mail:ledexport@furuier.com
Tel:86-755-61563456 Fax:86-755-61568736 Rev:A0 Page:1 of 5
Add:Rd.HuaChang Nan.Tongfuyu Zone.Dalang.Longhua.Baoan District.Shenzhen.China.

∅Absolute Maximum Rating

Item	Symbol	Absolute Maximum Rating	Unit
Forward Current	I_F	20	mA
Peak Forward Current	I_{FP}	120	mA
Reverse Voltage	V_R	5	V
Power Dissipation	P_D	80	mW
Operation Temperature	Topr	-35~+80	℃
Storage Temperature	Tstg	-40~+80	℃
Lead Soldering Temperature	Tsol	Max. 260° for 3sec Max.	

*I_{FP} Conditions:Pulse Width≤10msec duty≤1/10

*Tsol Conditions:4mm from the base of the epoxy bulb

∅TypicalOptical/ElectricalCharacteristics

Item	Symbol	Condition	Min.	Typ.	Max.	Unit
Forward Voltage	VF	IF=20mA	3.0	3.2	3.4	V
Reverse Current	IF	V_R=5V	—	—	10	uA
50% Power Angle	$2\theta_{1/2}$	IF=20mA	—	15	—	deg
Luminous Intensity	IV	IF=20mA	—	18000	20000	mcd
Peak Wavelength	λ_p	IF=20mA	520	523	525	nm
Recommend Forward Current	I_F(rec)	—	—	10~20	—	mA

Notes:

1. Absolute maximum ratings Ta=25° C .
2. Tolerance of measurement of forward voltage±0.1V.
3. Tolerance of measurement of peak Wavelength±2.0nm.
4. Tolerance of measurement of luminous intensity±15%.

∅Package Dimensions And Materials

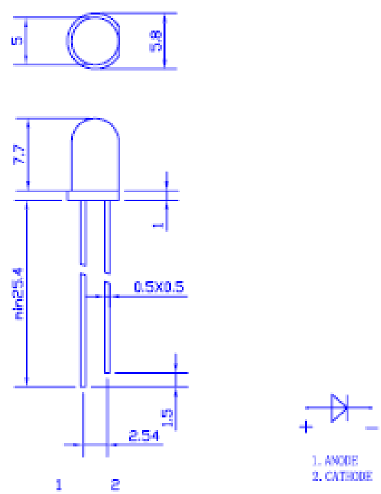

□ 0.5 SQUARE*2

Chip		Lens Color
Dice Material	Emitting Color	
InGaN	Pure green	WATER CLEAR

Notes:

1. All dimension units are millimeters
2. All dimension tolerance is ±0.2mm unless otherwise noted
3. An epoxy meniscus may extend about 1.5mm down the leads
4. Burr around bottom of epoxy may be 0.5mm max

Add:Rd.HuaChang Nan.Tongfuyu Zone.Dalang.Longhua.Baoan District.Shenzhen.China.
Http://www.furuier.en.alibaba.com E-mail:ledexport@furuier.com

Tel:86-755-61563456 Fax:86-755-61568736 Designed By:

∅Spatial Distribution

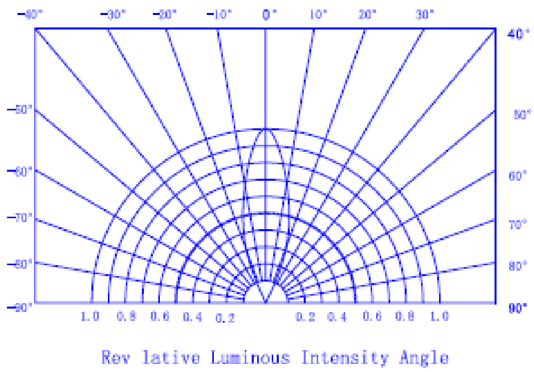

∅Reflow Temp/Time

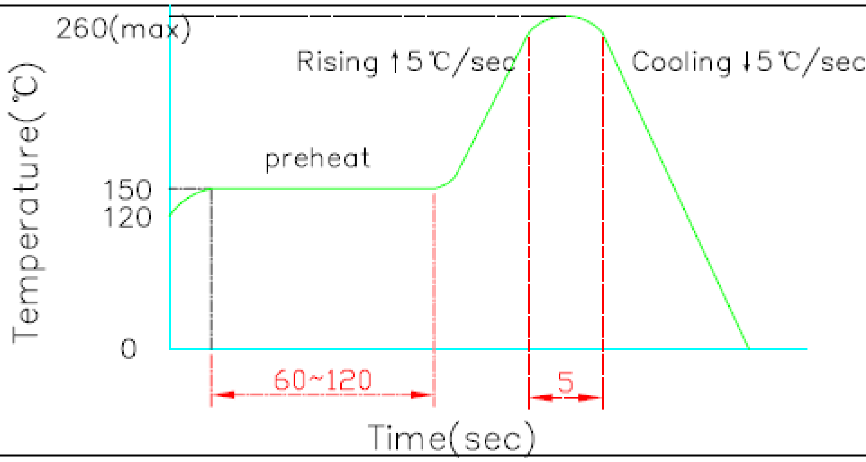

∅Soldering iron

Basic spec is≤5sec when 260℃. If temperature is higher, time should be shorter (+10℃-1sec) Power dissipation of iron should be smaller than 15W, and temperatures should be controllable. surface temperature of the device should be under 230℃

Electro-Optical Characteristic(Ta=25℃)

PARAMETER	SYMBOL	TEST CONDITIONS	Green		Orange		GaP Red		HI-EFF		Yellow		GaAlAs		Blue		UNIT
			TYP.	MAX.	TYP.	MAX.	TYP.	MAX.	TYP.	MAX.	TYP.	MAX.	TYP.	MAX.	TYP.	MAX.	
Forward Voltage	VF	IF=20mA	2.3	2.8	2.2	2.8	2.3	2.8	2.2	2.8	2.2	2.8	1.8	2.5	3.5	4.5	V
Reverse Current	IR	VR=5V		100		100		100		100		100		100		100	uA
Wavelength	λP	IF=20mA	570		635		700		625		590		660		430		nm
Spectral Line Halfwidth	△λ	IF=20mA	30		35		100		35		35		20		30		nm

Absolute Maximum Ratings(Ta=±25℃)

PARAMETER	Green	Orange	Gap Red	HI-EFF	Yellow	GaAlAs	Blue	UNIT
Reverse Voltage Per Segment or D.P.	5	5	5	5	5	5	5	V
Average Forward Current (IF)	25	25	25	25	25	30	50	mA
Peak Forward Current Per Segment Or Dp	200	200	200	200	200	200	200	mA
Power Dissipation	85	85	85	85	85	100	120	mW
Operating Temperature Range	-35℃~+80℃							
Recommend Storage Temperature Range	-35℃~+80℃							
Lead Solder Temperature(4mm From Body) 260℃for3sec								
Life:100000H								

Typical Electron-Optical Characteristic Curves25℃ Free Air Temperature Unless Otherwise Specified

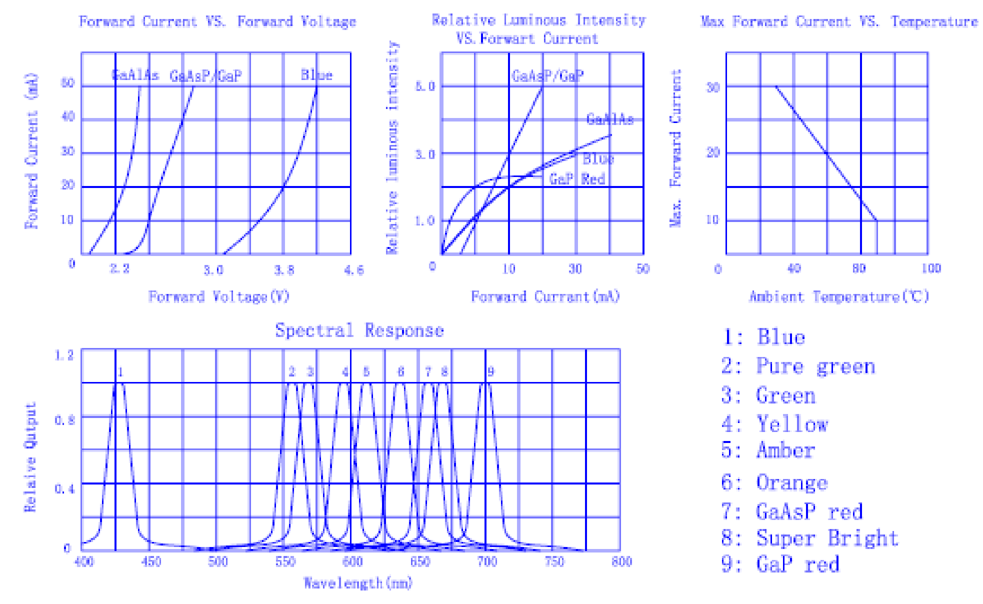

Add:Rd.HuaChang Nan.Tongfuyu Zone.Dalang.Longhua.Baoan District.Shenzhen.China.
Http://www.furuier.en.alibaba.com E-mail:ledmarket@furuier.com Rev:A0 Page:5 of 5
Tel:86-755-61563456 Fax:86-755-61568736

ANALOG DEVICES

Low Voltage Temperature Sensors

TMP35/TMP36/TMP37

FEATURES

Low voltage operation (2.7 V to 5.5 V)
Calibrated directly in °C
10 mV/°C scale factor (20 mV/°C on TMP37)
±2°C accuracy over temperature (typ)
±0.5°C linearity (typ)
Stable with large capacitive loads
Specified −40°C to +125°C, operation to +150°C
Less than 50 µA quiescent current
Shutdown current 0.5 µA max
Low self-heating

APPLICATIONS

Environmental control systems
Thermal protection
Industrial process control
Fire alarms
Power system monitors
CPU thermal management

GENERAL DESCRIPTION

The TMP35/TMP36/TMP37 are low voltage, precision centigrade temperature sensors. They provide a voltage output that is linearly proportional to the Celsius (centigrade) temperature. The TMP35/ TMP36/TMP37 do not require any external calibration to provide typical accuracies of ±1°C at +25°C and ±2°C over the −40°C to +125°C temperature range.

The low output impedance of the TMP35/TMP36/TMP37 and its linear output and precise calibration simplify interfacing to temperature control circuitry and ADCs. All three devices are intended for single-supply operation from 2.7 V to 5.5 V maximum. The supply current runs well below 50 µA, providing very low self-heating—less than 0.1°C in still air. In addition, a shutdown function is provided to cut the supply current to less than 0.5 µA.

The TMP35 is functionally compatible with the LM35/LM45 and provides a 250 mV output at 25°C. The TMP35 reads temperatures from 10°C to 125°C. The TMP36 is specified from −40°C to +125°C, provides a 750 mV output at 25°C, and operates to 125°C from a single 2.7 V supply. The TMP36 is functionally compatible with the LM50. Both the TMP35 and TMP36 have an output scale factor of 10 mV/°C.

FUNCTIONAL BLOCK DIAGRAM

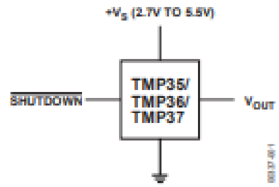

Figure 1.

PIN CONFIGURATIONS

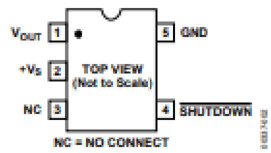

Figure 2. RJ-5 (SOT-23)

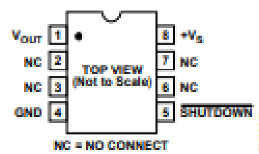

Figure 3. R-8 (SOIC_N)

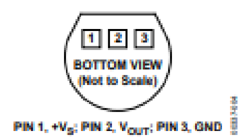

Figure 4. T-3 (TO-92)

The TMP37 is intended for applications over the range of 5°C to 100°C and provides an output scale factor of 20 mV/°C. The TMP37 provides a 500 mV output at 25°C. Operation extends to 150°C with reduced accuracy for all devices when operating from a 5 V supply.

The TMP35/TMP36/TMP37 are available in low cost 3-lead TO-92, 8-lead SOIC_N, and 5-lead SOT-23 surface-mount packages.

Rev. E

One Technology Way, P.O. Box 9106, Norwood, MA 02062-9106, U.S.A.
Tel: 781.329.4700 www.analog.com
Fax: 781.461.3113

APPENDIX B

COMPLETE SET OF OPTICAL SENSOR PLOTS

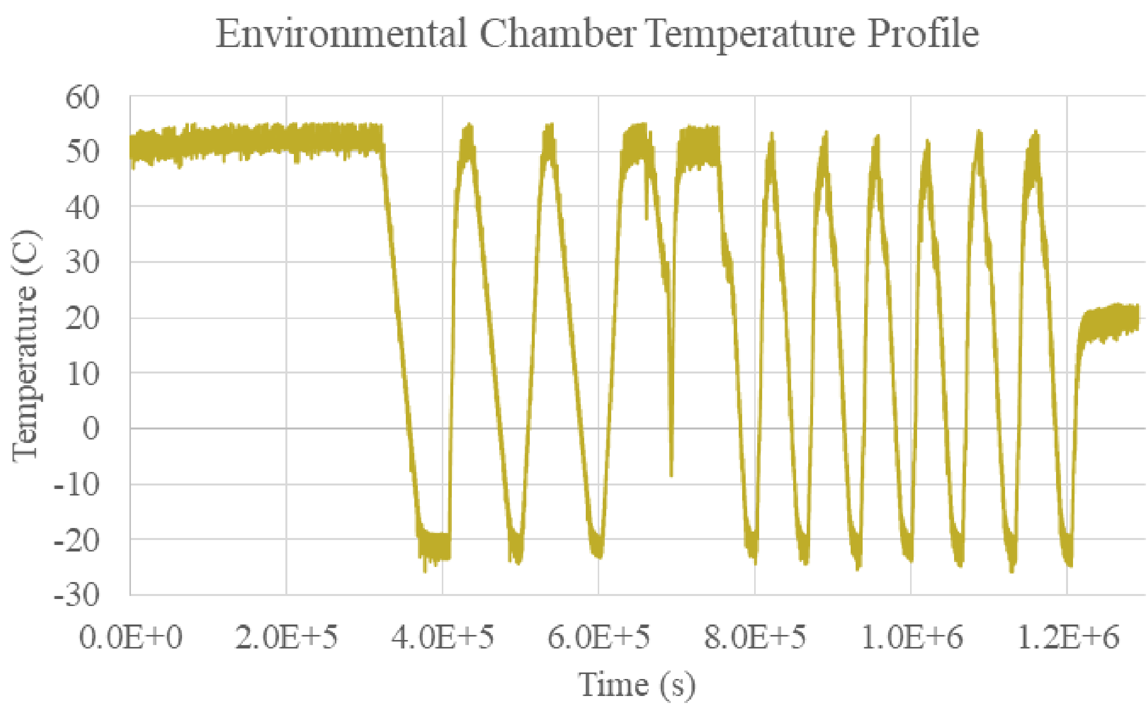

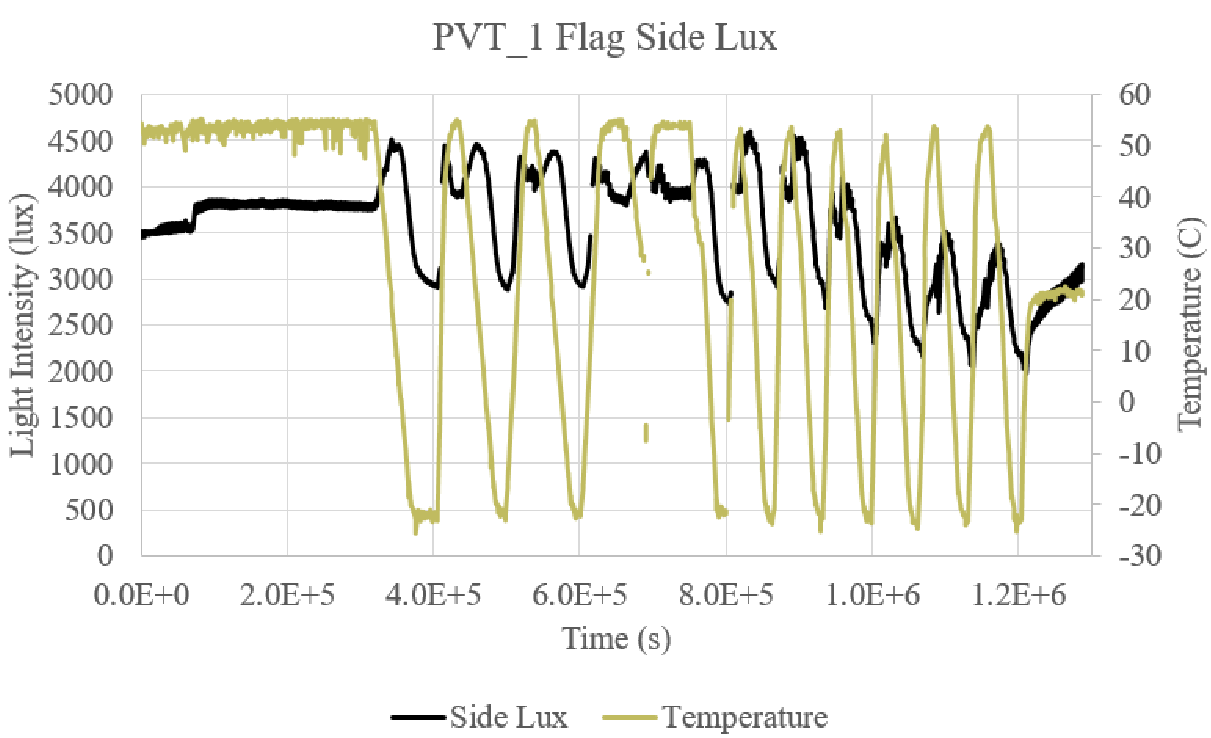

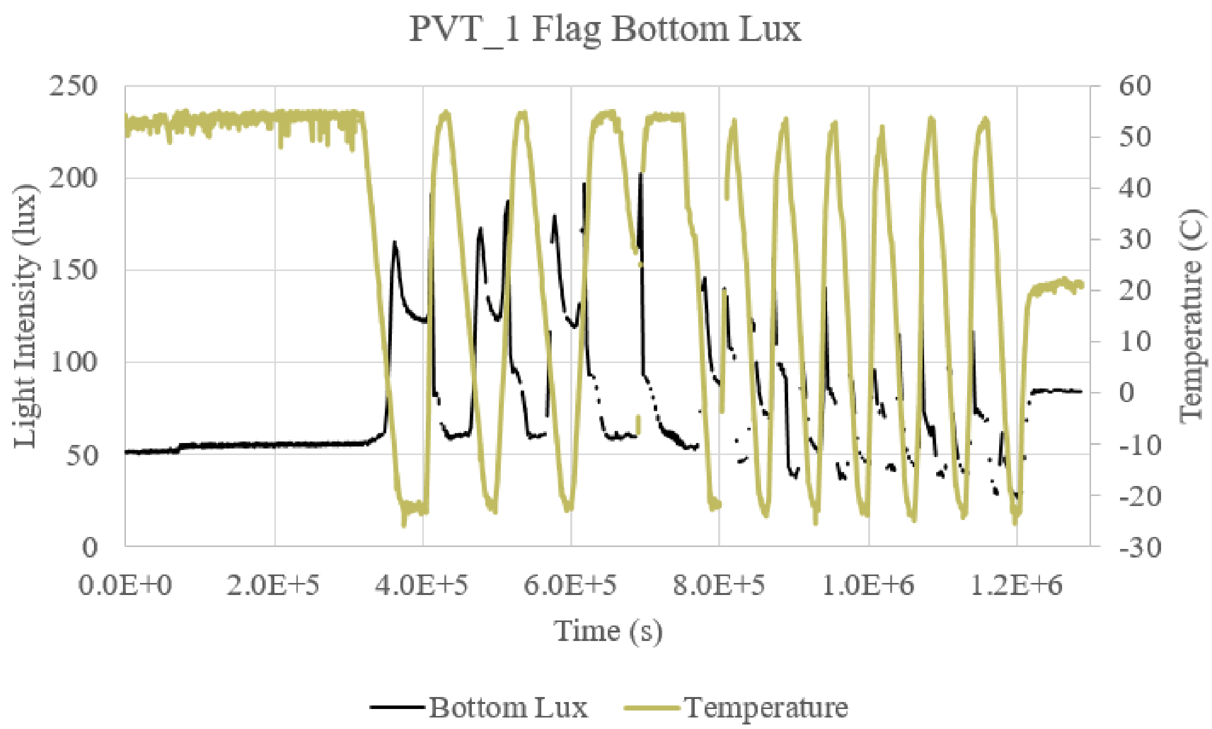
PVT_1 Flag Bottom Lux
Light Intensity (lux)
250
200
150
100
50
0
Temperature (C)
60
50
40
30
20
10
0
-10
-20
-30
0.0E+0
2.0E+5
4.0E+5
6.0E+5
8.0E+5
1.0E+6
1.2E+6
Time (s)
Bottom Lux
Temperature

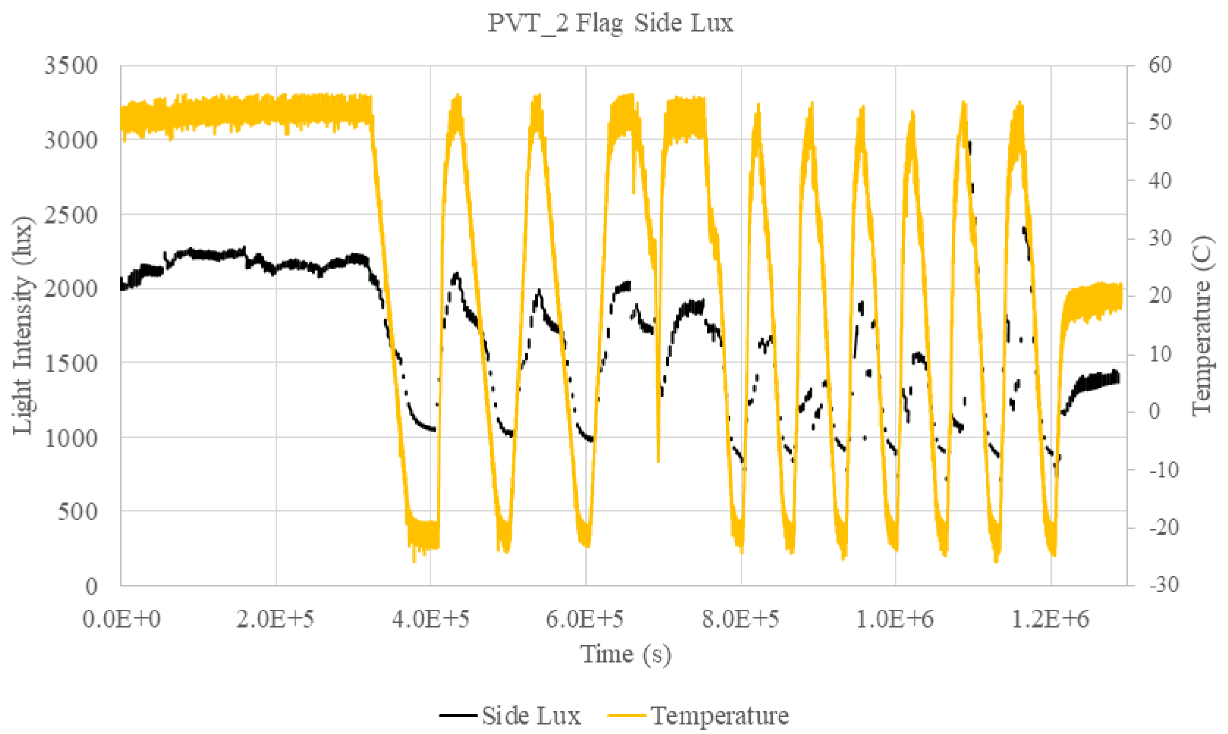
PVT_2 Flag Side Lux
Light Intensity (lux)
3500
3000
2500
2000
1500
1000
500
0
Temperature (C)
60
50
40
30
20
10
0
-10
-20
-30
0.0E+0
2.0E+5
4.0E+5
6.0E+5
8.0E+5
1.0E+6
1.2E+6
Time (s)
Side Lux
Temperature

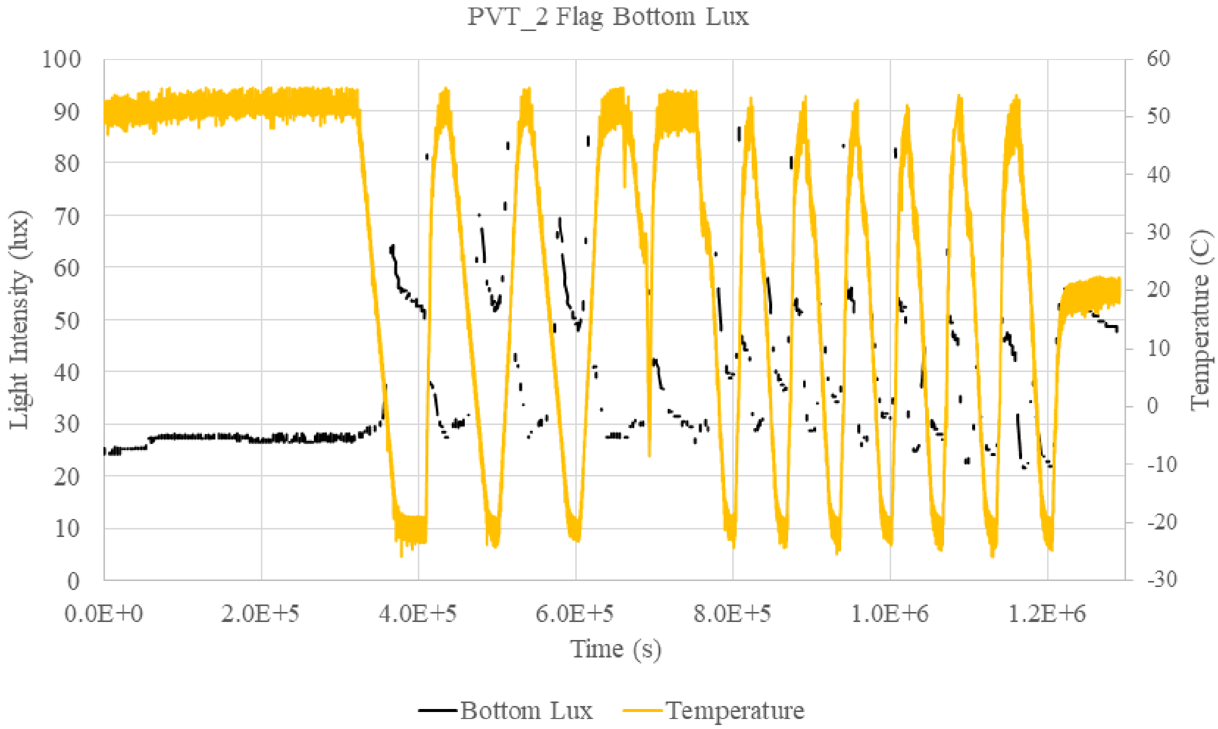
PVT_2 Flag Bottom Lux
Light Intensity (lux)
Temperature (C)
Time (s)
Bottom Lux
Temperature

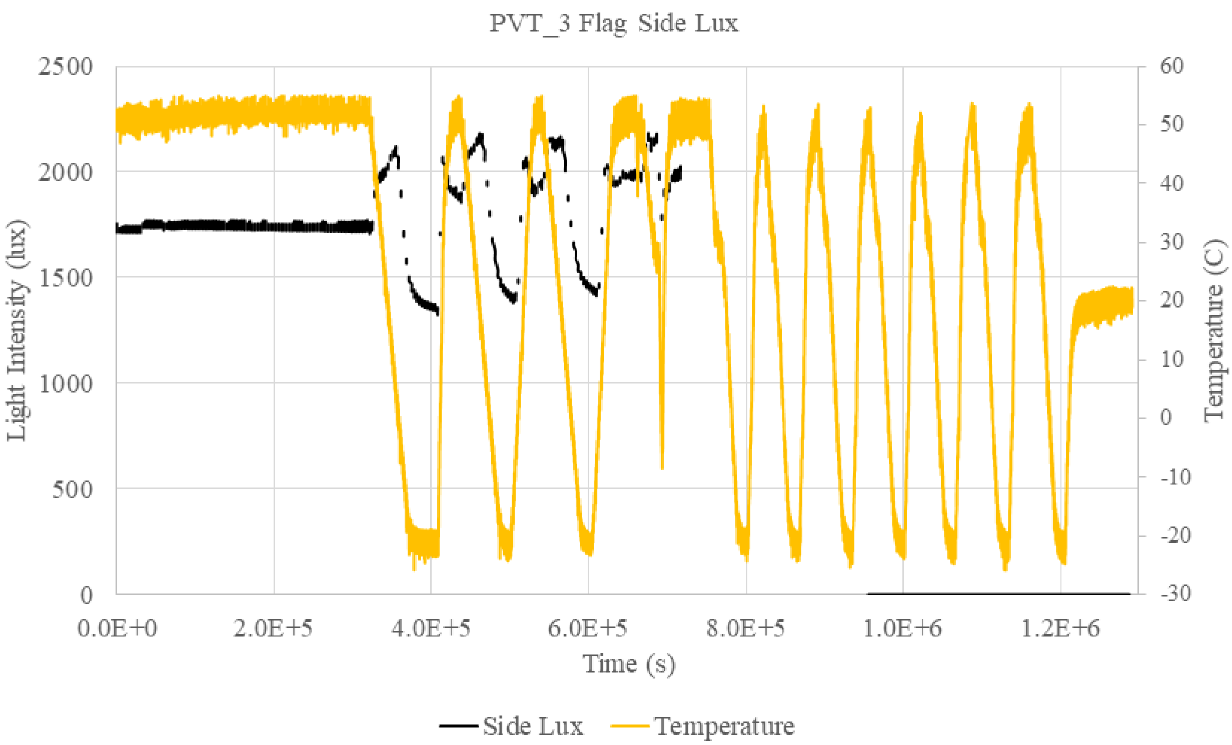
PVT_3 Flag Side Lux
Light Intensity (lux)
Temperature (C)
Time (s)
Side Lux
Temperature

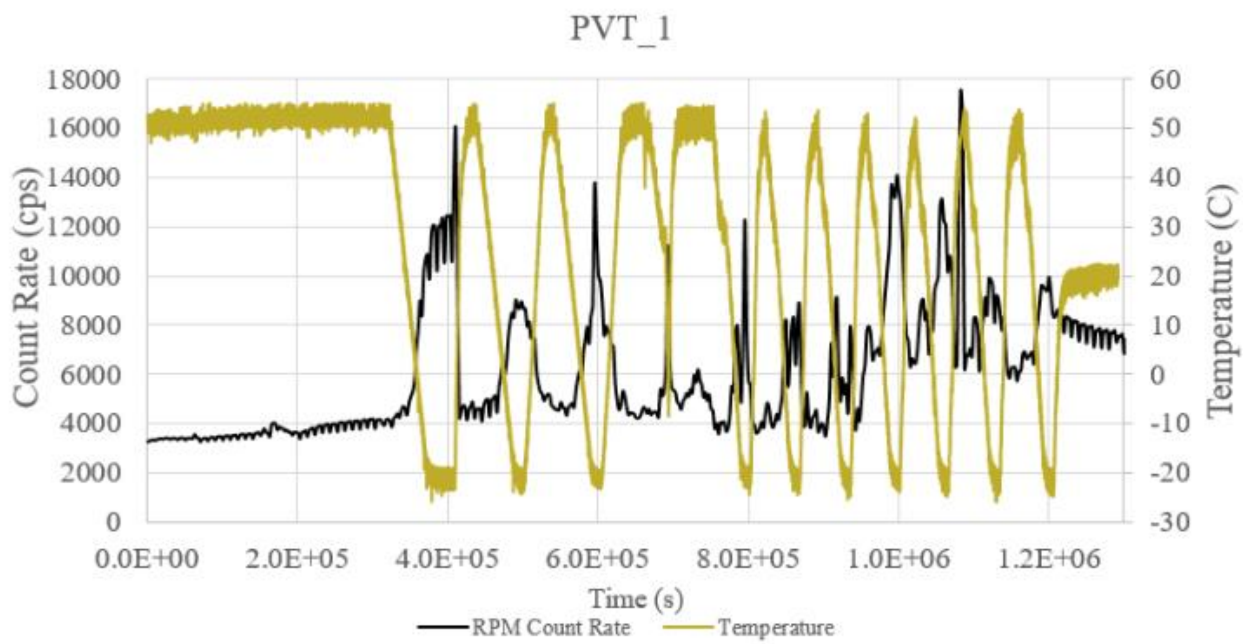
PVT_1
Count Rate (cps)
Temperature (C)
Time (s)
RPM Count Rate
Temperature

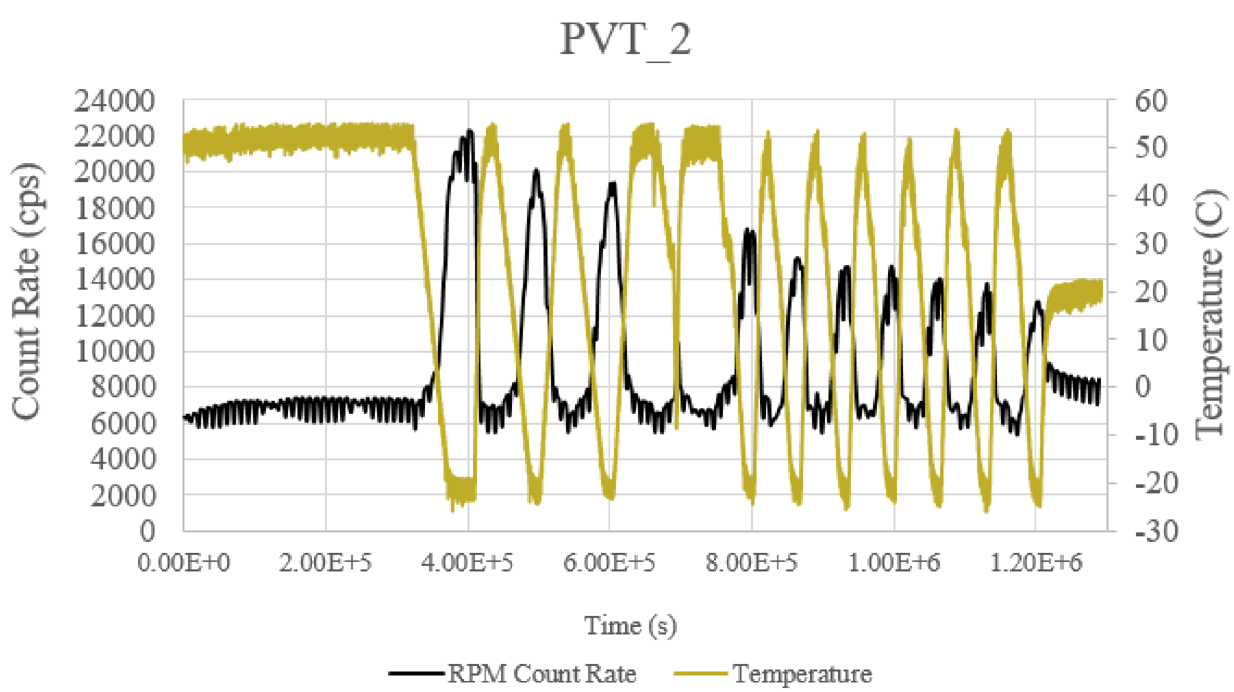
PVT_2
Count Rate (cps)
Temperature (C)
Time (s)
RPM Count Rate
Temperature

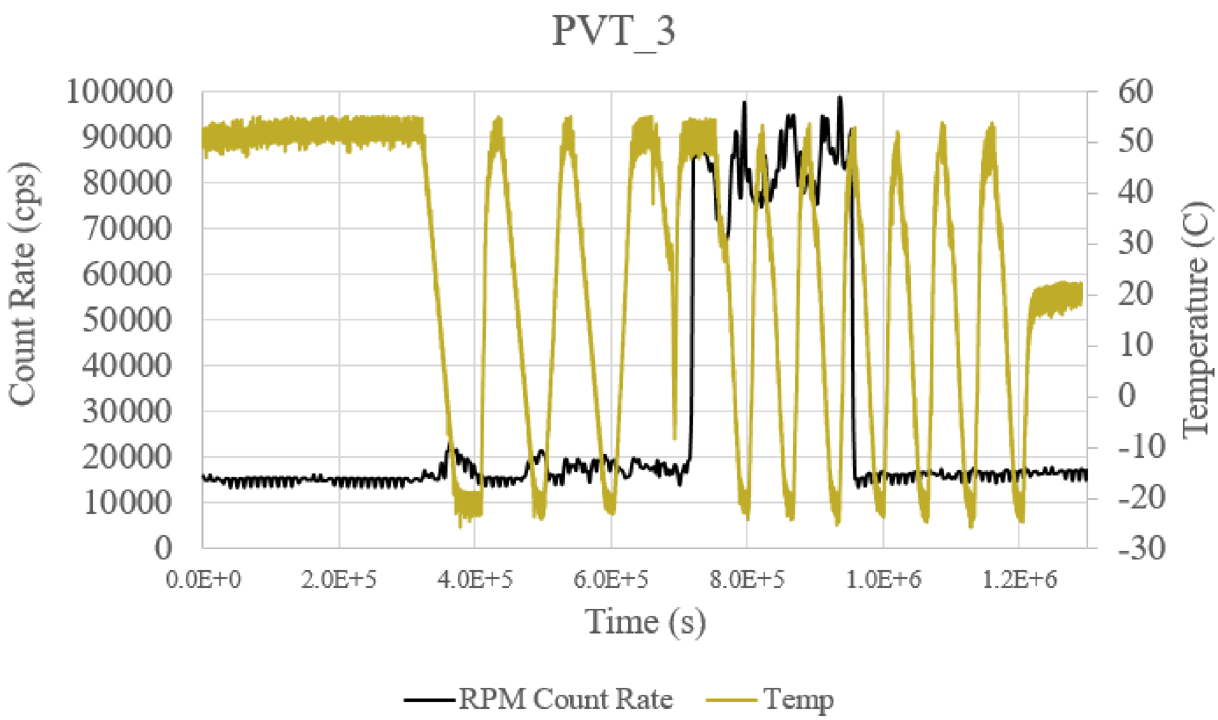
PVT_3
Count Rate (cps)
Temperature (C)
100000
90000
80000
70000
60000
50000
40000
30000
20000
10000
0
60
50
40
30
20
10
0
-10
-20
-30
0.0E+0
2.0E+5
4.0E+5
6.0E+5
8.0E+5
1.0E+6
1.2E+6
Time (s)
RPM Count Rate
Temp

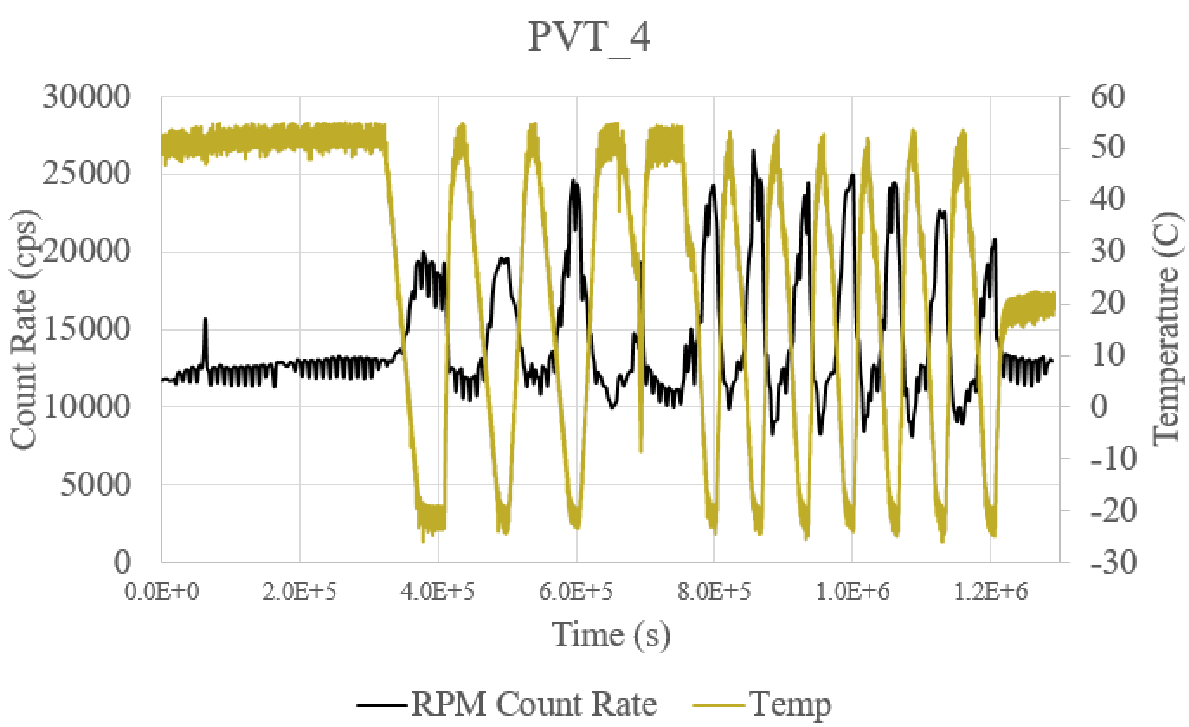
PVT_4
Count Rate (cps)
Temperature (C)
30000
25000
20000
15000
10000
5000
0
60
50
40
30
20
10
0
-10
-20
-30
0.0E+0
2.0E+5
4.0E+5
6.0E+5
8.0E+5
1.0E+6
1.2E+6
Time (s)
RPM Count Rate
Temp

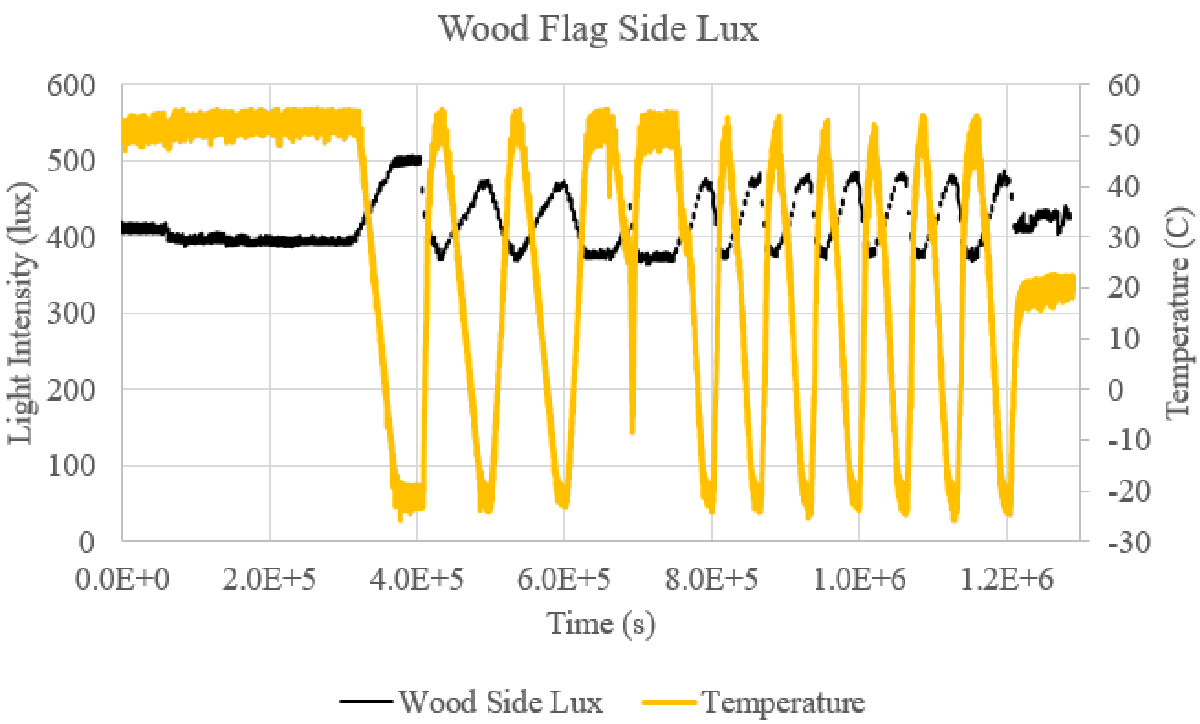

Wood Flag Side Lux
Light Intensity (lux)
600
500
400
300
200
100
0
Temperature (C)
60
50
40
30
20
10
0
-10
-20
-30
0.0E+0
2.0E+5
4.0E+5
6.0E+5
8.0E+5
1.0E+6
1.2E+6
Time (s)
Wood Side Lux
Temperature

APPENDIX C

HTA CALCULATION RESULTS

Table C. 1. HTA results for PVT_1

Experiment Time (s)	**Surface Temperature (C)**	**Surrounding Temperature (C)**	**Gr**	**Ra**	**Nu**	**h**	**Bi**	**Tc (C)**	**θc**
761134	32.52	27.00	4.982E+08	3.522E+08	71.094	2.102	0.148	31.908	0.889
769489	26.17	27.50	1.204E+08	8.514E+07	50.053	1.482	0.105	26.287	0.912
777718	12.50	9.50	3.548E+08	2.524E+08	65.515	1.834	0.129	12.204	0.901
786074	-8.50	-12.50	6.863E+08	4.923E+08	77.365	2.013	0.142	-8.966	0.883
794159	-18.75	-20.00	2.480E+08	1.783E+08	60.193	1.525	0.108	-18.843	0.926
802656	-18.75	-20.00	2.480E+08	1.783E+08	60.193	1.525	0.108	-18.863	0.909
810885	31.54	38.50	5.365E+08	3.785E+08	72.353	2.208	0.156	32.348	0.884
819240	49.12	48.00	7.416E+07	5.221E+07	44.352	1.389	0.098	49.027	0.917
827469	43.75	38.00	4.376E+08	3.087E+08	68.793	2.097	0.148	43.114	0.889
835824	28.61	26.00	2.402E+08	1.699E+08	59.364	1.750	0.123	28.342	0.898

Table C. 1 (continued)

Experiment Time (s)	Surface Temperature (C)	Surrounding Temperature (C)	Gr	Ra	Nu	h	Bi	Tc (C)	θc
844053	11.52	7.50	4.900E+08	3.489E+08	70.984	1.974	0.139	11.097	0.895
852408	-10.94	-14.00	5.406E+08	3.879E+08	72.937	1.888	0.133	-11.276	0.890
860636	-19.24	-20.00	1.509E+08	1.085E+08	53.244	1.349	0.095	-19.297	0.926
868991	-17.77	-17.50	5.124E+07	3.681E+07	40.790	1.043	0.074	-17.753	0.937
877220	35.45	43.00	5.449E+08	3.840E+08	72.607	2.243	0.158	36.336	0.883
885575	48.63	48.00	4.175E+07	2.939E+07	38.509	1.206	0.085	48.584	0.927
893804	42.77	35.50	5.731E+08	4.045E+08	73.561	2.227	0.157	41.917	0.883
902159	32.52	28.50	3.551E+08	2.510E+08	65.375	1.941	0.137	32.068	0.888
910388	14.94	10.00	5.776E+08	4.109E+08	73.912	2.072	0.146	14.398	0.890
918743	-7.03	-11.00	6.630E+08	4.753E+08	76.689	2.005	0.141	-7.490	0.884
926972	-18.75	-20.00	2.480E+08	1.783E+08	60.193	1.525	0.108	-18.853	0.918
935327	-21.68	-20.50	2.375E+08	1.708E+08	59.557	1.506	0.106	-21.574	0.910
943555	26.66	35.00	6.795E+08	4.797E+08	76.733	2.320	0.164	27.667	0.879

Table C. 1 (continued)

Experiment Time (s)	Surface Temperature (C)	Surrounding Temperature (C)	Gr	Ra	Nu	h	Bi	Tc (C)	θc
951910	46.68	48.00	8.774E+07	6.177E+07	46.227	1.447	0.102	46.795	0.913
960139	43.75	41.00	2.011E+08	1.418E+08	56.749	1.744	0.123	43.492	0.906
968494	33.50	28.50	4.410E+08	3.117E+08	68.973	2.048	0.144	32.910	0.882
976723	13.96	09.50	5.261E+08	3.743E+08	72.226	2.022	0.143	13.480	0.892
985078	-8.98	-12.50	6.045E+08	4.336E+08	74.970	1.950	0.138	-9.380	0.886
993307	-18.26	-20.00	3.449E+08	2.480E+08	65.307	1.655	0.117	-18.416	0.911
1001662	-18.75	-20.50	3.502E+08	2.519E+08	65.559	1.658	0.117	-18.921	0.902
1009890	32.52	39.50	5.301E+08	3.738E+08	72.131	2.207	0.156	33.331	0.884
1018245	49.12	48.00	7.416E+07	5.221E+07	44.352	1.389	0.098	49.027	0.917
1026474	43.26	38.00	4.006E+08	2.826E+08	67.306	2.051	0.145	42.689	0.892
1034829	30.08	27.00	2.791E+08	1.973E+08	61.599	1.821	0.128	30.395	1.102

Table C. 1 (continue)

Experiment Time (s)	Surface Temperature (C)	Surrounding Temperature (C)	Gr	Ra	Nu	h	Bi	Tc (C)	θc
1043058	8.11	3.50	5.991E+08	4.272E+08	74.647	2.049	0.145	7.610	0.892
1051413	-11.43	-16.50	9.345E+08	6.712E+08	83.560	2.144	0.151	-12.057	0.876
1060439	-22.66	-20.00	5.318E+08	3.825E+08	72.698	1.842	0.130	-22.253	0.847
1068794	-6.05	-4.00	3.060E+08	2.188E+08	63.275	1.694	0.120	-5.846	0.900
1077023	40.82	46.00	3.565E+08	2.511E+08	65.355	2.035	0.144	41.378	0.892
1090627	52.05	48.50	2.325E+08	1.637E+08	58.791	1.843	0.130	51.668	0.892
1098856	33.50	28.00	4.886E+08	3.453E+08	70.747	2.097	0.148	32.889	0.889
1107211	19.34	14.50	5.275E+08	3.746E+08	72.225	2.054	0.145	18.766	0.881
1115440	-2.64	-9.00	1.020E+09	7.308E+08	85.315	2.246	0.158	-3.390	0.882
1123795	-17.77	-20.00	4.415E+08	3.176E+08	69.426	1.759	0.124	-18.000	0.897
1132024	-20.71	-20.50	4.218E+07	3.034E+07	38.902	0.984	0.069	-20.699	0.948
1140379	13.96	19.50	5.694E+08	4.036E+08	73.557	2.125	0.150	14.635	0.878
1148607	48.14	47.50	4.272E+07	3.008E+07	38.727	1.211	0.085	48.097	0.933

Table C. 1 (continued)

Experiment Time (s)	Surface Temperature (C)	Surrounding Temperature (C)	Gr	Ra	Nu	h	Bi	Tc (C)	θc
1156962	49.12	48.00	7.416E+07	5.221E+07	44.352	1.389	0.098	49.027	0.917
1165200	44.24	40.00	3.139E+08	2.214E+08	63.358	1.942	0.137	43.799	0.896
1173546	33.01	28.50	3.981E+08	2.814E+08	67.248	1.996	0.141	32.490	0.885
1181775	13.48	8.50	5.963E+08	4.245E+08	74.513	2.079	0.147	12.933	0.890
1190130	-9.47	-13.50	7.042E+08	5.052E+08	77.868	2.019	0.142	-9.940	0.883
1198359	-18.75	-20.00	2.480E+08	1.783E+08	60.193	1.525	0.108	-18.854	0.917
1206714	-19.24	-19.00	4.685E+07	3.368E+07	39.911	1.015	0.072	-19.225	0.938
1214943	14.45	18.00	3.720E+08	2.638E+08	66.213	1.904	0.134	14.813	0.898
1223298	19.82	18.50	1.361E+08	9.653E+07	51.646	1.487	0.105	19.703	0.912
1231527	20.80	19.00	1.841E+08	1.305E+08	55.636	1.605	0.113	20.643	0.913
1239882	20.80	19.00	1.841E+08	1.305E+08	55.636	1.605	0.113	20.629	0.905

Table C. 1 (continued)

Experiment Time (s)	Surface Temperature (C)	Surrounding Temperature (C)	Gr	Ra	Nu	h	Bi	Tc (C)	θc
1248111	21.29	19.00	2.340E+08	1.659E+08	59.033	1.703	0.120	21.080	0.908
1256466	20.80	19.00	1.841E+08	1.305E+08	55.636	1.605	0.113	20.629	0.905
1264695	21.78	19.00	2.838E+08	2.012E+08	61.919	1.786	0.126	21.514	0.904

Table C. 2. HTA Results for PVT_2

Experiment Time (s)	Surface Temperature (C)	Surrounding Temperature (C)	Gr	Ra	Nu	h	Bi	Tc (C)	θc
756376	43.26	38.00	4.006E+08	2.826E+08	67.306	2.051	0.145	42.690	0.892
764715	29.59	28.50	9.676E+07	6.839E+07	47.420	1.408	0.099	29.499	0.916
772929	22.75	20.00	2.766E+08	1.960E+08	61.516	1.780	0.126	22.488	0.905
780346	3.71	0.50	4.396E+08	3.138E+08	69.166	1.880	0.133	3.388	0.900
788685	-19.24	-19.00	4.685E+07	3.368E+07	39.911	1.015	0.072	-19.225	0.938
796898	-19.73	-20.00	5.367E+07	3.860E+07	41.271	1.046	0.074	-19.746	0.942
805237	-5.08	-1.00	5.808E+08	4.148E+08	74.119	2.005	0.141	-4.609	0.884
813450	40.33	46.00	3.905E+08	2.751E+08	66.846	2.082	0.147	40.953	0.890
821789	49.61	48.50	7.298E+07	5.138E+07	44.176	1.385	0.098	49.518	0.918
830002	35.94	31.00	4.190E+08	2.960E+08	68.092	2.036	0.144	35.409	0.892
838341	23.73	20.00	3.745E+08	2.654E+08	66.306	1.919	0.135	23.315	0.889
846554	0.78	0.00	1.082E+08	7.725E+07	48.921	1.328	0.094	0.723	0.927

Table C. 2 (continued)

Experiment Time (s)	Surface Temperature (C)	Surrounding Temperature (C)	Gr	Ra	Nu	h	Bi	Tc (C)	θc
854893	-21.68	-19.50	4.313E+08	3.101E+08	69.018	1.752	0.124	-21.456	0.897
863106	-19.73	-20.50	1.544E+08	1.110E+08	53.546	1.354	0.096	-19.787	0.926
870649	-8.50	-3.50	7.441E+08	5.320E+08	78.838	2.115	0.149	-7.906	0.881
878862	40.82	46.00	3.565E+08	2.511E+08	65.355	2.035	0.144	41.377	0.892
887202	50.10	48.00	1.388E+08	9.775E+07	51.765	1.621	0.114	49.900	0.905
895415	42.29	38.00	3.272E+08	2.308E+08	64.021	1.951	0.138	41.846	0.896
903754	31.05	28.50	2.258E+08	1.596E+08	58.451	1.735	0.122	30.791	0.898
911967	8.11	6.50	2.003E+08	1.427E+08	56.902	1.577	0.111	7.972	0.915
920306	-14.84	-15.00	2.895E+07	2.079E+07	35.445	0.914	0.064	-14.849	0.944
928519	-18.75	-20.00	2.480E+08	1.783E+08	60.193	1.525	0.108	-18.853	0.918
936858	-17.29	-16.00	2.385E+08	1.713E+08	59.584	1.531	0.108	-17.174	0.910
945071	31.05	43.50	8.990E+08	6.335E+08	82.195	2.543	0.179	32.679	0.869

Table C. 2 (continued)

Experiment Time (s)	Surface Temperature (C)	Surrounding Temperature (C)	Gr	Ra	Nu	h	Bi	Tc (C)	θc
953410	45.70	48.50	1.852E+08	1.304E+08	55.579	1.742	0.123	45.985	0.898
961624	43.75	38.00	4.376E+08	3.087E+08	68.793	2.097	0.148	43.114	0.889
969963	30.08	27.00	2.791E+08	1.973E+08	61.599	1.821	0.128	29.752	0.893
978176	6.15	3.50	3.456E+08	2.464E+08	65.143	1.788	0.126	5.896	0.904
985593	-11.91	-14.00	3.699E+08	2.655E+08	66.399	1.718	0.121	-12.103	0.908
993932	-19.24	-20.00	1.509E+08	1.085E+08	53.244	1.349	0.095	-19.301	0.919
1002145	-17.77	-18.00	4.402E+07	3.163E+07	39.298	1.003	0.071	-17.783	0.944
1010484	35.45	43.00	5.449E+08	3.840E+08	72.607	2.243	0.158	36.412	0.873
1018697	48.63	48.00	4.175E+07	2.939E+07	38.509	1.206	0.085	48.588	0.933
1027036	41.31	37.50	2.930E+08	2.067E+08	62.299	1.896	0.134	40.892	0.890
1034453	29.59	28.00	1.422E+08	1.005E+08	52.140	1.546	0.109	29.457	0.916
1041074	13.48	10.00	4.079E+08	2.902E+08	67.814	1.901	0.134	13.128	0.899
1049413	-9.96	-12.00	3.482E+08	2.497E+08	65.393	1.704	0.120	-10.164	0.900

Table C. 2 (continued)

Experiment Time (s)	Surface Temperature (C)	Surrounding Temperature (C)	Gr	Ra	Nu	h	Bi	Tc (C)	θc
1057626	-20.70	-20.00	1.394E+08	1.003E+08	52.212	1.323	0.093	-20.649	0.928
1065966	-21.19	-20.50	1.387E+08	9.979E+07	52.153	1.319	0.093	-21.136	0.921
1074179	31.54	36.50	3.928E+08	2.772E+08	66.988	2.033	0.143	32.072	0.893
1082518	48.14	48.00	9.285E+06	6.537E+06	26.658	0.835	0.059	48.133	0.949
1090731	50.10	48.50	1.051E+08	7.400E+07	48.330	1.515	0.107	49.968	0.918
1098148	31.05	28.50	2.258E+08	1.596E+08	58.451	1.735	0.122	30.812	0.907
1105691	23.24	19.50	3.783E+08	2.682E+08	66.477	1.921	0.136	22.825	0.889
1113904	-0.20	-4.00	5.612E+08	4.012E+08	73.519	1.969	0.139	-0.598	0.895
1122243	-19.73	-20.00	5.367E+07	3.860E+07	41.271	1.046	0.074	-19.747	0.936
1130456	-20.70	-20.00	1.394E+08	1.003E+08	52.212	1.323	0.093	-20.649	0.927
1138796	1.76	5.50	4.775E+08	3.402E+08	70.549	1.949	0.138	2.182	0.887
1147009	44.73	46.50	1.203E+08	8.472E+07	49.971	1.558	0.110	44.880	0.915
1155348	49.61	48.00	1.065E+08	7.500E+07	48.491	1.518	0.107	49.466	0.910

Table C. 2 (continued)

Experiment Time (s)	Surface Temperature (C)	Surrounding Temperature (C)	Gr	Ra	Nu	h	Bi	Tc (C)	θc
1163561	48.63	47.00	1.094E+08	7.704E+07	48.814	1.524	0.108	48.494	0.917
1171900	34.47	28.50	5.257E+08	3.716E+08	72.040	2.139	0.151	33.739	0.878
1180114	17.38	11.00	7.324E+08	5.208E+08	78.381	2.205	0.156	16.640	0.884
1188453	-7.03	-9.50	4.027E+08	2.885E+08	67.768	1.781	0.126	-7.287	0.896
1196666	-18.75	-20.00	2.480E+08	1.783E+08	60.193	1.525	0.108	-18.853	0.917
1205005	-21.19	-20.50	1.387E+08	9.979E+07	52.153	1.319	0.093	-21.136	0.921
1213218	12.50	16.00	3.781E+08	2.684E+08	66.499	1.900	0.134	12.629	0.963
1221557	14.94	18.50	3.702E+08	2.625E+08	66.130	1.905	0.134	15.333	0.890
1229770	17.87	19.00	1.161E+08	8.234E+07	49.659	1.432	0.101	17.958	0.922
1238110	20.31	19.00	1.341E+08	9.506E+07	51.450	1.484	0.105	20.194	0.911
1246325	18.85	19.00	1.539E+07	1.091E+07	30.232	0.872	0.062	18.857	0.950
1254662	20.31	19.00	1.341E+08	9.506E+07	51.450	1.484	0.105	20.195	0.912
1262875	20.80	19.00	1.841E+08	1.305E+08	55.636	1.605	0.113	20.643	0.913